6-20-2022 10:00 AM

Quantitative Assessment of Cardiac Functional Response after External Beam Radiotherapy using Non-invasive Multi-Modality Imaging

Oi Wai Chau, *The University of Western Ontario*

Supervisor: Gaede, Stewart, *The University of Western Ontario*

A thesis submitted in partial fulfillment of the requirements for the Doctor of Philosophy degree in Medical Biophysics

6-20-2022 10:00 AM

Quantitative Assessment of Cardiac Functional Response after External Beam Radiotherapy using Non-invasive Multi-Modality Imaging

Oi Wai Chau

Supervisor: Gaede, Stewart, *The University of Western Ontario*
A thesis submitted in partial fulfillment of the requirements for the Doctor of Philosophy degree in Medical Biophysics

Abstract

External beam radiation treatment is often included in standard breast cancer and non-small cell lung cancer patients' curative management. With the advances in radiation treatment (RT) techniques, such as the development of intensity-modulated radiation therapy and volumetric modulated arc therapy, local and regional control benefits are established. However, both cancer type survivors are prone to develop radiation-induced cardiac disease in their cured life. Furthermore, our laboratory previously demonstrated an inflammatory response in canine models using ^{18}FDG/PET imaging during the initial year following RT.

Hence, the overall goal of this thesis is to assess early functional changes and inflammation response in the heart after irradiation in both animal and patient pilot studies with the use of multi-modality imaging. Additionally, planning studies were undertaken to investigate the potential of reducing dose to the heart and substructure, including the left ventricle and the left anterior descending artery, which are unintentionally subjected to a higher dose during RT. Various RT planning techniques including deep-inspiration breath-hold and 4D Robust optimization, which can be applied to treat breast cancer are also examined. This is aimed to provide clinically feasible alternative options for patients who are non-compliant to breath-hold, without compromising target coverage.

In this thesis, we established a clinically feasible protocol to assess early cardiac functional changes and inflammation response of current radiation treatment techniques that are dedicated to minimizing cardiac dose and radiation-induced cardiac toxicity. This included multi-modality cardiac imaging assessment using hybrid PET/MR and CT perfusion imaging with serial blood work performed. Additionally, from the extensive dosimetric heart sparing treatment planning study, we were able to demonstrate/present clinical feasible free-breathing options for patients who are non-compliant with breath-

hold treatment. In the future, the benefits of cardiac dose mitigation strategies can be evaluated with the use of multi-modality imaging techniques.

Keywords

Radiotherapy, breast cancer, non-small cell lung cancer, radiation-induced toxicity, cardiac imaging, hybrid PET/MRI, inflammation, perfusion, treatment planning, robust optimization, deep-inspiration breath-hold

Summary for Lay Audience

With the advancement in radiotherapy techniques, the benefits of positive tumour biological response and progression in breast cancer and non-small cell lung cancer are observed. However, unintentional radiation-induced cardiac toxicity was reported in both cancer type survivors after their treatment. With the use of multi-modality functional cardiac imaging, the early effects on cardiac blood flow, function and inflammatory responses to radiotherapy were assessed from animal models to patient pilot studies before and after radiation treatment, featured in three chapters of this thesis. The feasibility of the non-invasive imaging assessment that we demonstrated may be useful in developing future patient-specific strategies, including early cardiac toxicity detection to minimize post-radiation risk. Moreover, through an extensive radiation dose distribution comparison among various radiotherapy treatment planning techniques, such as deep-inspiration breath-hold and robust optimization, the clinical feasibility in sparing various aspects of the heart are be compared and evaluated. Therefore, the cardiac exposure in future cancer patients can be minimized without compromising target coverage, especially for patients who are not compliant to heart-sparing techniques. In the future, the benefits of cardiac dose mitigation strategies can be evaluated with the use of multi-modality imaging techniques.

Co-Authorship Statement

This thesis consists of manuscripts that are submitted to and previously published in peer-reviewed journals.

Chapter two was adapted from the manuscript titled: “Changes in Myocardial Blood Flow in a Canine Model of Left-Sided Breast Cancer Radiotherapy”, which was submitted to *Physics & Imaging in Radiation Oncology* by Oi-Wai Chau, O El-Sherif, M Mouawad, J Sykes, J Butler, H Biernaski, R A deKemp, J M Renaud, G Wisenberg, F S Prato, and S Gaede. The study was conceived and designed by S Gaede, O El-Sherif, G Wisenberg, F S Prato and myself. The study was performed by J Sykes, O El-Sherif and S Gaede. The images were obtained by J Butler, H Biernaski, O El-Sherif. O El-Sherif, M Mouawad, R A deKemp, J M Renaud and I were responsible for analyzing, interpreting the data and preparing figures. And I wrote the whole manuscript with assistance from F S Prato and G Wisenberg. All the authors edited, revised and approved the final version of the manuscript.

Chapter three was adapted from the manuscript titled: “Dosimetric Planning Comparison for Left-sided Breast Cancer Radiotherapy: “The Clinical Feasibility of Four Dimensional-Computed Tomography Based Treatment Planning Optimization”, published in *Cureus* (in press; DOI: 10.7759/cureus.24777) by Oi-Wai Chau, H Fakir, M Lock, R Dinniwell, F Perera, A Erickson, S Gaede. The study was conceived and designed by S Gaede, H Fakir and myself. The treatment planning was performed by me and a selected review was performed by H Fakir, A Erickson, M Lock, R Dinniwell, F Perera. I was responsible for analyzing, interpreting the data and preparing figures. The manuscript was written by me with the assistance from S Gaede. All the authors edited, revised and approved the final version of the manuscript.

Chapter four was adapted from a manuscript titled: “Assessing Acute Cardiac Inflammation One Month after Left-sided Breast Cancer Radiotherapy with Hybrid PET/MRI”, which was submitted to *Breast Cancer Research and Treatment* by Oi-Wai Chau, A Islam, M Lock, E Yu, R Dinniwell, B Yaremko, M Brackstone, W Pavlosky, J

Butler, H Biernaski, M Kovacs, C Graf, G Wisenberg, F S Prato, S Gaede. The study was conceived and designed by A Islam, J Butler, G Wisenberg, F S Prato, S Gaede and myself. The images were obtained by J Butler and H Biernaski. A Islam and I were responsible for analyzing, interpreting the data, and preparing figures. I wrote the whole manuscript with assistance from A Islam, G Wisenberg, F S Prato and S Gaede. All the authors edited, revised and approved the final version of the manuscript.

Chapter five was adapted from an original research article titled: "Multi-Modality Imaging Assessment of the Heart Before and After Stage III Non-Small Cell Lung Cancer Radiotherapy", published in the *Advances in Radiation Oncology* 2022 (in press; DOI:10.1016/j.adro.2022.100927) by Oi-Wai Chau, A Islam, E Yu, M Qu, J Butler, H Biernaski, A Sun, J-P Bissonnette, A MacDonald, C Graf, A So, G Wisenberg, T-Y Lee, F S Prato, S Gaede. The study was conceived and designed by S Gaede, F S Prato, G Wisenberg, T-Y Lee, E Yu, A So and myself. The images were obtained by J Butler and H Biernaski. A Islam, G Wisenberg, F S Prato, S Gaede and I were responsible for analyzing, interpreting the data, and preparing figures. The manuscript was written by me with assistance from G Wisenberg, F S Prato, S Gaede. All the authors edited, revised and approved the final version of the manuscript.

Acknowledgments

This thesis would not be possible without the generous continuous support and expertise from the multi-disciplinary team across the city (the Departments of Radiation Oncology, Cardiology, Medical Biophysics and Nuclear Medicine) and the patient community. I am sincerely fortunate and grateful to have been surrounded by individuals who have provided me the support and growth.

I would like to begin by thanking our sources of funding, including the Translational Breast Cancer Research Unit, the Lawson Strategic Research Fund and the Canadian Institutes of Health Research for making this research possible.

Thank you to my advisory committee, Dr. Frank Prato, for continuous guidance support, patience & motivational constructive feedback for my projects, starting from the project initiation to reviewing my manuscript. I enjoy all the encouraging and inspirational long chats on research and life. Dr. Edward Yu, thank you for always being super approachable and especially for your continuous effort in patient recruitment and clinical support. Dr. Aaron So, thank you for providing me with the technical support and guidance in cardiac CT and research design.

My sincere gratitude to our cardiology partners including Dr. Gerald Wisenberg, Anna Mcdonald, and Dr. Ali Islam, for helping me navigating the cardiology clinical workspace, coordinating patients' workflow and recruitment, and critically reviewing my manuscripts. Sincere and special thanks to Chantelle Graf, thank you for being the best coordinator we can have, you are the reason for our success! Thank you to our oncology partners, including Dr. Michael lock, Dr. Muriel Brackstone, Dr. Melody Qu and Dr. Rob Dinniwell for continuous support in patient recruitment, without their efforts and hard work in patient recruitment, this thesis would not be possible. To Dr. Hatim Fakir and Abigail Erickson, thank you for teaching me the standard treatment planning workflow.

To my imaging collaborators, John Butler and Heather Biernaski, Tony Wales, and Jennifer Hadway, thank you for your support in imaging and your dedication to ensuring patients are the most comfortable they can during the scans. Thank you Dr. Omar El-Sherif, Dr. Ben Wilk, Dr. William Provosky, Dr. Rob de Kempe, Dr. Michael Kovacs for continuing tech support. Thank you Dr. Ting-Yim Lee, for his support and guidance on the technical and equipment in CT imaging.

To my lab administrators and supporters, including Barbara Barons, Shelagh Ross and Anne Leaist, thank you for their kindest support and for helping me navigate and schedule different facilities across the city. Thank you Jeff Kempe for always being so kind, inclusive and patient in my (non-tech-savvy) brain. To Heather Young, Timothy Yau, Dr. Mathew Mouawad, Dr. Derek Gillies, Dr. John Patrick, Mathew Van Oirschot, Zoe & all the wonderful coop students (Delaney, Megan, Daniel, Owen[s], Brandon, Tom, Nate and McKenzie), thank you for always being super supportive and making my days at lab more enjoyable. I wish you all the greatest success in your future endeavors.

Thank you to all the LRCP staff, patients and family, who give me the clinical exposure day to day at the centre. Through witnessing all the dedication to improving care and building connections with the community, the centre has been a safe space to let me grow and ask questions.

To my primary supervisor Dr. Stewart Gaede, thank you for believing me and taking me as a student. You have inspired me to grow and establish skillsets in every aspect of research and in clinical physics, with a lot of freedom in my interest area and pace as well as to explore other interesting areas such as public health. I am truly grateful for your open-minded mentorship, which enables me to seek consult, to mentor and thank you for your patience in my writing, which always has to be improved. I feel truly fortunate and lucky to have had the opportunity to learn from you and work alongside you throughout this experience.

Thank you to all my friends, Jill Hu, Olivia Tong, Charmainne Cruje, Danny Yang, Sabrina Chong, Bhavini Rathod, Joshua Lee, Lindsay Deng, Jimmy Li, Lyla Mu, Golafsoun Ameri, Jessica Rodgers, Salma Dammak, Roberta Piazza, Linda Lo, Jessica

Ye, Sharon Quershi, Andrea Kassay & many more, for all the long chats, late-night gatherings, food trips that make my graduate studies memorable. I am very grateful to have met all of you wonderful people.

Lastly, to my family, thank you for the unconditional love, caring, sacrifices and support for me to pursue higher education. Kenneth, thank you for being the best supportive brother and always being by my side. Mom and dad, I love you. Thank you for everything that you have taught, given and inspired me, this accomplishment would not be possible without every effort you have put into nourishing me.

Table of Contents

List of Tables

List of Figures

List of Appendices

List of Abbreviations

2D-RT	Two-dimensional radiotherapy
3D-CRT	3D-conformal radiotherapy
AIF	Arterial input function
CAD	Coronary artery disease
CTA	Computed tomography angiography
CTP	CT perfusion imaging
CVD	Cardiovascular disease
DCE-MRI	Dynamic contrast-enhanced MRI
DIBH	Deep-inspiration breath-hold
ECV	Extracellular volume matrix
ESR	Erythrocyte sedimentation rate
FDG	Fluorodeoxyglucose
HF	Heart failure
hs-CRP	High-sensitivity C reactive protein
hs-TnT	High-sensitivity troponin T
IMC	Internal mammary chain
IMRT	Intensity-modulated radiotherapy
LAD	Left anterior descending coronary artery

LCX	Left circumflex coronary artery
LGE	Late gadolinium enhancement
LV	Left ventricle
LVEDV	LV end-diastolic volume
LVEF	Left ventricular ejection fraction
LVESV	LV end-systolic volume
MBF	Myocardial blood flow
MHD	Mean heart dose
MI	Myocardial infarction
MPR	Myocardial perfusion reserve
MRAC	MR-based PET attenuation correction
PET	Positron emission tomography
PCI	Percutaneous coronary intervention
QUANTEC	Quantitative Analysis of Normal Tissue Effects in the Clinic
RC	Right coronary artery
RICD	Radiation induced cardiac disease
RT	Radiation treatment
SEM	Standard error of mean
SV	Stroke volume

SUV_{bw}	Standard uptake of the myocardium based on body weight
T1	Longitudinal recovery time
VMAT	Volumetric modulated arc therapy

Chapter 1

1 Introduction

In this thesis introduction, several topics are covered in order to highlight the importance of accounting for radiation-induced cardiac toxicity in two cancer types: breast cancer and non-small cell lung cancer. The topics include the clinical endpoints of radiation-induced cardiac toxicity, current curative management of both cancer types and specific radiation treatment techniques aiming to minimize normal tissue dose, including the heart. This is followed by a summary explanation of the progression of radiation damage in the heart. Lastly, various imaging techniques and biomarkers for assessing/detecting radiation induced cardiac disease are presented.

1.1 Breast Cancer

Breast cancer is the most frequently diagnosed cancer among women worldwide.[1] It is estimated that about 1 in 8 Canadian women will develop breast cancer during their lifetime and 1 in 33 will die from it. [2] In Canada, from 2011-2017, the 5-year survival rate is 89% for all stages combined.[3]

Breast cancer arises in the epithelium of the ducts or lobules in the breast glandular tissue. The initial cancerous growth is confined to the duct or lobule ("in situ"), is generally symptomless, and has minimal potential for spread (metastasis).

Radiation treatment (RT) plays an integral role in curative management, with well-established local and regional control benefits.[4-5] In Canada, almost two thirds of female breast cancer receive radiation treatment.[6] With the introduction RT, the 10-year risks of any locoregional or distance first recurrence and the 15-year risk of breast cancer mortality were reduced by 15.7%, (35% to 19.3%) and 21.2%, (63.7% to 42.5%) in a retrospective study.[7]

However, a landmark paper that included patients treated with breast RT in 75 randomized trials, reported the cardiac mortality increase risk is 0.3% for nonsmokers and 1.2% for persistent smokers.[8] Moreover, patients in 22 countries (diagnosed in breast

cancer and received adjuvant RT before 1990) with 6.7 years mean length of follow-up presented with a causal effect of higher radiation dose on cardiac mortality in left-sided versus right-sided affected breast cancer (rate ratio, left vs right, 1.04).[9]

A population-based cohort study of breast cancer survivors during the non-CT based RT period (1999-2007) in Denmark and Sweden, presented an increased risk of radiation-related cardiac morbidity after left-sided RT compared with right-sided RT (incidence rate ratio: 1.18; 95% CI: 1.07-1.30) with 3.6 Gy greater mean heart dose in the left-sided cohort.[10] Whereas during the CT-based RT period (2008-2016), no difference in risk of cardiac events in left-sided vs right-sided was reported in early-stage breast cancer (10-year) survivors.[11]

A retrospective study of patients diagnosed from 2000 to 2009 identified from the SEER-Medicare database demonstrated that left-breast-affected patients had a small increase in their risk of percutaneous coronary intervention after RT and a subsequent increase in the cardiac mortality risk with a subdistribution hazard ratio of 2.02.[12]

Overall, these published studies have shown with RT techniques, breast cancer survivors are benefited with better survival and local control. Nevertheless, especially the left-sided-affected cohort are prone to develop radiation-related cardiac disease and the clinical symptoms can manifest into cardiac mortality.

1.2 Curative management of breast cancer

Standard breast cancer curative management includes breast cancer surgery, adjuvant hormonal therapy, adjuvant chemotherapy and radiation therapy which are discussed in the subsequent sections.

1.2.1 Breast Cancer Surgery

Breast cancer surgery is one of the main components of curative breast cancer management. It consists of either modified radical mastectomy, quadrantectomy, excisional biopsy or wide local excision with sentinel lymph node biopsy with/without

axillary lymph node dissection. Wide local excision is commonly followed with whole-breast irradiation, with/without a boost to the tumour bed.[13]

1.2.2 Mastectomy

Mastectomy can be removing one breast (unilateral or single mastectomy) or both s breasts (bilateral or double mastectomy). It is reported that after mastectomy, RT decreases the 20-year breast cancer mortality risk by 8.1% and lowers the overall mortality in node-positive disease (risk ratio 0.89) reported in a meta-analysis study.[14]

1.2.3 Adjuvant Hormonal Therapy

Hormonal therapy is also recognized as endocrine therapy with the basis of estrogen linking to the pathogenesis of breast cancer.[15] Tamoxifen antagonizes the growth of estrogen-dependent breast cancer. Five years duration of tamoxifen treatment is the standard adjuvant endocrine therapy for women with estrogen-positive blood-free breast cancer.[15] For patients with hormone receptor positive early-stage breast cancer, the current guidelines suggest extending hormone therapy for 10 years.[16] Yet, the use of tamoxifen or aromatase inhibitors may associate with increased risk of ischemic heart disease, myocardial infarction and venous thrombosis, according to the American Heart Association Cardiovascular Disease in Women and Special Populations Committee of the Council on Clinical Cardiology.[17]

1.2.4 Adjuvant Chemotherapy

Up to the mid-1990s, adjuvant chemotherapy for breast cancer, comprised mainly of cyclophosphamide, methotrexate, and 5-fluorouracil (CMF), were prescribed to premenopausal women/women aged <50 years with positive lymph nodes.[13] It was reported with no elevation of cardiovascular disease (CVD) risk compared with surgery alone.[13]

In the 1990s, anthracycline-containing regimens were introduced with the FDA's approval of doxorubicin (due to its significant antitumor activity published in experimental tumour studies during 1969 and 1970), including 4xAC (doxorubicin, cyclophosphamide), 4xEC (epirubicin, cyclophosphamide), 5xFAC (AC with 5-

fluorouracil) and 5-6xFEC (EC with 5-fluorouracil).[13] Systemic therapy was also increasingly delivered to premenopausal women without axillary lymph node metastasis. Chemotherapy used since 1997 was reported to have a higher risk of chronic heart failure (HF) (sHR 1.35).[13] Dexrazoxane is a cardioprotective agent approved by the FDA for use in advanced breast cancer patients treated with anthracyclines-containing regimens[18], which significantly reduces the risk of HF.

Trastuzumab is a humanized monoclonal antibody targeted against the extracellular part of HER2, which inhibits the proliferation of the cells overexpressing the HER2 oncogenic activation.[19] An elevated risk of cardiotoxicity in a cohort of trastuzumab-treated early-stage breast cancer patients was previously reported.[20] The cumulative incidence of major cardiac events was higher compared with an age-matched healthy population; and patients receiving sequential therapy with both anthracyclines and trastuzumab were at a higher risk.[20]

1.3 Radiation-induced cardiac toxicity: clinical endpoints

The foremost data obtained regarding the harmful effects of radiation on the cardiovascular system was from the survivors of the Hiroshima and Nagasaki atomic bombings, which depicted a 9.5% of cardiac mortality rate.[21]

Radiation-induced cardiac disease (RICD) was initially characterized by the diffuse interstitial fibrosis typically observed in the left ventricle (LV) myocardium, which is dominant in the anterior and lateral walls, represented as an outcome of damaged myocardium microcirculation with subsequent ischemia.

The radiation-related cardiovascular event which resulted from radiation treatment was frequently defined as a cardiovascular hospital discharge diagnosis, cardiosurgical intervention, or death due to cardiovascular disease (CVD). CVD is classified as cardiomyopathy, myocardial infarction, coronary heart disease (CAD), angina, arrhythmia, stiff or leaking heart valves. It is important to note that CVD mainly is diagnosed after decades of patient-cured life.

1.3.1 Coronary Artery Disease (CAD)

Coronary artery disease is the most common manifestation of RICD with an incidence of up to 85%,[22] resulting from coronary arteries stenosis and atherosclerosis development, microcirculatory damage, and sustained inflammation. In terms of coronary artery stenosis, the lumen narrowing is related to endothelial injury in the coronaries, platelet aggregation, thrombosis and replacement of damaged coronary intima cells by myofibroblasts.[23] CAD is generally diagnosed by echocardiography and CT imaging. Coronary artery bypass graft and percutaneous coronary intervention (PCI) are common practices for CAD management.[23]

1.3.2 Pericardial Disease

Acute pericarditis is recognized as a short-term complication of radiation-induced inflammation of the pericardium. Pericardial calcifications, thickening, effusion, and constrictions can be detected through imaging such as T2-weighted MRI. In the later term, collagen and fibrin will replace the normal adipose tissue of the heart. Persistent inflammation fibrosis of the pericardium is characterized as chronic constrictive pericarditis that can progress to heart failure. An autopsy study showed a large proportion of patients who had undergone mediastinal radiation had some form of the pericardial disease usually effusion or constriction identified.[24] Frequently, the pericardial disease is managed with (1) diuretics and anti-inflammation drugs, (2) pericardial stripping for constrictive pericarditis, (3) pericardiocentesis for large effusions/tamponade.[23]

1.3.3 Valvular dysfunction

Irradiated valve cusps and leaflets can induce fibrotic changes and thickening, with or without calcification.[23] A case-control study of 5-year Hodgkin lymphoma survivors reported that the radiation dose to the heart valves can linearly increase the risk for clinically significant valvular heart disease with a dose above 30 Gy.[25] Currently, most of the studies reporting RICD endpoints of valvular disease are from Hodgkin lymphoma patients treated with mediastinal irradiation[25-28], which is more detrimental to the left-sided valves (responsible for controlling blood delivery to the whole body) regardless of the dose distribution,[29] and suggesting higher pressures in the systemic circulation (a

more forceful hemodynamics), which may further damage the fragile valve. Surgical or transcatheter aortic valve replacements are performed in severe cases.[23]

1.3.4 Cardiac sarcoidosis

Cardiac sarcoidosis is a rare inflammatory condition where clusters of immune cells form granulomas in the heart, which can give rise to arrhythmia and heart failure. Traditionally, echocardiography and late gadolinium enhancement (LGE) MRI are used in the diagnosis of cardiac sarcoidosis (CS). With nuclear imaging, ^{18}FDG/PET has a reported sensitivity and specificity for the detection of cardiac sarcoid disease as high as 89.9% and 81.4%, respectively.[30] Immunosuppressive regimens in the form of corticosteroids generally play a major role in CS treatments.

1.3.5 Arrhythmia

Arrhythmia is presented as triggered activity from active inflammation to re-entry scar formation. Transient and asymptomatic arrhythmia may occur within a year of therapy, but permanent damage to the cardiac nodes and bundle branch blocks may manifest in later years after RT completion.[23] Patients are generally managed with a pacemaker or cardiac resynchronization, or prescribed with beta-blockers, and calcium channel blockers for anti-arrhythmic therapy.[23]

1.3.6 Myocardial Infarction (MI)

Acute myocardial infarction is identified as an event of myocardial necrosis caused by myocardial ischemia, such as the atheromatous process (activation of a plaque) which prevents blood flow through the coronaries.[31] Acute MI is classified based on the presence or absence of ST-segment elevation on the ECG and is further categorized into subtypes of infarction (cause by coronary atherothrombosis or cardiac intervention such as PCI and stent).[32]

1.3.7 Congestive Heart Failure (HF)

Congestive heart failure may result from widespread sarcoidosis of the myocardium, excessive inflammation leading to adverse LV remodeling, with a decline in left ventricular ejection fraction (LVEF) and death.

It is interesting to note that a case-control study, which studied heart failure as the first cardiovascular diagnosis of breast cancer survivors treated during 1980-2009, found in the absence of anthracyclines, breast RT was not associated with increased HF risk.[33]

Patients with heart failure symptoms from radiation are often prescribed beta-blockers, angiotensin-converting enzyme inhibitors, and diuretics.[23]

1.4 Types of Breast Irradiation

Adjuvant whole breast and partial breast irradiation are often delivered in curative breast cancer management. Traditionally, whole-breast irradiation is performed in a tangential manner, usually prescribed with a dose of 50 Gy in 25 fractions or 42.5 Gy in 16 fractions using 2 tangential photon beams. The Radiation Therapy Oncology Group (RTOG) published consensus guidelines on the dose coverage contour boundaries of the whole breast, chest wall, and nodal volume used for CT-based RT planning.[34]

Partial breast irradiation is delivered using intraoperative radiation, brachytherapy or external beam techniques.[35-37] It is aimed to irradiate the tumour bed rather than the whole breast, and a single treatment using photons or electrons can be given at the time of surgery. Two large partial breast irradiation trials (NSABP B-39 / RTOG 0413 – RAPID [38.5Gy in 10 twice daily])[38-39] published promising results (acceptable toxicity rate and ipsilateral breast-tumour recurrence) in low-risk breast cancer patients with a shorter treatment duration. It is aimed that smaller volume of breast tissue can be treated with larger fractions in a shorter treatment fractionation regime.

For advanced stage breast cancer, both the European Organization for Research and Treatment of Cancer (EORTC 22922)[40] and the National Cancer Institute of Canada Clinical Trials Group (MA.20)[41] studies demonstrated that locoregional RT (with irradiation of regional nodes in patients with high volume nodal disease or high-risk N0-1 disease) with prior surgery improves locoregional control and decreases rates of distant

metastasis, breast pain and treatment-related symptoms, with the cost of worsening cosmetic results (moderate to severe fibrosis risk)[39,42].

Note that when the internal mammary chain, supraclavicular or axillary modes and chest wall are irradiated, this can lead to considerable exposure of the heart and lungs in both left and right-sided RT, especially in case of axillary nodal metastases.[8,43-44]

1.4.1 Radiation Treatment Techniques

After decades of two-dimensional radiotherapy (2D-RT), CT-based planning has become a standard-of-care.[45] CT-based RT planning allows for an accurate anatomical location and its vicinity to the breast and lungs and, subsequently, an accurate description of cardiac and substructure radiation exposure. The advancement of RT techniques, including utilizing 3D-conformal radiotherapy (3D-CRT), intensity-modulated radiotherapy (IMRT), and volumetric arc radiotherapy (VMAT), have constituted improved conformal dose distributions. However, it is not certain whether the advances in RT techniques can reduce the prevalence of cardiac complications or simply delay the timing of their onset with further reduction of radiation dose received in the heart.

1.4.2 3-Dimensional conformal radiation therapy (3D-CRT)

For cancer patients who were irradiated before the era of 3DCT RT planning, the individual CT information was unavailable, such that the estimation of cardiac and substructure doses in the treatment plan for retrospective evaluation is impossible. Through incorporating the treatment planning software with 3D anatomy structure dataset, 3D-CRT can calculate accurate 3D dose distributions to the treated breast and also nearby organs at risk, including the heart.

A retrospective study of 3D-CRT, which published results on irradiated patients in Germany from 1998-2008 demonstrated lower cardiac mortality than patients treated without RT.[46] Moreover, NRG Oncology RTOG 0319 [47] was the first prospective cooperative group trial to evaluate 3D-CRT as a method of accelerated partial breast irradiation (APBI) for stage I or II invasive breast cancer patients. The prescription dose of 38.5 Gy in 10 fractions was often delivered in terms of a point dose.[47] Overall, with a

median follow-up period of 8 years, durable ipsilateral breast tumour control was shown, similar to other published APBI trials (using brachytherapy).[47]

Advanced RT techniques for treating breast cancer are currently available aiming for better target coverage and sparing the normal tissue including the heart, and are presented/discussed in the following sections.

1.4.3 Intensity-modulated Radiotherapy (IMRT)

Forward and inverse planned intensity-modulated RT has been considered to further conform the dose distribution, specifically to the target, and to minimize the dose to critical structures.[48] In addition, IMRT beams delivered by a dynamic multi-leaf collimator can provide a rapid and efficient dose delivery compared to 3D-CRT.

1.4.4 Volumetric Modulated Arc Therapy (VMAT)

VMAT was developed in 2007, a novel RT technique equipped with the benefits of highly conformal dose distributions, improvements in target volume coverage and normal tissue sparing by the synchronized variation of the gantry rotation speed and treatment field shape in combination with the involvement of multi-collimator leaves motions and dynamic dose rate during RT. However, Sakka et al. have shown that VMAT techniques in left-sided breast RT have a greater low dose volume to the heart and left anterior descending artery (LAD) compared to IMRT.[49]

1.4.5 Deep Inspiration Breath-hold (DIBH)

To address the concern of heart dose, many centres utilize a deep-inspiration breath-hold (DIBH) approach to maximize the distance between the heart and the irradiated breast. The respiratory signal is viewed as a surrogate of an internal organ motion, through monitoring, and the heart is typically furthest from the treated breast during the end of inspiration. For centers that do not acquire respiratory signal, the patients usually undergo a large inhale then hold. It is noted that breath-hold treatment requires patient compliance and education/training prior to treatment (15-30 minutes)[50], and not every patient manages DIBH RT.

Deep-inspiration breath-hold consists of voluntary and involuntary techniques. Usually the breath-hold automatically triggers the beam delivery at specific portions of the breathing cycle. This requires either measuring the changes in the pressure exerted by the breathing induced motion of the diaphragm against the bellows system, or video tracking of an external marker on patient such as the real time position management system (Varian RPM systems, Varian Medical Systems, Palo Alto, USA) or surface guided RT system (SGRT) (AlignRT, Vision RT Ltd, London, United Kingdom) that are discussed in the proceeding sections.

1.4.5.1 Active breathing Control (ABC)

The active breathing control (ABC) procedure is an involuntary technique which consists of apparatus that can halt breathing at any predetermined position along the breathing cycle. The device usually incorporates a mouthpiece, spirometer and valve connected in series.[51] Once activated by the operator, the valve will close at a specific lung volume, thereby halting the airflow and causing a corresponding breath-hold of typically 10-45s.[51] The ABC procedure can be adapted for planning CT acquisition with minimal motion artifacts.[51] However, it holds the disadvantages of compliance issues and invasiveness to patient.

In a prospective trial of left-sided breast cancer patients, the mean heart dose was significantly reduced by ≥20% in 88% of patients ($p < .001$) with the use of active breathing control and proven to be well tolerated and preserved local control.[52]

1.4.5.2 Voluntary deep-inspiration breath-hold (vDIBH)

The voluntary deep-inspiration breath-hold techniques utilize respiratory gating techniques that can correspondingly optimize patient positioning and intra-fraction motion monitoring. The Varian RPM system[53] consists of an infrared camera mounted on the wall and surrounded by infrared lights. A marker box with reflective dots is placed on the patient and used as surrogate to measure the expansion of the patient's thorax during breathing from 2 degrees of freedom (DOF).[53] Alternatively, surface-guided radiation therapy (SGRT) has emerged with combinations of optical sensors and algorithms that can permit 3D optically surface scanning of patient's surface and detection of positional

offsets which could be corrected in 6 DOF.[54] It holds the basic principle of photogrammetry, which is defined as the process of optical describing a 3D object with the information obtained from 2D images. Photogrammetry measures the distance between two points residing on a plane parallel to the imaging plane, through quantifying the distance on an image with a known scale. Therefore, the patient surface can be compared with a reference surface, followed by computing the displacements required to bring the two surfaces into alignment. The accuracy of SGRT systems was reported within 5 mm for DIBH positioning and monitoring[54], and agreeable to spirometry-based positioning.[55] Overall, SGRT enables a more robust RT setup (compared to traditional tattoo setup), which is contact-less, non-invasive and can longitudinally gate/monitor patient's breath-hold throughout the treatment. Note, the reproducibility for both respiratory gating techniques from fraction to fraction can be a limitation. Furthermore, testing features of SGRT such as skin colors, room lighting, thermal signature and deformable registration algorithms can be challenging.[56]

1.4.6 Prone Breast

In the prone position, gravity is exploited to further separate the breast and surrounding normal tissues, leading to less radiation exposure to the heart and lungs. Prone positioning tangential-field whole-breast and partial breast RT showed promise in reducing the heart dose in left-breast-affected women of larger volume and right-breast-affected women regardless of the breast volume; however, left-breast-affected women of smaller breast volume were less benefitted from prone positioning, comparing the normal-tissue doses of the ipsilateral lung, heart, chest wall and LAD doses.[57]

1.5 Breast RT Cardiac Dose Guideline

The Quantitative Analysis of Normal Tissue Effects in the Clinic (QUANTEC) was formed by a group of physicians and researchers to provide data and reliable predictive models on relationships between dose-volume parameters and the normal tissue complication for RT planning in 2Gy per fraction. For the whole heart, it is suggested to have the volume of the heart receiving 25 Gy or more to be less than 10% ($V25_{Gy}$Heart <10%) for <1% long-term cardiac mortality; and for the pericardium, it is recommended

to have the mean dose <26Gy and $V30_{Gy}$ <36% for <15% toxicity risk of pericarditis.[58] However, a population-based study identified that QUANTEC guidelines were not violated in any of the cardiovascular deaths in women with early-stage breast cancer.[59] The risk of radiation-induced cardiac death at 10 years appeared to be very low according to the classification of mean heart dose (MHD) <3.3 Gy and max LAD dose <45.4 Gy, which suggested the need for the dose constraints of heart and LAD to be re-evaluated in future studies.[59]

In a retrospective study, Darby et al. presented the overall average of MHD which was 4.9 Gy from 2D-RT and the overall ratio of major coronary events increased linearly with the MHD by 7.4% per gray, with no apparent threshold.[60] Regarding this retrospective model, the baseline cardiovascular risk was not known since the real dosimetric data and true location of the heart compared to the irradiated volume were not available in all patients (MHD was estimated), and there was an imbalance of comorbidities among treatment groups. Van der Bogaardt et al.[61] later validated Darby's model in breast cancer survivors treated with 3D-RT using available dosimetric data, given that lots of variability in heart position could exist. They concluded after a nine-year follow-up that the cumulative incidence of coronary events surged by 16.5% per Gy of MHD and that the LV V_{5Gy} was the best predictor of risk.[61]

A worldwide systematic review done by Drost et al.[62] on whole breast RT studies after 2014, reported a 3.6 Gy total MHD based on 84 left-sided breast cancer studies and a lower MHD of 1.7 Gy from 65 regimens with breathing control. Frequently the apex of the heart is close, or even within the radiation field, resulting in a maximum dose exposure of the heart up to >20 Gy.[63] A 3D-CRT study on breast cancer suggested the LAD radiation dose should be considered in RT planning and the dose should be kept as low as possible.[64] Particularly, the women receiving a mean dose of 1-5 Gy to the mid LAD had an adjusted odds ratio of 0.9 for a later coronary intervention compared to women receiving a mean dose of 0-1 Gy to the mid LAD.[64]

In order to (1) manage/monitor the progression of radiation-induced cardiac toxicity efficiently and (2) evaluate the clinical effectiveness of cardiac dose mitigation strategies

including current and advanced RT techniques, acute microvascular level radiation damage/changes in patients and/or animal models need to be studied. This can allow early interventions to minimize breast cancer patients from the aforementioned radiation-related cardiac toxicity at the later term. The proceeding section will begin with a brief introduction of radiation damage to heart at the micro and macrovascular level.

1.6 Micro and Macrovascular level Radiation Damage

Radiation leads to the formation of free radicals that disrupts the DNA strands integrity, which can precipitate molecular damage. Tissue malfunction ultimately occurs when the cell's ability to repair itself is overwhelmed.[65] At an acute stage, radiation damage at the microvascular level is identified.

Endothelial injury in the cardiomyocytes and coronaries can lead to a proinflammatory and profibrotic environment as a host defense response. By secreting chemokine (C-C motif) ligand 2 (CCL2), which attracts monocytes that will later differentiate into M1-like macrophages, will be responsible for removing cellular debris, minimizing the area of apoptosis, and segregating injured from healthy tissue.[66] It is proceeded with the generation of reactive oxygen species, cytokine and adhesion molecules, which interacts with the leukocytes and platelets and target the inflammation (to clear the injury).[67] Pro-inflammatory cytokine release includes IL-6, tumour necrosis factor (TNF)-α, transforming growth factor (TGF)-β. TGF-β activation under ionizing radiation contributes to many cellular processes such as epithelial cell growth, mesenchymal cell proliferation, and extracellular matrix synthesis.[68] Platelet aggregation, thrombosis, and replacement of the damaged cells by myofibroblasts can eventually rupture vessel walls via oxidative stress (loss of thromboresistance).

At the later stage, the damaged heart initiates cell recruitment through chemokine (C-X3-C motif) ligand 1 (CX3CL1) to attract monocytes, which differentiate into M2-like reparative macrophages within the tissue.[66] This begins the reparative phase of the healing process; whereby invading leukocytes secrete cytokines which provide support to endogenous tissue. Lymphocytes, including T helper cells, are present at low levels and

are suggested to mediate the transition from proinflammatory to reparative cell recruitment.[66] Together, these cells operate the healing process, stimulating angiogenesis to restore blood supply to the area at risk, and stimulating fibroblast reorganization and extracellular matrix synthesis to generate a stable, collagen-rich scar.[66]

Intimal lesions following radiation exposure consist primarily of fibrous tissue. Increased vascular permeability post-radiation is mediated in part by histamine and accumulating endothelial cell death, causing fibrinogen leak outside the vessels.[68] Fibrinogen is converted to fibrin and evolves into fibrous tissue over time.[68] This can lead to the narrowing of the vessels commonly diagnosed as atherosclerosis. The decreased ratio of effective blood vessels to myocytes, ultimately will manifest in the development of cardiac sequelae and myocardial cell death.[69]

1.7 Non-small Cell Lung Cancer (NSCLC)

Lung cancer is the second most commonly diagnosed cancer worldwide (11.4% of total cases)[1] and is classified into two major histological types, non-small cell lung cancer (NSCLC) and small cell lung cancer, depending on the neuroendocrine features. NSCLC comprises 85% of all lung cancer originating from the epithelial cells of the lung of the central bronchi to terminal alveoli.[70] The poor prognosis of lung cancer patients compared to other cancer survivors has been shown, with the age-standardized mortality rate (number of total deaths of patients worldwide) being 11.2% (male) to 25.9% (female).[1]

Radiation treatment is among the standard curative management for NSCLC patients. As discussed previously, it is important to note that radiation may induce unintentional injury of the myocardial tissue, during and after NSCLC RT due to the proximity of the heart to the target tumour. From stage III NSCLC patients receiving dose-escalated RT of 74 Gy in 30 fx in 6 trials, at 8.8 years follow-up, 23% of patients had their first cardiovascular event with heart doses associated with the events on a univariable analysis.[71] Since lung cancer patients are usually diagnosed at an older age, cardiac comorbidities including ischemic heart disease and cardiac arrhythmia are commonly reported.[72] Moreover, data from an Austrian center demonstrated that NSCLC patients

(stage I-IV) presented with at least one coexisting cardiovascular disease (CVD) in 67.2% of the population.[73] A US-based study of 95167 patients showed that CVD may increase mortality in patients with stage I-IIIB disease, while there is no difference in survival in stage IV patients.[74]

Locally advanced NSCLC patients with underlying CVD were presented with a 2-year cumulative incidence estimate of major adverse cardiac events of 11.7%.[75] Additionally, for cardiac intervention, a case-control study of cardiac revascularization in patients who had previous thoracic RT found that there was an increase mortality risk up to 5 years after coronary artery stenting (hazard ratio = 4.2, 95% CI: 1.8-9.5).[76]
Overall, NSCLC patients are commonly treated with surgery, with or without adjuvant chemotherapy and RT, and chemotherapy and RT for unresectable disease, which is discussed in the subsequent section.

1.8 Standard Curative Treatment of NSCLC

1.8.1 Lung Cancer Surgery

Targeted lung cancer screening programs have shown lung cancer incidence rates between 1% [77] and 1.6% [78], with the majority of patients diagnosed with early-stage disease and treated with curative-intent surgery only, whereas the other patients received chemo or radiation treatment.

1.8.2 Chemotherapy - NSCLC

From the practice guideline published by American Society for Radiation Oncology (ASTRO), the optimal chemotherapy regimen for use in conjunction with concurrent thoracic RT is not known, however, the 2 most common regimens etoposide/cisplatin (EP) and carboplatin/paclitaxel (PC) were assessed in a completed phase 3 clinical trial (NCT01494558).[79] EP was suggested to be superior to weekly PC in terms of OS in the setting of concurrent chemoradiation for unresectable stage III NSCLC.[80-81] Another chemotherapy regimen, Cetuximab, which was examined in RTOG 0617, showed no OS benefit.[82]

1.8.3 Dose of NSCLC RT

The ASTRO practice guideline recommended a minimum dose of 60 Gy in 2 Gy once-daily fractions of external RT for locally advanced NSCLC patients managed by RT alone, with a cost of treatment-related side effects such as esophagitis and pneumonitis.[79] For dose escalation beyond 60 Gy with combined modality concurrent chemoradiation, it is reported with no associated clinical benefits.[79]

Furthermore, RTOG 0617 compared standard dose (60 Gy) versus high-dose (74 Gy) radiation with concurrent chemotherapy and determined the efficacy of cetuximab for stage III NSCLC.[82] Of 496 eligible patients accrued, at a median follow-up of 5.1 years, V_{5Gy}Heart along with tumour location, radiation dose, esophagitis/dysphagia etc. were factors that affected OS.[82]

1.9 Lung RT Cardiac Dose Guideline

The heart dose in NSCLC RT planning has historically not been the main priority, given the later toxicities are acceptable for patients with relatively poor prognosis.[83] A retrospective study of locally advanced NSCLC patients treated with median prescription of 66 Gy, with the planning CT heart location recontoured according to the RTOG 0617 guidelines, compared $V50_{Gy}$Heart <25% versus ≥25%, reported the 1-year OS rates were 70.2% versus 46.8% and the 2-year OS rates were 45.9% versus 26.7% ($p < 0.0001$).[84] Moreover, it was reported that the median $V50_{Gy}$Heart was significantly higher (20.8% versus 13.9%, $p < 0.0001$) for patients with cardiac toxicity.[84] From RTOG 0617 trial reported that at a median follow-up of 2 years and 5.1 years, $V5_{Gy}$Heart and $V30_{Gy}$Heart were factors that affected stage III NSCLC OS.[82,85]

For early-stage NSCLC patients treated with SBRT, in a median follow-up of 34.8 months, a multivariate analysis by Stam et al.[86] showed that the maximum dose on the left atrium (HR: 1.005/Gy) and the dose of 90% of the superior vena cava (HR: 1.025/Gy) were significantly associated with non-cancer death in this patient group.

A study of 11101 NSCLC patients (stage T1 to T4, treated with 55 Gy in 20 fractions), presented the dose-sensitive region at the base of the heart, where higher doses were associated with worse patient survival using voxel-by-voxel CT permutation testing ($p < 0.001$).[87] Furthermore, Schytte et al.[88] found in NSCLC patients treated with 3D-CRT a

worsened OS in the group of patients with a mean LV dose greater than 14.5 Gy in 30 to 40 fractions.

1.10 Previous canine model study done on understanding cardiac inflammation post irradiation

A study of the effects of radiation in an animal model, particularly at the heart region, was done previously. Our laboratory demonstrated a progressive global myocardial inflammatory response during the initial year following RT using hybrid ^{18}FDG/PET imaging in canine models (n=5).[89] The increased global inflammatory signal uptake was detected as early as one-week post-single-fraction irradiation of a biological equivalent LAD dose compared to standard breast RT under breath-hold condition.[89] The inflammatory signal was correlated with the myocardial dose and further confirmed with immunohistochemistry (CD45) at 12-months.[89] The study suggested that inflammation PET imaging should be considered in future clinical studies to monitor the early changes in cardiac function that progress into radiation-induced cardiac toxicity.

1.11 Non-invasive Cardiac Imaging for RICD

The available imaging techniques to detect or monitor RICD in patients non-invasively are listed in the proceeding section.

1.11.1 Echocardiography

Transthoracic echocardiography has been recommended in cardiovascular medicine and oncology articles as a primary imaging biomarker for LV dysfunction during and after the administration of potentially cardiotoxic cancer-related treatment.[18,90] A LVEF measurement of less than or equal to 40% is identified as heart failure using echocardiography.[91] Baseline global longitudinal strain imaging using 2D speckle tracking echocardiography or doppler tissue imaging is also recommended to measure myocardial deformation with high sensitivity for early detection of LV dysfunction.[92] However, conventional echocardiography is limited to the detection of macrovascular changes in the heart functions. To detect microvascular changes in response to radiation, medical imaging other than echocardiography is needed.

1.11.2 SPECT imaging

SPECT is a traditionally widely used diagnostic tool for the detection of myocardial prefusion defects with the capacity to differentiate reversible perfusion defects from irreversible perfusion defects. Imaging using ^{99}Tc/SPECT in left-sided breast cancer patients have reported increased myocardial perfusion defects and abnormalities starting from 6-months post-RT.[93-95] A systematic review done by Kaidar-Person et al. reported regional perfusion defects in the apical and anterolateral aspects of the LV with a correlation between the proportion of LV within the RT-field.[96] Moreover, a retrospective study of early-stage breast cancer patients found a statistically significant higher prevalence of stress SPECT perfusion abnormalities particularly in the LAD territory at 12 years post-RT among left (59% incidence) vs right-side (8% incidence) irradiated patients.[97]

1.11.3 PET imaging and ^{18}FDG

Positron emission tomography (PET) utilizes radionuclide tracer techniques and an external detector system to produce images of in vivo radionuclide distribution. The image intensity presented as standard uptake value (SUV) (equation 1) reflects the functionality instead of the anatomy of the imaged organ. PET allows non-invasive evaluation of the myocardial metabolism, blood flow, and function, using physiological substrates prepared with the positron-emitting radionuclide. Positron emitting radionuclides, such as fluoro-2-deoxyglucose (^{18}FDG) which has a 110-minute half-life, are produced using a cyclotron. The advancement of 3D cardiac imaging using PET has been equipped with crystal camera technology, high-speed electronics, and software to lessen the dead time and better locate random and scattered events.[98]

$$[1] SUV = Activty\ (MBq/kg)/[injected\ dose\ MBq/Weight(kg)]$$

^{18}FDG/PET is the most studied tracer of nuclear inflammation imaging, which has been used for staging primary cancer and detecting metastasis.[99] ^{18}FDG/PET imaging changes in terms of the whole heart were studied in NSCLC patients, with increasing SUVmean cardiac values significantly predictive of an overall trend of improved overall survival.[100] However, the study lacked suppression of healthy myocyte glucose uptake. Hence, it is

possible that the increased ^{18}FDG/PET in the myocardium was due to the increased glucose metabolism of healthy myocytes.

Furthermore, the use of ^{18}FDG/PET was reported for enhanced detection of cardiac sarcoidosis[101], granulomatous disease, and equipped with a sensitivity and specificity of 89% and 78% in detection.[102] Other PET cardiac imaging approaches include the use of ^{18}F-NaF, which can detect coronary calcifications and microcalcifications. ^{68}Ga-pentixafor (68 minutes half-life) is another tracer for detection of arterial wall inflammation in comparison to ^{18}FDG and the uptake was correlated to the degree of calcification in the corresponding lesions.[103]

1.11.3.1 Glucose Suppression in ^{18}FDG PET imaging

Fasting for 12-hours before ^{18}FDG/PET imaging and a special diet preparation including high fat, low carbohydrate, and low protein is required to suppress normal myocytes glucose. Under fasting and aerobic conditions, long-chain fatty acids are the main energy supplier in the heart (65 -70%) and the rest (15 - 20%) of the energy supply comes from glucose.[104] Cardiac myocytes utilize glucose as an energy source via GLUT4,[105] while macrophages undergo glycolysis mainly via GLUT1 and GLUT3,[106] and are not insulin-dependent. As a result, ^{18}FDG uptake in cardiac inflammatory lesions is not expected to be reduced with the diet protocol.

The administration of heparin prior to ^{18}FDG injection aims at increasing blood-free fatty acid. Such an approach will further induce fat-dominated metabolism, which decreases ^{18}FDG accumulation in the myocardium. However, 5% of the time the suppression of uptake in normal myocytes failed even under the best diet and fasting protocols.[107]

1.11.4 PET imaging $^{13}NH_3$

$^{13}NH_3$/PET is capable of performing myocardial perfusion imaging with a flow-dependence property with a 10-minute half-life. $^{13}NH_3$ extraction by the myocardial tissue is metabolically trapped by the glutamine synthetase reaction as ^{13}N-labeled glutamine.[108] One-tissue compartmental tracer kinetic model can be utilized for $^{13}NH_3$/PET perfusion analysis (equation 2). Semi-automated analysis programs, such as

FlowQuant© (University of Ottawa Heart Institute) had the tracer kinetic model implemented.[109]

$$[2] C_t(t) = K_1 e^{-k_2 t} * C_{LV}(t)$$

in which K_1 [ml/min/g] and k_2 [min^{-1}], are regional uptake and clearance parameters; whereas $C_t(t)$ and $C_{LV}(t)$ are the concentration of $^{13}NH_3$ in the myocardial tissue and in the LV blood respectively. K_1 is related to myocardial blood flow (MBF) according to the Renkin-Crone function (equation 3):

$$[3] K_1 = \left(1 - \mathrm{a} \times \mathrm{e}^{-\frac{\mathrm{b}}{\mathrm{MBF}}}\right) \times \mathrm{MBF}$$

For $^{13}NH_3$ the K_1 quantity is approximated $\left(1 - \mathrm{a} \times \mathrm{e}^{-\frac{\mathrm{b}}{\mathrm{MBF}}}\right) \approx 1$ for MBF less than 6 ml/min/g, with a and b parameters estimated with a weighted least-squares algorithm.[98] Rasmussen et al.[110] presented no differences in MBF between irradiated and non-irradiated myocardium from breast cancer patients post-irradiation using $^{13}NH_3$/PET at an average of 7 years. Up to this point, no serial longitudinal MBF assessment using $^{13}NH_3$/PET has been performed and reported on breast cancer patients.

1.11.5 Hybrid PET/MR

Clinical hybrid PET/MRI was introduced in 2011 with the capability tof imaging with two modalities simultaneously. The equipment challenges of integrating a PET ring into the MRI bore include (a) optimization of the RF/MRI receive coils to minimize the attenuation of the PET signal while maintaining agreeable performance to the dedicated MRI only coils and (b) MR-based PET attenuation correction (MRAC) that is comparable to CT-based PET attenuation correction. Currently, manufacturer-provided software cardiac-MRAC has been reported with an excellent correlation with CT correction.[111]

1.11.6 MR imaging

Cardiovascular magnetic resonance is a non-invasive, ionizing radiation-free approach to cardiac diagnosis. A significant limitation of MR imaging of the heart is that patients often have pacemakers or defibrillators in their cardiac care management and were therefore excluded.

The capability of MRI to acquire cine images of wall motion throughout the cardiac cycle is considered the gold standard for the quantification of ejection fraction (LVEF), end-diastolic volumes (LVEDV), and end-systolic volumes (LVESV), but requires short breath holds of about 15 seconds. Cine imaging can identify cardiac function that is progressing towards heart failure.[112] The normal range of MR cardiac functional parameters measured using steady-state free precession cine images of healthy individuals was previously established.[113] However, it is known that LVEF can remain within normal limits even in the presence of significant cardiac diastolic dysfunction and comorbidities, and is more common in elderly women diagnosed with heart failure with preserved LVEF (HFpEF),[114] which is considered a multifactorial etiology. Hence, additional imaging or biomarkers are often required to further confirm the decline of cardiac function in these patients.

T1 mapping can be used to quantify the extent of diffuse fibrosis with the increased extracellular space (due to leakiness of the membrane) in a quantifiable fashion. (See extracellular volume matrix section). Moreover, the T2 relaxation rate increases in tissue containing an increase in extracellular water, i.e., edema resulting in a hyperintense signal in T2-weighted MRI.

1.11.6.1 Extracellular volume matrix (ECV)

The combination of pre-and post-contrast T1 maps can give a direct measure of the extracellular volume (ECV), a volume fraction (see equation 4), where the expansion relates to myocardial fibrosis and correlates to more likelihood of cardiac events.[115] The quantification of ECV can only be performed with MR imaging using contrast agents of gadolinium chelate that accumulate in the extracellular space.

$$[4] ECV = (1 - hematocrit\ ratio)\left(\frac{\frac{1}{Post\ contrast\ T1\ myocardium} - \frac{1}{native\ T1\ myocardium}}{\frac{1}{Post\ contrast\ T1\ LV\ blood\ pool} - \frac{1}{native\ T1\ LVblood\ pool}}\right)$$

1.11.7 Late Gadolinium Enhancement Imaging (LGE)

Late gadolinium enhancement imaging (LGE) is the non-invasive standard for determining both ischemic and non-ischemic focal fibrosis of the myocardium.[116-117] It

has been validated with excellent accuracy as a marker of irreversible damage post-MI in animals as well as biopsies.[117] LGE imaging depicts the relative difference in longitudinal recovery times (T1) between enhancing areas of fibrosis or scar and normal nulled myocardium, due to the combination differences in myocardial blood flow and volume of distributions of gadolinium contrast. However, diffuse fibrosis can go undetected on LGE imaging because of the absence of normal reference myocardium and the limited spatial resolution for identification of microscopic interstitial fibrosis, hence showing a poor correlation with collagen volume calculated from endomyocardial biopsies.[118]

1.11.8 MR perfusion

Using dynamic contrast-enhanced MRI (DCE-MRI), MBF (expressed in mL/min/g) can be estimated using three different common quantitative methods: Fermi function modelling, the Tofts model (equation 5), and the gamma function model. The three modeling methods were previously compared and agreed with each other from human subjects under rest and cold pressor test stress conditions[119] using a series of T1 weighted images acquired while a bolus of gadolinium is circulating through the LV cavity and myocardial wall. Evaluation of myocardial perfusion assessed by stress DCE-MRI has shown promise to predict the risk for major adverse cardiovascular events (MACE) in large systemic meta-analysis studies.[120]

$$[5] C_t(t - t_0) = K^{trans} \int_0^t C_p(\tau) e^{-k_{ep}(t-t_0-\tau)}\, d\tau = K^{trans} e^{-k_{ep}(t-t_0)} \int_0^t C_p\,(\tau) e^{k_{ep}\tau} d\tau$$

where k_{ep} is the flux rate constant, C_t is the contrast concentration in the myocardial tissue and C_p is the blood plasma concentration derived from the AIF corrected by an assumed blood hematocrit value. The relationship between K^{trans} and MBF is represented in equation 6:

$$[6] K^{trans} = E * MBF$$

where E is the extraction fraction, represents a measure of the permeability surface area product and the rate of perfusion in the myocardium.[121] Note Tong et al. recorded an absolute measurement of extraction fraction of 0.5 at rest for normal canine myocardium with Gd-DTPA.[122]

1.11.8.1 Assignment of Coronary Territories

Frequently, the myocardial segments are sorted according to their supplying coronary arteries during data analysis, based on the American Heart Association 17 segment model for the short-axis tomographic plane.[123] The segment at the apex (17th segment) in all patients is usually excluded for analysis because of significant movement.

1.11.9 CT imaging

Coronary computed tomography angiography (CTA) provides an opportunity to evaluate the extent and severity of anatomical stenosis but are poor predictors of hemodynamically significant stenosis. On the other hand, dynamic CT perfusion imaging (CTP) provide good correlation with the current standard catheter-based fractional flow reserve (FFR) technique in identifying hemodynamically significant stenosis lesions,[124] and can be used for the differentiation between hemodynamically significant and non-significant coronary artery lesions. However, depending on the software and algorithm used for perfusion calculation, various papers published with different thresholds have been reported. Bamberg et al. reported the cutoff of MBF was 75 ml/min/100g under adenosine-induced stress conditions using a model-based parametric deconvolution method, related to hemodynamically significant coronary artery stenosis measured by FFR of 0.75 or less.[124] In addition, So et al. validated the effectiveness of a whole-heart coverage CT system to minimize the image noise and artifacts for CT myocardial perfusion detection.[125]

Myocardial perfusion reserve (MPR), also known as coronary flow reserve, is the ratio between stress and rest blood flow measurements. MPR is the theoretical gold standard alternative to FFR for assessing myocardial ischemia in CAD with a powerful prognostic[126] and diagnostic factor (AUC 0.916).[127] However, pharmacological stress is necessary for the measurement of MPR calculation. The MPR value in the ischemic segments (1.56 ± 0.41) was significantly lower than that in the non-ischemic segments (2.53 ± 0.7) in symptomatic patients with suspected or known CAD.[127]

1.11.9.1 Pharmacologic vasodilator stress protocols and tracers

Currently, available vasodilator agents include dipyridamole, adenosine, and regadenoson are commonly used during CT myocardial perfusion assessment. Adenosine induces direct coronary arteriolar vasodilation through the specific activation of the A_{2A} receptor, which accelerates the myocardial perfusion by 3.5 to 4-fold.[128] Meanwhile, the mechanism of dipyridamole is based on blockage of adenosine reabsorption and dobutamine is based on inotropic property. The protocol and guideline for performing cardiac stress test recommended that adenosine be given as a continuous infusion at a rate of 140 mcg/kg/min over a 4–6-minute for CAD detection.[128] Since the myocardial regions supplied by stenotic coronary arteries have an attenuated hyperemic response, depending upon the severity of the stenosis and coronary flow reserve limitation, a relative flow heterogeneity is induced for assessment.

1.12 Biomarkers

Biomarkers in cardio-oncology (a field of cardiology that focuses cardiovascular disease as side effect of oncology treatment) serve 3 main purposes: (1) enhance pre-therapy cardiac risk stratification, (2) distinguish subclinical evidence of cardiotoxicity during therapy, and (3) guide the long-term cardiovascular monitoring/management of cancer survivors.[129]

1.12.1 Troponin

Troponin is a protein complex that modulates the contraction and relaxation of striated muscle (skeletal and cardiac but not in smooth muscles). It is composed of three subunits: troponin I, T, and C (TnI, TnT andex TnC).[130] Cardiac-Specific troponins are useful to convey prognostic information and guide therapeutic decisions regarding patients with acute coronary syndromes.[131]

According to the American College of Cardiology (ACC) and the European Society of Cardiology (ESC), acute myocardial infarction (MI) should be diagnosed if cTnI or cTnT levels are higher than the 99th percentile using high-sensitivity cardiac troponin assay (hs-cTNT level 14ng/L), detected within 24-hour after the index clinical event, which had a

sensitivity and specificity of 95% and 80%.[132] Values in the intermediate zone suggest minor myocardial damage.[133-134]

It has been reported that the mean cTnI levels for left-breast-affected patients were significantly higher after RT compared with baseline, whereas cTnI levels of the right-sided patients remained unaffected.[135] Skyttä et al. reported the increase in hs-cTnT level during adjuvant 3D-CRT was positively associated with the cardiac radiation doses for the whole heart and LV, but the difference in hs-cTnT level and LVEF before and 3 weeks after RT was not significant.[136]

A 3 years follow-up of breast cancer patients, echocardiography assessing LV function was compared with baseline, after completion of RT and 3 years after RT, along with hs-cTnT and N-terminal pro-brain natriuretic peptide (proBNP) measurements; with results demonstrating that LVEF and SV had significantly declined at 3 years compared to baseline.[137]

1.12.2 Interleukin-6 (IL-6)- cytokine

Interleukin-6 is a protein produced by various cells and cytokines. Cytokines have multiple roles to play within the body, particularly within the immune system to help regulate the body's immune response. IL-6 test is useful in the evaluation of diabetes, stroke, or cardiovascular disease.[138]

1.12.3 C-reactive protein (CRP)

IL-6 levels are often found to be elevated in the bloodstream during inflammation, followed by the liver with the production of CRP reactants. CRP involves attaching microorganisms and ruptured cellular components via phosphocholine, a precipitating factor to selective activation of phagocytosis.[139] High-sensitivity C-reactive protein (hs-CRP) is an inflammation marker that predicts incident MI, stroke, peripheral arterial disease, and sudden cardiac death among healthy individuals without a history of cardiovascular disease.[140] Hs-CRP levels of less than 1, 1 to 3, and greater than 3 mg/L are associated with lower, moderate, and higher cardiovascular risks respectively.[140]

1.12.4 Erythrocyte Sedimentation Rate (ESR)

The erythrocyte sedimentation rate is a surrogate marker of acute inflammation, associating with the elevation of fibrinogen concentrations, the main clotting protein, and alpha globulins. The plasma viscosity was measured by assessing the tendency for the red blood cells to aggregate and 'fall' through the non-uniformly viscous plasma.[139] It is depicted that CRP is a better indicator of inflammation than the erythrocyte sedimentation rate, with higher sensitivity and responsive efficiency.[139]

1.13 Anti-inflammation and Cardioprotective medication

It is known that if inflammation occurs early, preceding but predictive of subsequent functional changes, then there may be a role for early treatment with anti-inflammatory and/or cardioprotective medication.

The Canakinumab Anti-inflammatory Thrombosis Outcome Study (CANTOS) is a randomized trial investigating canakinumab, a therapeutic monoclonal antibody targeting IL-1β, a cytokine that is central to the inflammatory response and that drives the IL-6 signaling pathway.[141] The trial involved patients with previous MI and hs-CRP of 2mg or more per liter.[141] And compared three doses of canakinumab with placebo (administered subcutaneously every 3 months).[141] The primary efficacy endpoint was nonfatal MI, stroke or cardiovascular death. At 4 years, the median reduction from baseline in the hs-CRP was 41% greater in the group that received canakinumab than the placebo group; with 3.90 cardiac events per 100 person-years in the 300 canakinumab.[141]

Additionally, angiotensin receptor blockers, beta-blockers and ACE-inhibitors are cardioprotective medications that can prevent the deterioration of the heart evolving to heart failure. Efficacy of these cardioprotective medications were evaluated with promising cardiac toxicity reduction results in large trials involving patients receiving trastuzumab chemotherapy.[142-144]

1.14 Selected up to date literature - Breast RT with cardiac imaging

1.14.1 ^{18}FDG/PET imaging

Jo et al.[145] conducted a retrospective study evaluating the irradiated myocardium in both the staging and post-RT PET/CT images of breast cancer patients who underwent 3D-CRT. The whole myocardium was segmented into three sections based on the dose threshold. The ^{18}FDG/PET uptake of the myocardium irradiated with more than 30 Gy significantly increased after RT even at the one-year follow-up.[145] And the degree of ^{18}FDG/PET uptake increase significantly correlated with the radiation dose to the myocardium.[143] However, glucose suppression was not performed in the PET imaging. In our study, glucose suppression was performed, and the myocardium was segmented according to the AHA heart model for better location of radiosensitive substructure of the heart.

1.14.2 MR imaging

Bergom et al.[144] evaluated anthracycline-based chemotherapy and 3D-CRT node-positive breast cancer patients using cardiac MRI (cine and LGE). No abnormal clinical findings were identified among LVEF, LVEDV and LVESV and LGE in N=15 left-sided and N=5 right-sided patients at a median 8.3 years post RT.[146] However, correlations between ventricular mean dose, V10 and V25 and LV mass were seen with left ventricular mass index.[146]

1.14.3 Echocardiographic imaging

Clasen et al.[147] conducted a prospective longitudinal cohort study of patients treated with photon or proton thoracic RT, with echocardiographic data at 3 time points: before RT initiation (T0), within 3 days before 6 weeks after the end of RT (T1) and 5 to 9 months after RT completion (T2). At the T1 timepoint, there was a modest decrease in LVEF of borderline significance.[145] And the associations between MHD and LVEF were modest, demonstrating only a slight decrease in cardiac function per 100 cGy increase in MHD.[147]

1.14.4 CT imaging

Coronary artery calcium has been shown to be associated with traditional CAD risk factors rather than cardiac dosimetry.[148] A study which compared 15915 breast cancer patients receiving RT (2005-2016) with coronary artery calcium (CAC) scores extracted from non-contrast planning CT scans (of all stages) using deep-learning algorithm, presented with a strong association with CVD risk (median following time of 51.2 months).[148] CAC scoring is demonstrated as a fast and low-cost tool to identify patients at increased risk of CVD.

Gaasch et al.[149] conducted a prospective Save-Heart trial with left-sided breast cancer patients who received DIBH RT with analysis of individual baseline risk factors for CVD and evaluated individual CVD risk profiles using three frequently used prediction tools (Procam, Framingham and Reynolds score).[150] The 10-year CVD excess absolute risk (EAR) was further estimated using individual mean heart dose of RT plans in free-breathing and DIBH. The study demonstrated that all CVD prediction tools were comparable and could easily be integrated into daily clinical practice, which can help identifying high-risk patients who may benefit from primary prevention.[150]

1.15 Thesis outline

In this thesis, changes of FDG PET/MR resting myocardial perfusion post irradiation in a canine model representing a standard left-sided breast cancer patient RT will first be presented, subsequent with a dosimetric comparison of a variety of cardiac sparing techniques in left-sided breast RT, followed by an early (at 1-month post RT) cardiac functional response presentation of a hybrid PET/MRI pilot study on left-sided breast cancer patients treated with RT. And lastly, a feasibility study of comprehensive functional multi-modality imaging assessment of the heart 6-weeks after NSCLC RT in two patients is presented.

There were several research objectives:

(1) Through the measurement of myocardial blood flow, the first goal in this thesis was to assess the effect of radiation on perfusion from 1-week to 1-year in a clinically relevant

model similar to patients exposed to left-sided breast cancer RT. We will then correlate any changes in perfusion with our previously reported changes in ^{18}FDG uptake reflective of inflammation.

(2) Second goal was through extensive dosimetric comparison among various treatment planning techniques in combination with IMRT and VMAT, including 4D Robust optimization, DIBH and standard 4D Untag Average, it is aimed to (a) identify the clinical feasibility of aforementioned techniques in sparing of the heart and its substructure; (b) address whether 4D Robust optimization can outperform DIBH and conventional 4D-CT techniques; and (c) determine the clinical feasibility of IMRT versus VMAT.

(3) Third goal was to investigate the utility of hybrid PET/MRI and serial blood work to detect early inflammatory response and cardiac functionality changes after left-sided breast cancer radiation therapy at 1-month follow-up.

(4) Fourth goal was, through collection of comprehensive functional imaging data with imaging sessions before and 6-weeks after NSCLC RT, to demonstrate the feasibility and sensitivity of these methods to assess early functional response (at 6-weeks follow-up) in the heart after RT.

Overall, this thesis will demonstrate the feasibility of non-invasive multi-modality imaging assessment of early cardiac functional response after breast and NSCLC RT from animal model to pilot studies of cancer patients. Imaging microvascular inflammation in RICD will allow us to consider new techniques to enhance pre-cardiac risk stratification, minimize or eliminate heart complications in future cancer patients and guide long-term cardiovascular monitoring/management of cancer survivors. And the extensive comparison of cardiac dose mitigation techniques can minimize cardiac exposure in future left-sided breast cancer patients without compromising target coverage. Regarding left-sided breast cancer patients who are not compliant with breath-hold RT techniques, in this thesis we demonstrated that conventional 4D-CT based free-

breathing RT approaches are also clinically feasible, and beneficial to the dose sparing of the LAD under current standard guidelines.

1.16 References

[1] Sung H, Ferlay J, Siegel R, Laversanne M, Soerjomataram I, et al. Global Cancer Statistics 2020: GLOBOCAN Estimates of Incidence and Mortality Worldwide for 36 Cancers in 185 Countries. CA Cancer J Clin. 2021;71(3):209-249

[2]Brenner D, Weir H, Demers A, Ellison L, Louzado C, et al. Projected Estimates of Cancer in Canda in 2020. CMAJ. 2020;192(9):E199-205

[3]Canadian Cancer Statistics Advisory Committee in collaboration with the Canadian Cancer Society. Canadian Cancer Statistics 2021. Toronto: Canadian Cancer Society. Retrieved from cancer.ca/Canadian-Cancer-Statistics-2021-EN

[4]Clarke M, Collins R, Darby S, Davies C, Elphinstone P, et al. and Early Breast Cancer Trialists' Collaborative Group, Effects of radiotherapy and of differences in the extent of surgery for early breast cancer on local recurrence and 15-year survival: an overview of the randomised trials. Lancet. 2005;366(9503):2086-2016

[5]McGale P, Early Breast Cancer Trialists' Collaborative Group, Taylor C, Correa C, Cutter D, et al. Effect of radiotherapy after mastectomy and axillary surgery on 10-year recurrence and 20-year breast cancer mortality: meta-analysis of individual patient data for 8135 women in 22 randomised trials. Lancet. 2014;383(9935):2127-2135

[6]Mittmann N, Seung SJ, Liu N, Saskin R, Hoch J, et al. Population-based utilization of radiation therpay by a Canadian breast cancer cohort. Curr Oncol. 2014;21(5):e715-717

[7]Darby S, Early Breast Cancer Trialists' Collaborative Group, McGale P, Correa C, Taylor C, et al. Effect of radiotherapy after breast-conserving surgery on 10-year recurrence and 15-year breast cancer death: meta-analysis of individual patient data for 10, 801 women in 17 radomised trials. Lancet. 2011;378(9804):1707-1716

[8]Taylor C, Correa C, Duane F, Aznar M, Anderson S, et al. Estimating the Risks of Breast Cancer Radiotherapy: Evidence From Modern Radiation Doses to the Lungs and Heart and From Previous Randomized Trials. J Clin Oncol. 2017;35(15):1641-1649

[9]Henson K, McGale P, Darby S, Parkin M, Wang Y and Taylor C. Cardiac mortality

after radiotherapy, chemotherapy and endocrine therapy for breast cancer: Cohort study of 2 million women from 57 cancer registries in 22 countries. Int J Cancer. 2020; 147(5):1437-1449

[10]McGale P, Darby S, Hall P, Adolfsson J, Bengtsson N, et al. Incidence of heart disease in 35000 women treated with radiotherapy for breast cancer in Denmark and Sweden. Radiother Oncol. 2011;100(2):167-175

[11] Milo M, Thorsen L, Johnsen S, Nielsen K, Valentin J, et al. Risk of coronary artery disease after adujuvant radiotherapy in 29662 early breast cancer patients: A population-based Danish Breast Cancer Group study. Radiother Oncol. 2021;157(1):106-113

[12] Boero I, Paravati A, Triplett D, Hwang L, Matsuno R, et al. Modern Radiation Therpay and Cardiac Outcomes in Breast Cancer. Int J Radiat Oncol Biol Phys. 2015;94(4):700-708

[13] Boekel N, Schaapveld M, Gietema J, Russell N, Poortmans P, Theuws J, et al. Cardiovascular Disease Risk in a Large, Population-Based Cohort of Breast Cancer Survivors. Int J Radiat Oncol Bio Phys. 2015;94(5):1061-1072

[14]McGale P, Taylor C, Correa C, Cutter D, Duane F, et al. Effect of radiotherapy after mastectomy and axillary surgery on 10-year recurrence and 20-year breast cancer mortality: meta-analysis of individual patient data for 8135 women in 22 randomised trials. Lancet. 2014;383(9935):2127-2135

[15]Clemons M and Goss P. Estrogen and the risk of breast cancer. N Engl J Med, 2001; 344(4):276-285

[16]Early Breast Cancer Trialists' Collaborative Group. Tamoxifen for early breast cancer: an overview of the randomised trials. Early Breast Cancer Trialists' Collaborative Group. Lancet. 1998;351(9114):1451-1467

[17]Mehta L, Watson K, Barac A, Beckie TH, Bittner V, et al. Cardiovascular disease and breast cancer: where these entities intersect: A scientific statement from the American Heart Association. 2018;137(8):e30-66

[18]Armenian S, Lacchetti C, Barac A, Carver J, Constine L, et al. Prevention and monitoring of cardiac dysfunction in survivors of adult cancers: American Society of Clinical Oncology Clinical Practice Guideline. J Clin Oncol. 2017;35(1):893-911

[19]Molina M, Codony-Servat J, Albanell J, Rojo F, Arribas J, et al. Trastuzumab (Herceptin), a Humanized Anti-HER2 Receptor Monoclonal Antibody, Inhibits Basal and Activated HER2 Ectodomain Clevage in Breast Cancer Cells. Cancer Res. 2001;61(12):4744-4749

[20]Thavendiranathan P, Abdel-Qadir H, FIscher H, Camacho X, Amir E, et al. Breast Cancer Therapy-Related Cardiac Dysfunction in Adult Women Treated in Routine Clinical Practice: A Population-Based Cohort Study. J Clin Oncol. 2016;34(19):2239-2246

[21]Shimizu Y, Kodama K, Nishi N, Kasagi F, Suyama A, et al. Radiation exposure and ciculatory disease risk: Hiroshima and Nagasaki atomic bomb survivor data, 1950-2003. BMJ. 2010;340:b5349

[22]Chang H-M, Okwuosa T, Scarabelli T, Moudgil R and Yeh E. Cardiovascular Complications of Cancer Therapy: Best Practices in Diagnosis, Prevention, and Management - Part 2. J Am Coll Cardiol. 2017;70(20):2552-2565

[23]Belzile-Dugas E and Eisenberg M, Radiation-Induced Cardiovascular Disease: Review of an Underrecognized Pathology. J Am Heart Assoc. 2021;10(18):e021686

[24]Veinot J. and Edwards W. Pathology of Radiation-Induced Heart Disease: A Surgical and Autopsy Study of 27 cases. Hum Pathol. 1996;27(8):766-773

[25]Cutter D, Schaapveld M, Darby S, Hauptmann M, van Nimwegen F, et al. Risk for Valvular Heart Disease After Treatment for Hodgkin Lymphoma. J Natl Cancer Inst. 2015;107(4):djv008

[26]Galper S, Yu J, Mauch P, Strasser J, Silver B, et al. Clinically signficant cardiac disease in patients with Hodgkin lymphoma treated with mediastinal irradiation. Blood. 2011;117(2):412-418

[27]Bijl J, Roos M, Leeuwen-Segarceanu E, Vos J, Bros W-J, et al. Assessment of Valvular Disaorders in Survivors of Hodgkin's Lymphoma Treated by Mediastinal Radiotherapy ± Chemotherapy. Am J Cardiol. 2016;117(4):691-696

[28]van Rijswijk J, Farag E, Bouten C, de Boer O, van der Wal A, et al. Fibrotic aortic valve disease after radiotherapy: an immunohistochemical study in breast cancer and

lymphoma patients. Caridovasc Pathol. 2020;45:107176

[29]Cuomo J, Sharma G, Conger P and Weintraub N. Novel concepts in radiation-induced cardiovascular disease. World J Cardiol. 2016;8(9):504-519

[30]Skali H, Schulman A and Dorbala S. 18F-FDG PET/CT for the Assessment of Myocardial Sarcoidosis. Curr Cardiol Rep. 2013;15(4):352

[31]Thygesen K, Alpert J, Jaffe A, Simoons M, Chaitman B, et al. Third Universal Definition of Myocardial Infarction. J Am Coll Cardiol. 2012;60(16):1581-1598

[32]Anderson J and Morrow D. Acute Myocardial Infarction. N Engl J Med. 2017;376: 2053-2064

[33]Boekel N, Duane F, Jacobse J, Hauptmann M, Schaapveld M, et al. Heart failure after treatment for breast cancer. Eur J Heart Fail. 2020;22(2):366-374

[34]White J, Tai A, Arthur D, Buchholz T, MacDonald S, et al. Breast Cancer Atlas for Radiation Therapy Planning: Consensus Definition. Radiation Therapy Oncology Group, 2012.

[35]Coles C, Griffin C, Kirby A, Titley J, Agrawal R, et al. Partial-breast radiotherapy after breast conservation surgery for patients with early breast cancer (UK IMPORT LOW trial): 5-year results from a multicentre, randomised, controlled, phase 3, non-inferiority trial. Lancet. 2017;390(10099):1048-1060

[36]Livi L, Meattini I, Marrazzo L, Simontacchi G, Pallotta S, et al. Accelerated partial breast irradiation using intensity-modulated radiotherapy versus whole breast irradiation: 5-year survival analysis of a phase 3 randomised controlled trial. Eur J Cancer. 2015;51(4):451-463

[37]Vaidya J, Wenz F, Bulsara M, Tobias J, Joseph D, et al. Risk-adapted targeted intraoperative radiotherapy versus whole-breast radiotherapy for breast cancer: 5-year results for local control and overall survival from the TARGIT-A randomised trial. Lancet. 2014;83(1):603-613

[38]Vicini F, Cecchini R, White J, Arthur D, Julian T, et al. Long-term primary results of accelerated partial breast irradiation after breast-conserving surgery for early-stage breast cancer: a randomised, phase 3, equivalence trial. Lancet. 2019;394(1):2155-2164

[39]Whelan T, Julian J, Berrang T, Kim D-H, Germain I, et al. External beam accelerated partial breast irradiation versus whole breast irradiation after breast conserving surgery in women with ductal carcinoma in situ and node-negative breast cancer (RAPID): a randomised controlled trial. Lancet. 2019;394(10215):2165-2172

[40]Poortmans P, Collette S, Kirkove C, Van Limbergen E, Budach V, et al. Internal Mammary and Medical Supraclavicular Irradiaiton in Breast Cancer. N Engl J Med. 2015;373(4):317-327

[41]Whelan T, Olivotto I, Parulekar W, Ackerman I, Chua B, et al. Regional Nodal Irradiation in Early-Stage Breast Cancer. N Engl J Med. 2015;373(1):307-316

[42]Bartelink H, Maingon P, Poortmans P, Weltens C, Fourquet A, et al. Whole-breast irradiation with or without a boost for patients treated with breast-conserving surgery for early breast cancer: 20-year follow-up of a randomised phase 3 trial. Lancet Oncol. 2015;16(1):47-56

[43]Taylor C, Brønnum D, Darby S, Gagliardi G, Hall P, et al. Cardiac dose estimates from Danish and Swedish breast cancer radiotherapy during 1977-2001. Radiother Oncol. 2011;100(2):176-183

[44]Taylor C, Wang Z, Macaulay E, Jagsi R, Duane F, et al. Exposure of the Heart in Breast Cancer Radiation Therapy: A Systematic Review of Heart Doses Published During 2003 to 2013. Int J Radiat Oncol Bio Phys. 2015;93(4):845-853

[45]Bucci K, Bevan A and Roach M. Advances in radiation therapy: conventional to 3D, to IMRT, to 4D, and beyond. CA Cancer J Clin. 2005;55(2):117-134

[46]Merzenich H., Bartkowiak D, Schmidberger H, Schmidt M, Schwentner L, et al. 3D conformal radiotherapy is not associated with the long-term cardiac mortaliy in breast cancer patients: a retrospective cohort study in Germany (PASSOS-Heart Study). Breast Cancer Res Treat. 2017;161(1):143-152

[47]Rabinovitch R, Moughan J, Vicini F, Pass H, Wong J, et al. Long-Term Update of NRG Oncology RTOG 0319: A Phase 1 and 2 Trial to Evaluate 3-Dimensional Conformal Radiation Therapy Confined to the Region of the Lumpectomy Cavity for Stage I and II Breast Carcinoma. Int J Radiat Oncol Biol Phys. 2016;96(5):1054-1059

[48]Mohan R, Wang X, Jackson A, Bortfeld T, Boyer A, et al. The potential and

limitations of the inverse radiotherapy technique. Radiother Oncol. 1994;32(3):232-248

[49]Sakka M, Kunzelmann L, Metzger M and Grabenbauer G. Cardiac dose-sparing effects of deep-inspiration breath-hold in left breast irradiation is IMRT more beneficial than VMAT? Strahlenther Onkol. 2017;193(10):800-811

[50]Latty D, Stuart K, Wang W and Ahern V. Review of deep inspiration breath-hold techniques for the treatment of breast cancer. J Med Radiat Sci. 2015;62(1):74-81

[51]Wong J, Sharpe M, Jaffray D, Kini V, Robertson J, et al. The use of active breathing control (ABC) to reduce margin for breathing motion. 1999;44(4):911-919

[52]Eldredge-Hindy H, Lockamy V, Crawford A, Nettleton V, Werner-Wasik M, et al. Active Breathing Coordinator reduces radiation dose to the heart and preserves local control in patients with left breast cancer: Report of a prospective trial. Pract Radiat Oncol. 2015;5(1):4-10

[53]Kubo H, Len P, Minohara S and Mostafavi H, et al. Breating-synchronized radiotherapy program at the University of California Davis Cancer Center. Med Phys. 2000; 27(2):346-353

[54]Hamming V, Visser C, Batin E, McDermott L, Busz D, et al. Evaluation of a 3D surface imaging system for deep inspiration breath-hold patient positioning and intra-fraction monitoring. Radiat Oncol. 2019;14(1):4-11

[55]Xiao A, Crosby J, Malin M, Kang H, Washinton M, et al. Single-institution report of setup margins of voluntary deep-inspiration breath-hold (DIBH) whle breast radiotherpay implemented with real-time surface imaging. J Appl Clin Med Phys. 2018;19(4):205-213

[56]Freislederer P, Kügele M, Öllers M, Swinnen A, Sauer T, et al. Recent advances in surface guided radiation therapy. Radiat Oncol. 2020;15(187):1-11

[57]Kirby A, Evans P, Donovan E, Convery H, Haviland J, et al. Prone versus supine positioning for whole and partial-breast radiotherapy: A comparison of non-target tissue dosimetry. Radiother and Oncol. 2010;96(2):178-184

[58]Gagliardi G, Constine L, Moiseenko V, Correa C, Pierce L, et al. Radiation Dose-Volume Effects in the Heart. Int J Radiat Oncol Biol Phys. 2010;76(3):S77-85

[59]Beaton L, Bergman A, Nichol A, Aparicio M, Wong G, et al. Cardiac death after breast radiotherapy and the QUANTEC cardiac guidelines. Clin Transl Radiat Oncol.

2019;19(1):39-45

[60]Darby S, Ewertz M, McGale P, Bennet A, Blom-Goldman U, et al. Risk of ischemic heart disease in women after radiotherapy for breast cancer. N Engl J Med, 2013;368(11): 987-998

[61]van den Bogaard V, Ta B, van der Schaaf A, Bouma A, Middag A, et al. Validation and Modification of a Prediction Model for Acute Cardiac Events in Patients with Breast Cancer Treated with Radiotherapy Based on Three-Dimensional Dose Distributions to Cardiac Substructures. J Clin Oncol. 2017;35(11):1171-1178

[62]Drost L, Yee C, Lam H, Zhang L, Wronski M, et al. A Systematic Review of Heart Dose in Breast Radiotherapy. Clin Breast Cancer. 2018;18(5):e819-e824

[63]Taylor C, Nisbet A, McGale P and Darby S. Cardiac Exposures in Breast Cancer Radiotherapy: 1950s-1990s. Int J Radiat Oncol Biol Phys. 2007;69(5):1484-1495

[64]Wennstig A-K, Garmo H, Isacsson U, Gagliardi G, Rintelä N, et al. The relationship between radiation doses to coronary arteries and location of coronary stenosis requiring interventation in breast cancer suriviors. Rad Oncol. 2019;14(1):40

[65]Hirshfeld J, Ferrari V, Bengel F, Bergersen L, Chambers C, et al. 2018 ACC/HRS/NASCI/SCAI/SCCT Expert Consensus Document on Optimal Use of Ionizing Radiation in Cardiovascular Imaging-Best Practices for Safety and Effectiveness. J Am Coll Cardiol. 2018;71(24):2811-2828

[66]Thackeray J and Bengel F. Molecular Imaging of Myocardial Inflammation with Positron Emission Tomography Post-Ischemia: A Determinant of Subsequent Remodelling or Recovery. JACC Cardiovasc Imaging. 2018;11(9):1340-1355

[67]Venkatesulu B, Mahadevan L, Aliru M, Yang X, Bodd M, et al. Radiation-Induced Endothelial Vascular Injury: A Review of Possible Mechanisms. JACC Basic Transl Sci. 2018;3(4):563-572

[68]Yang E, Marmagkiolis K, Balanescu D, Hakeem A, Donisan T, et al. Radiation-Induced Vascular Disease- A State-of-the-Art Review. Front Cardiovasc Med, 2021;8:652761

[69]Paris F, Kang A, Capodieci P, Juan G, Ehleiter D, et al. Endothelial apoptosis as the

primary lesion initiating intestinal radiation damage in mice. Science. 2001;293(5528):293-297

[70]Molina J, Yang P, Cassivi S, Schild S and Adjei A. Non–Small Cell Lung Cancer: Epidemiology, Risk Factors, Treatment, and Survivorship. Mayo Clin Proc. 2009;83(5)584-594

[71]Wang K, Eblan M, Deal A, Lipner M, Zagar T, et al. Cardiac toxcity after radiotherapy for stage III non-small-cell lung cancer: pooled analysis of dose-escalation trials delivering 70 to 90 Gy. J Clin Oncol. 2017;35(13):1387-1394

[72]Banfill K, Giuliani M, Aznar M, Franks K, McWilliam A, et al. Cardiac toxicity of thoracic radiotherapy existing evidence and future directions. J Thorac Oncol. 2021;16(2):216-227

[73]Kocher F, Fiegl M, Mian M, Hilb W. Cardiovascular comorbidities and events in NSCLC: often underestimated but worth considering. Clin Lung Cancer. 2015; 16(4):305-312

[74]Kravchenko J, Berry M, Arbeev K, Lyerly H, Yashin A and Akushevich I. Cardiovascular comorbidities and survival of lung cancer patients: Medicare data based analysis. Lung Cancer. 2015;88(1):85-93

[75]Atkins K, Rawal B, Chaunzwa T, Lamba N, Bitterman D, et al. Cardiac radiation dose, cardiac disease and mortality in patients with lung cancer. J Am Coll Cardiol. 2019;73(23):2976-2987

[76]Dubois C, Pappas C, Belmans A., Erven K., Adriaenssens T, et al. Clinical outcome of coronary stenting after thoracic radiotherapy: a case-control study. Heart. 2010; 96(9):678-682

[77]de Koning H, van der Aalst C, de Jong P, Scholten E, Nackaerts K, et al. Reduced lung-cancer mortality with volume CT screening in a randomized trial. N Engl J Med. 2020;382(6):503-513

[78]Crosbie P, Balata H, Evison M, Atack M, Bayliss-Brideaux V, et al. Second round results from the Manchester 'Lung Health Check' community-based targeted lung cancer screening pilot. Thorax. 2019;74(7):700-704

[79]Rodrigues G, Choy H, Bradley J, Rosenzweig K, Bogart J, et al. Definitive radiation therapy in locally advanced non-small cell lung cancer: Executive summary of an American Society for Radiation Oncology (ASTRO) evidence-based clinical practice guideline. Pract Radiat Oncol. 2015;5(3):141-148

[80]Liang J, Bi N, Wu S, Chen M, Lv C, et al. Etoposide and cisplatin versus paclitaxel and carboplatin with concurrent thoracic radiotherapy in unresectable stage III non-small cell lung cancer: a multicenter randomized phase III trial. Ann Oncol. 2017;28(4):777-783

[81]Bi N, Liu L, Liang J, Wu S, Chen M, et al. Efficacy and safety of concurrent chemoradiotherapy in ECOG 2 patients with locally advanced non-small-cell lung cancer: a subgroup analysis of a randomized phase III trial. BMC Cancer. 2020; 20(1):278

[82]Bradley J, Hu C, Komaki R., Masters G, Blumenschein G, et al. Long-Term Results of NRG Oncology RTOG 0617: Standard-Versus HIgh-Dose Chemoradiotherpay With or Without Cetuximab for Unresectable Stage III Non-Small Lung Cancer. J Clin Oncol. 2020;38(7):706-714

[83]Zhang T, Snir J, Boldt G, Rodrigues G, Louie A, et al. Is the importance of heart dose overstated in the treatment of non-small cell lung cancer? A systematic review of the literature. Int J Radiat Oncol Biol Phys. 2019;104(3):582-589

[84]Speirs C, DeWees T, Rehman S, Molotievschi A, Velez M, et al. Heart dose is an independent dosimetric predictor of overall survival in locally advanced non-smell lung cancer. J Thorac Oncol. 2017;17(2) :293-301

[85]Bradley J, Paulus R, Komaaki R, Masters G, Blumenschein G, et al. Standard-dose versus high-dose conformal radiotherapy with concurrent and consolidation carboplatin plus paclitaxel with or without cetuximab for patients with stage IIIA or IIIB non-small-cell lung cancer (RTOG 0617): a randomised, two-by-two factorial phase 3 study. Lancet Oncol. 2015;16(2):187-199

[86]Stam B, Peulen H, Guckenberger M, Mantel F, Hope A, et al. Dose to heart substrucutres is associated with non-cancer death after SBRT in stage I-II NSCLC patients. Radiother Oncol. 2017;123(3):370-375

[87]McWilliam A, Kennedy J, Hodgson C, Osorio E, Faivre-Finn C, et al. Radiation dose to heart base linked with poorer survival in lung cancer patients. Eur J Cancer. 2017;85:106-113

[88]Schytte T, Hansen O, Stolberg-Rohr T and Brink C. Cardiac toxicity and radiation dose to the heart in definitive treated non-small cell lung cancer. Acta Oncol. 2010;49(7):1058-1060

[89]El-Sherif O, Xhaferllari I, Butler J, deKemp R, Renaud J, et al. [18F]FDG cardiac PET imaging in a canine model of radiation-induced cardiovascular disease associated with breast cancer radiotherapy. Am J Physiol Heart Circ Physiol. 2019;316(3):H586-H595

[90]Zamorano J, Lancellotti P, Munoz D, Aboyans V, Asteggiano R, et al. 2016 ESC Position Paper on cancer treatments and cardiovascular toxicity developed under auspices of the ESC Committee for Practice Guidelines. Eur Heart J. 2016;37(36):2768-2801

[91]Bozkurt B, Coats A, Tsutsui H, Abdelhamid M, Adamopoulos S, et al. Universal Definition and Classification of Heart Failure: A Report of the Heart Failure Society of America, Heart Failure Association of the European Society of Cardiology, Japanese Heart Failure Society and Writing Committee of the Universal Definition of Heart Failure. J Card Fail. 2021;23(3):352-380

[92]Plana J, Galderisi M, Barac A, Ewer M, Ky B, et al. Expert consensus for multimodality imaging evaluation of adult patients during and after cancer therapy: A report from the American Society of Echocardiography and the European Association of Cardiovascular Imaging. Eur Heart J Cardiovas Imaging. 2014;15(10):1063-1093

[93]Lind P, Pagnanelli R, Marks L, Borges-Neto S, Hu C, et al. Myocardial perfusion changes in patients irradiated for left-sided breast cancer and correlation with coronary artery distribution. Int J Radiat Oncol Bio Phys. 2003;55(4):914-920

[94]Hardenbergh P, Munley M, Bentel G, Kedem R, Borges-Neto S, et al. Cardiac perfsuion changes in patients treated for breast cancer with radiation therapy and doxorubicin: perlimanary results. Int J Radiat Oncol Bio Phys, 2001;49(4):1023-1028

[95]Sioka C, Exarchopoulos T, Tasiou I, Tzima E, Fotou N, et al. Myocardial perfusion imaging with 99mTc-tetrofosmin SPECT in breast cancer patients that received

postoperative radiotherapy: a case-control study. Radiat Oncol. 2011;6:151

[96]Kaidar-Person O, Zagar T, Oldan J, Matney J, Jones E, et al. Early cardiac perfusion defects after left-sided radiation therapy for breast cancer: is there a volume repsonse? Breast Cancer Res Treat. 2017;164(2):253-262

[97]Correa C, Litt H, Hwang W-T, Ferrari V, Solin L, et al. Coronary artery findings after left-sided compared with right-sided radiation treatment for early-stage breast cancer. J Clin Oncol. 2007;25(21):3031-3037

[98]deKemp R, Yoshinaga K and R. Beanlands. Will 3-dimensional PET-CT enable the routine quantification of myocardial blood flow? J Nucl Cardiol. 2007;14(3):380-397

[99]Moghbel M, Al-Zaghal A, Werner T, Constantinescu C, Høilund-Carlsen P, et al. The role of PET inevaluating atherosclerosis: a critical review. Semin Nucl Med. 2018;48(6):488-497

[100]Vinogradskiy Y, Diot Q, Jones B, Castillo R, Castillo E, et al. Evaluating Positron Emission Tomography-Based Functional Imaging Changes in the Heart After Chemo-Radiation for Patients With Lung Cancer. Int J Radiat Oncol Biol Phys. 2020;106(5):1063-1070

[101]Wisenberg G, Thiessen J, Pavlosky W, Butler J, Wilk B, et al. Same day comparison of PET/CT and PET/MR in patients with cardiac sarcoidosis. J Nucl Cardiol. 2020; 27(6):2118-2129

[102]Youssef G, Leung E, Mylonas L, Nery P, Williams K, et al. The Use of 18F-FDG PET in the Diagnosis of Cardiac Sarcodosis: A Systematic Review and Metaanlaysis Including the Ontario Experience. J Nucl Med. 2012;53(2):241-248

[103]Kircher M, Tran-Gia J, Kemmer L, Zhang X, Schirbel A, et al. Imaging Inflammation in Atherosclerosis with CXCR4-Directed 68Ga-Pentixafor PET/CT: Correlation with 18F-FDG PET/CT. J Nucl Med. 2020;61(5):751-756

[104]Neely J, Rovetto M and Oram J. Myocardial utilization of carbohydrate and lipids. Prog Cardiovasc Dis. 1972;15(3)289-329

[105]Armoni M, Harel C, Bar-Yoseph F, Milo S and Karnieli E. Free fatty acids repress the GLUT4 gene expression in cardiac muscle via novel response elements. J Biol Chem.

2005;280(1);34786-34795

[106]Fu Y, Maianu L, Melbert B and Garvey W. Facilitative glucose transporter gene expression in human lymphocytes, monocytes, and macrophages: a role for GLUT isoforms 1,3, and 5 in the immune response and foam cell formation. Blood Cells Mol Dis. 2004;32(1):182-190

[107]Larson S, Pieper J, Hulten E, Ficaro E, Corbett J, et al. Characterization of a highly effective preparation for suppression of myocardial glucose utilization. J Nucl Cardio. 2020;27(3):1-21

[108]Bergman S, Hack S, Tewson T, Welch M and Sobel B. The Dependence of Accumulation of 13NH3 by Myocardium on Metabolic Factors and its Implications for Quantitative Assessment of Perfusion. Circulation. 1980;61(1):34-43

[109]Lortie M, Beanlands R, Yoshinaga K, Klein R, DaSilva J, et al. Quantification of myocardial blood flow with 82Rb dynamic PET imaging. Eur J Nucl Med Mol Imaging. 2007;34(11):1765-1774

[110]Rasmussen T, Kjær A, Lassen M, Pedersen A, Specht L, et al. No changes in myocardial perfusion following radiation therapy of left-sided breast cancer: A positron emission tomography study. J Nucl Cardiol. 2021;28(5):1923-1932

[111]Vontobel J, Liga R, Possner M, Clerc O, Mikulicic F, et al. MR-based attenuation correction for cardiac FDG PET on a hybrid PET/MRI scanner: comparison with standard CT attenuation correction. Eur J Nucl Med Mol Imaging. 2015;42(10):1574-1580

[112]Bellenger N, Davies L, Francis J, Coats A and Pennell D. Reduction in Sample Size for Studies of Remodeling in Heart Failure by the Use of Cardiovascular Magnetic Resonance. J Cardiovasc Magn Reson. 2000;2(4):271-278

[113]Maceira A, Prasad S, Khan M and Pennell D. Normalized Left Ventricular Systolic and Diastolic Function by Steady State Free Precession Cardiovascular Magnetic Resonance. J Cardiovasc Magn Reson. 2009;8(3):417-426

[114]Upadhya B, Taffet G, Cheng C-P and Kitzman D. Heart failure with preserved ejection fraction in the elderly: scope of the problem. J Mol Cell Cardiol. 2015;83(1):73-87

[115]Sado D, Flett A, Banypersad S, White S, Maestrini V, et al. Cardiovascular magnetic resonance measurement of myocardial extracellular volume in health and disease. Heart. 2012;98(19):1436-1441

[116]Gulati A, Jabbour A, Ismail T, Guha K, Khwaja J, et al. Association of fibrosis with mortality and sudden cardiac death in patients with nonischemic dilated cardiomyopathy. JAMA. 2013;309(9):896-908,

[117]Kim R, Wu E, Rafael A, Enn-Ling C, Parker M, et al. The use of contrast-enhancement magnetic resonance imaging to identify reveresible myocardial dysfunction. N Engl J Med. 2000;343(20):1445-53

[118]Parsai C, O'Hanlon R, Prasad S and Mohiaddin R. Diagnostic and prognostic value of cardiovascular magnetic resonance in non-ischaemic cardiomyopathies. J Cardiovasc Magn Reson. 2012;14(1):54

[119]Borrazzo C, Galea N, Pacilio M, Luisa A and Preziosi E. Myocardial blood flow estimates from dynamic contrast-enhanced magnetic resonance imaging: three quantitative methods. Phys Med Biol. 2018;63(1):1-12

[120]Lipinski M, McVey C, Berger J, Kramer C and Salerno M. Prognostic Value of Stress Cardiac Magnetic Resonance Imaging in Patients With Known or Suspected Coronary Artery Disease: A Systematic Review and Meta-Analysis. J Am Coll Cardiol. 2013;62(9):826-838

[121]Soubron S and Buckley D. Tracer kinetic modelling in MRI: estimating perfusion and capillary permeability. Phys Med Biol. 2011;57(2):R1-33

[122]Tong C, Prato F, Wisenberg G, Lee TY, Carroll E and Sandler D. Measurement of the extraction efficiency and distribution volume for Gd-DTPA in normal and diseased canine myocardium. Magn Reson Med. 1993;30:337-346

[123]Cerqueira M, Weissman N, Dilsizian V, Jacobs A, Kaul S, et al. Standardized Myocardial Segmentation and Nomenclature for Tomographic Imaging of the Heart. Circulation. 2002;105(4):539-542

[124]Bamberg F, Becker A, Schwarz F, R. Marcus, Greif M., von Ziegler F, et al. Detection of Hemodynamically Signifcant Coronary Artery Stenosis: Incremental

Diagnostic Value of Dynamic CT-based Myocardial Pefusion Imgaing. Radiology. 2011; 260(3):689-698

[125]So A, Imai Y, Nett B, Jackson J, Nett L, et al. Technical Note: Evaluation of a 160mm/256-row CT scanner for whole-heart quantitative myocardial perfusion imaging. Med Phys. 2016;43(8):4821-4832

[126]Gould K, Johnson N, Baterman T, Beanlands R, Bengel F, et al. Anatomic versus physiologic assessment of coronary artery disease. Role of coronary flow reserve, fractional flow reserve and positron emission tomogrpahy imaging in revascularization decision making. J Am Coll Cardio. 2013;62(18):163901653

[127]Huang I-L, Wu M-T, Hu C, Mar G-Y, Lee T-Y, et al. Quantitative low-dose rest and stress CT mycardial perfusion imaging with a whole-heart coverage scanner improves functional assessment of coronary artery disease. Int J Cardiol Heart Vasc. 2019;24:100381

[128]Henzlova M, Duvall L, Einstein A, Travin M and Verberne H. ASNC imaging guidelines for SPECT nuclear cardiology procedures: Stress, protcols, and tracers. J Nucl Cardiol. 2016;23(3):606-639

[129]Zaha V, Hayek S, Alexander K, Beckie T, Hundley G, et al. Future Perspectives of Cardiovascular Biomarker Utilization in Cancer Survivors: A Scientific Statement From the American Heart Association. Circulation. 2021:144(25):e551-e553

[130]Skeik N and Patel D. A review of troponins in ischemica heart disease and other conditions. Int J Angiol. 2007;16(2):53-58

[131]Braunwald E, Antman E, Beasley J, Califf R, Cheitlin M, et al. ACC/AHA 2002 guideline update for the management of patients with unstable angina and non-ST-segment elevation myocardial infarction-summary article: A report of the American College of Cardiology/American Heart Association task force on practice guidelin. J Am Coll Cardiol. 2002;40(7):1366-1374

[132]Reichlin T., Hochholzer W, Bassett S, Steuer S, Stelzig C, et al. Early diagnosis of myocardial infarction with sensitive cardiac troponin assays. N Engl J Med. 2009;361(9):858-867

[133]Antman E. Decision making with cardiac troponin tests. N Engl J Med. 2002; 346(26):2079-2082

[134]Panteghini M, Pagani F, K-T Yeo, Apple F, Christenson R and Dati F. Evaluation of Imprecision for Cardiac Troponin Assays at Low-Range Concentration. Clin Chem. 2004;50(2):327-332

[135]Erven K, Florian A, Slagmolen P, Sweldens C, Jurcut R, et al. Subclinical Cardiotoxicity Detected by Strain Rate Imaginag up to 14 months After Breast Radiation Therapy. Int J Radiat Oncol Biol Phys. 2013;85(5):1172-1178

[136]Skyttä T, Tuohinen S, Boman E, Virtanen V, Raatikainen P, et al. Troponin T-release associates with cardiac radiation doses during adjuvant left-sided breast radiotherapy. Radiat Oncol. 2015;10(141):1-8

[137]Skyttä T, Tuohinen S, Luukkaala T, Virtanen V, Raatikainen P, et al. Adjuvant radiotherapy-induced cardiac changes among patients with early breast cancer: a three-year follow-up study. Acta Oncol. 2019;58(9):1250-1258

[138]Qu D, Liu J, Lau C-W and Huang Y. IL-6 in diabetes and cardiovascular complications. BR J Pharmacol. 2014;171(15):3595-3603

[139]Harrison M, Erythrocyte sedimentation rate and C-reactive protein. Aust Prescr. 2015;38(3):93-94

[140]Bassuk S, Rifai N and Ridker P, High-Sensitivity C-Reactive Protein: Clinical Importance. Curr Probl Cardiol. 2004;29(8):439-493

[141]Ridker P, EverettB, Thuren T, MacFadyen J, Chang W, Ballantyne C, et al. Antiinflammatory Therapy with Canakinumab for Atherosclerotic Disease. N Engl J Med. 2017;377(12):1119-1131

[142]Pituskin E, Mackey J, Koshman S, Jassal D, Pitz M, et al. Multidisciplinary Approach to Novel Therapies in Cardio-Oncology Research (MANTICORE 101-Breast): A Randomized Trial for the Prevention of Trastuzumab-Associated Cardiotoxicity. J Clin Oncol. 2017;35(8)870-877

[143]Gulati G, Heck S, Ree A, Hoffmann P, Schulz-Menger J, et al. Prevention of cardiac dysfunction during adjuvant breast cancer therapy (PRADA): a 2 × 2 factorial,

randomized, placebo-controlled, double-blind clinical trial of candesartan and metoprolol. Eur Heart J. 2016;37(21):1671-1680

[144]Geuna E, Lombardi P, Martinello R, Garino D, Bonzano A, et al. Treatment with Beta-Blockers and ACE-Inhibitors in Breast Cancer Patients Receiving Adjuvant Trastuzumab-Based Therapy and Developing Mild Cardiac Toxicity: A Prospective Study. Cancers(Basel). 2020;12(2):327

[145]Jo I-Y, Lee J-W, Kim W-C, Min C-K, Kim E-S, et al. Relationship between changes in myocardial F-18 fluorodeoxyglucose uptake and radiation dose after adjuvant three-dimensional conformal radiotherapy in patients with breast cancer. J Clin Med. 2020;9(3):666

[146]Bergom C, Rubenstein J, Wilson J, Welsh A, Ibrahim E-S, et al. A Pilot Study of Cardiac MRI in Breast Cancer Survivors After Cardiotoxic Chemotherapy and Three-Dimensional Conforomal Radiotherapy. Front Oncol. 2020;10:1-10

[147]Clasen S, Shou H, Freedman G, Plastaras J, Taunk N, et al. Early cardiac effects of contemporary radiation therapy in patients with breast cancer. Int J Radiat Oncol Biol Phys. 2021;93(4):836-844

[148]Tjessem K, Bosse G, Fosså K, Reinertsen K, Fosså S, et al. Coronary calcium score in 12-year breast cancer survivors after adjuvant radiotherapy with low to moderate heart exposure - Relationship to cardiac radiation dose and cardiovascular risk factors. Radiother Oncol. 2015;114(3):328-334

[149]Gal R, van Velzen S, Hooning M, Emaus M, van der Leij F, et al. Identification of Risk of Cardiovascular Disease by Automatic Quantification of Coronary Artery Calcifications on Radiotherapy Planning CT Scans in Patients with Breast Cancer. JAMA Oncol. 2021;7(7):1024-1032

[150]Gaasch A, Schönecker S, Simonetto C, Eidemüller M, Pazos M, et al. Heart sparing radiotherapy in breast cancer: the importance of baseline cardiac risks. Radiat Oncol. 2020:15(1):117

Chapter 2

2 Changes in Myocardial Blood Flow in a Canine Model of Left Sided Breast Cancer RT

Left-sided breast cancer patients receiving adjuvant radiotherapy are at risk for coronary artery disease, and/or radiation mediated effects on the microvasculature. Previously our laboratory (El-Sherif et al.) demonstrated in canines with hybrid ^{18}FDG/PET a progressive global inflammatory response during the initial one year following treatment. To evaluate corresponding changes in perfusion, in the same cohort, myocardial blood flow (MBF) was semi-quantitatively measured and the results analysis is presented in this chapter.

2.1 Introduction

It was projected that in 2021, breast cancer will account for 25% of the total yearly female cancer incidence in Canada.[1] Advances in adjuvant radiation therapy of the breast improves both local control and overall survival.[2-3] However, patients with left-sided breast cancer are at a greater risk for the later development of radiation-mediated effects on the heart, including effects on the major coronary arteries, as well as vasculature due to the proximity of the heart to the radiation beam.[4] A worldwide systematic review done by Drost et al. on whole breast radiotherapy studies after 2014 reported a 3.6 Gray (Gy) total mean whole heart dose based on 84 left-sided breast cancer studies and a lower mean heart dose of 1.7 Gy from 65 regimens with breathing control.[5] The left anterior descending artery located in the anterior region of the heart, which is closer to the left breast, receives a substantially higher mean dose of 12.4 Gy.[5] Darby et al. has reported a linear relationship between major coronary events such as myocardial infarction and death from ischemic heart disease and radiation dose without a threshold (7.4% per Gy mean heart dose).[6] Several studies have reported myocardial perfusion deficits following radiotherapy (RT) for left-sided breast at 6 or more months, detected using mainly single photon emission tomography (SPECT). However without measurements performed prior to 6 months, any early postulated effects of radiation on myocardial blood flow and/or metabolism are purely conjecture.[8-11] Rasmussen et al. reported no differences in MBF

between irradiated and non-irradiated myocardium using ^{13}N ammonia ($^{13}NH_3$) PET imaging of breast cancer patients at an average of 7 years post-irradiation.[12] Up to this point, no serial longitudinal MBF assessments have been done which include early post treatment timepoints (i.e., before 6 months post RT) except for a single canine study of Yan et al.,[13] which studied animals at 3 time points (months 3, 6, and 12 after radiation. However the clinical relevance of the findings are uncertain, as in that study a single fraction dose of 20 Gy was used which far exceeds the single dose equivalent of a typical clinical RT protocol. Hence, as the early effects of radiation remain unknown and given the importance of this issue clinically, we wished to assess and monitor the cardiac response to irradiation longitudinally, to look for both its early and late manifestations. In a canine model of left-sided breast cancer RT, we measured the changes in myocardial blood flow post cardiac irradiation using both $^{13}NH_3$ PET and dynamic contrast enhanced MRI (DCE-MRI) with semi-quantitative measurements done concurrently using hybrid PET/MRI. These semi-quantitative measurements of blood flow were compared and each correlated to the progression of cell-mediated inflammation previously determined using fluorodeoxyglucose (^{18}FDG). Measurements performed at 1-week, 1-month, 3-months, 6-months and 12-months in five canines were compared to baseline values.

2.1.1 Aim

Through the measurement of myocardial blood flow, we will assess the effect of radiation on perfusion in canines from one week to one year in a clinically relevant model similar to patients exposed to left-sided breast cancer RT. We will correlate any changes in perfusion with our previously reported changes in ^{18}FDG uptake reflective of inflammation.

2.2 Method

In five adult female, bred-for-research hounds (21 - 26 kg), cardiac perfusion and inflammation imaging was performed on a hybrid PET/MRI system (Biograph mMR; Siemens AG). The study was approved by the Animal Care Committee of Western University (Protocol 2014-005). All animals at the start of the study were 1 year old and

were anesthetized during imaging and irradiation using propofol (4-6 mg/kg) and maintained with 2% isoflurane. Cardiac perfusion imaging was performed at baseline, 1-week, 1-month, 3-months, 6-months and 12-months following focused cardiac external beam irradiation. The same animal cohort that was used in this perfusion study was used in our previously published ^{18}FDG study[14] in which all animals underwent suppression of glycolysis by cardiomyocytes, which included diet, fasting, injection of heparin and infusion of intralipid. Note however that the injection of heparin and the infusion of intralipid were only applied after the MBF data acquisition was completed. Rate pressure product (RPP) of each animal at each imaging timepoint was determined from the heart rate and systolic blood pressure measured using the physiologic ECG and respiratory unit and the wireless pulse sensor connected to the scanner (Siemens AG).

2.2.1 Radiation delivery

A fast-helical CT and a contrast enhanced CT (discovery VCT, GE Healthcare) were performed on all animals for radiation treatment planning. Manual contouring of the heart, left ventricle (LV), left circumflex (LCX) and the left anterior descending coronary artery (LAD) perfusion regions were performed on the contrast enhanced CT and overlaid on the fast-helical CT for radiation treatment planning. All animals were irradiated with a TrueBeam linear accelerator (Varian Medical Systems) with the biological equivalent LAD dose for a left-sided breast patient in a single fraction.[14-15] An α/β ratio of 2.5 Gy was used to convert the multi-fractionated scheme maximal dose to 0.4cm^3 of LAD ($D_{0.4}$ ~30 Gy in 25 fractions prescribed to a focal point at the LAD) to a single ~9 Gy in one fraction.[15] The treatment plans consisted of two, 180^o , 6MV photon arcs and deliberately focused on to the myocardial region supplied by the LAD while intentionally avoiding the basal anterolateral portion of the LV and the LCX artery itself in order to compare cardiac function in irradiated vs. minimally-irradiated segments. Dose was calculated using the adaptive convolve dose algorithm implemented on our Pinnacle^3 treatment planning system (Phillips Radiation Oncology Systems). The single fraction mean doses delivered to the whole heart (1.7 Gy), LV (2.2 Gy) and the coronary arteries (LAD (5.5 Gy) and LCX (1.1 Gy)) are the typical values observed in left-sided breast cancer radiotherapy patients (when converted back to multi-fraction dose).[5] The

average dose delivered to the myocardium regions supplied by LAD was 2.4 Gy, by LCX was 2.4 Gy and within the overlap regions was 3.1 Gy.

2.2.2 Imaging

Cardiac perfusion was longitudinally assessed using $^{13}NH_3$ for the PET imaging component, along with simultaneous dual bolus dynamic contrast enhanced MR (DCE-MR) imaging using a hybrid PET/MR system (mMR, Siemens Medical Systems). Cardiac perfusion was imaged at rest. Perfusion was assessed with an injection of $^{13}NH_3$ (~5 M Bq/kg). (See figure 2.1 for imaging protocol.) The PET data was acquired in list-mode and retrospectively binned into 16 time periods 12×10s, 2×30s, 1×60s, 1×360s. All PET data was reconstructed using an iterative 3D ordered subset expectation maximization algorithm (OSEM) with 3 iterations, 21 subsets, 172×172×127 matrix size and a 4mm Gaussian smoothing filter, which yielded a voxel size of 2.08×2.08×2.03 mm.

Concurrent with $^{13}NH_3$ imaging, DCE-MR imaging was performed utilizing the 2D fast gradient echo sequence (syngo MR B20P) under breath-hold condition with 6mm slice thickness, ECG-gated end-diastolic phase, 164.02 ms repetition time, 1.01ms echo time, time between saturation pulse and signal acquisition = 100 ms, FOV matrix = 270x360, flip angle =10^o and a total scan time of 60 R-R intervals. The volume ratio of the injected Gadolinium chelate (Gd-DPTA) (Magnevist; Berlex Canada; Lachine, Quebec, Canada) was 1:10, i.e. the injection that produced the low blood concentration was 0.4 ml (0.01 mmol/kg of Gd-DTPA) and the one that produced the high blood concentration was 4 ml (0.1 mmol/kg Gd-DTPA). Each bolus was followed by 11 ml saline at a rate of 3 ml/s. The dual bolus injection was set up following the dual-bolus injection scheme stated by Ishida et al. using a two-syringe power injector with programmable pause functionality.[16] The bolus with 4 ml contrast was injected 25 seconds after the 0.4 ml bolus. T1-weighted late gadolinium enhanced whole heart imaging was performed using 3D-FLASH sequence with 407.28 ms triggered repetition time (based on R-R interval), 1.4 ms echo time, 270 inversion time, FOV matrix = 250x320, slice thickness of 0.9 mm and flip angle = 20^o and were collected only at 6-months and 12-months follow-up, to identify any specific focal enhancement.

The imaging protocol for ^{18}FDG was adopted from a previously validated study reported by Prato et al., which is capable of identifying abnormal accumulation of inflammatory cells within the heart following coronary occlusion.[17] Glucose uptake of cardiomyocytes was suppressed in all animals through fasting and an intravenous injection of heparin immediately followed by a 20% lipid infusion, 20 mins prior to the injection of ^{18}FDG. The ^{18}FDG data were acquired in list mode triggered by respiration, 60 mins after the injection, using a single static frame (20 mins duration). The ^{18}FDG measurements done in these animals have been published previously, where the standard uptake values remained persistently elevated compared with baseline (1.1 ± 0.03 vs. 2.6 ± 0.19, $P < 0.05$).[14] The presence of myocardial inflammation was confirmed histologically through ex-vivo analysis using an anti-CD45 antibody, when the animals were sacrificed

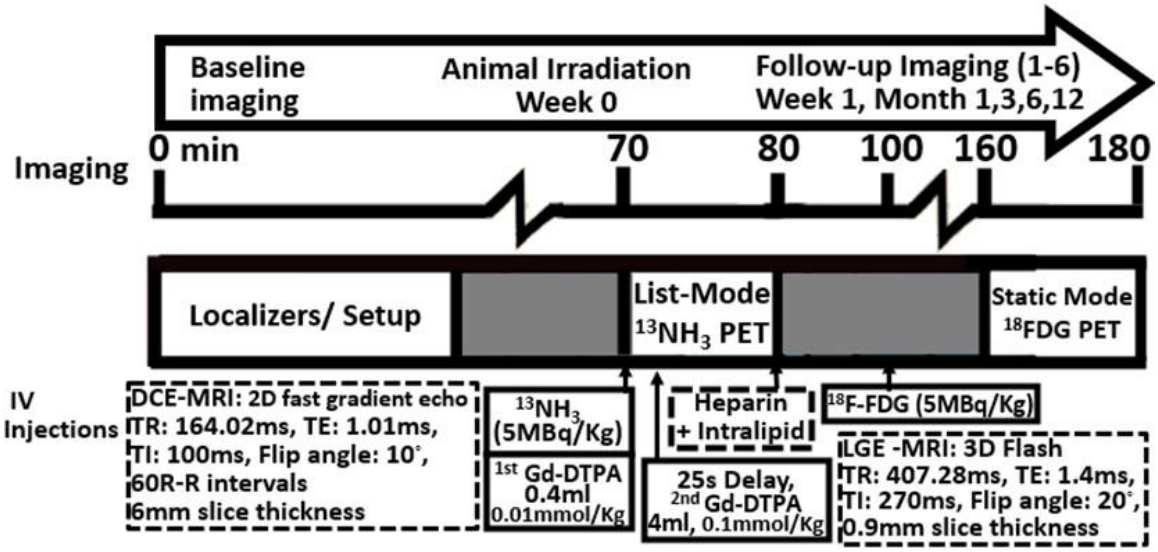

Figure 2.1 Overview of the PET/MRI imaging protocol and timing of the baseline, 1 week, 1,3,6 and 12 months follow-up imaging protocol. This protocol incudes the ^{18}FDG details that have been previously reported.[14]

following the 1-year imaging session.[14] However, no assessment for myocardial fibrosis was done on the pathological specimens.

2.2.3 Data analysis

Myocardial blood flow (MBF) determined from the $^{13}NH_3$ injection was assessed using a one tissue-compartment tracer kinetic model of the first 4 minutes of data, as

implemented in a semi-automated analysis program, FlowQuant© (University of Ottawa Heart Institute):

$C_t(t) = K_1 e^{-k_2 t} * C_{LV}(t)$, in which K_1 [ml/min/g] and k_2 [min^{-1}], are regional uptake and clearance parameters; $C_t(t)$ and $C_{LV}(t)$ are the concentration of $^{13}NH_3$ in the myocardial tissue and in the left ventricle blood. K_1 is related to MBF according to the Renkin-Crone function: $K_1 = \left(1 - a \times e^{-\frac{b}{MBF}}\right) \times MBF$, using a and b parameters measured previously in dogs.[18] The parameters K_1 and k_2, are estimated parameters using a weighted least-squares algorithm.[19] (See figure 2.2) For $^{13}NH_3$ the quantity is approximated $\left(1 - a \times e^{-\frac{b}{MBF}}\right) \approx 1$ for MBF less than 6 ml/min/g.[18]

Three short axis slices including basal, mid and apex, of the myocardium DCE-MR images were contoured on ITK-SNAP (Version 3.6.0)[20] according to a 16-segment canine heart model (See figure 2.3). The mid slice LV blood pool contour was selected as the region for the arterial input function. A MATLAB v.R2019b (MathWorks®, Natick, Massachusetts, USA) based quantitative software program was created to automate the Toft's model (shown in figure 2.2) deconvolution of the MRI derived curve fitting methods in order to calculate K^{trans}. Regarding the dual bolus curve fitting method (DB), the signal intensity curve of the small bolus arterial input function (AIF) was magnified by a factor of ten according to the bolus ratio of contrast material injected. The time intensity curve and the myocardial tissue curves from the 0.4 ml bolus were truncated. The conventional 4 ml Gd-DTPA bolus myocardial tissue curves were fitted with the magnified arterial input curve using the Toft's model:[21-22]

$$C_t(t - t_0) = K^{trans} \int_0^t C_p(\tau) e^{-k_{ep}(t - t_0 - \tau)} d\tau = K^{trans} e^{-k_{ep}(t - t_0)} \int_0^t C_p(\tau) e^{k_{ep}\tau} d\tau,$$

where k_{ep} is the flux rate constant, C_t is the contrast concentration in the myocardial tissue and C_p is the blood plasma concentration derived from the AIF corrected by an assumed blood hematocrit value of 0.45. The MBF later was calculated from K^{trans} obtained from each curve fitting method using the relation that equals the extraction fraction multiplied by the MBF. An extraction fraction of 0.5 was used as reported by Tong et al. for normal canine myocardium for Gd-DTPA.[23] Figure 2.4 and 2.5 shows the ideal curve fitting scenarios for AIF and myocardial tissue curves following DB DCE-MR. Note that for both $^{13}NH_3$ and DB DCE-MRI determination, a one-tissue compartment model is

assumed as shown in figure 2.2. Late gadolinium enhancement-MR (LGE-MR) images were analysed using circle CVI42 version 5.11 (Circle Cardiovascular Inc., Calgary, Canada). The detection of scar or fibrosis in the form of a focal enhancement, was based on the signal threshold versus reference myocardium technique (mean ± 5 SD signal intensity), with the mean obtained from a mid-slice of the left ventricle judged to correspond to non-irradiated remote myocardium.[24]

2.2.4 Statistical Analysis

Statistical analyses were performed in SPSS IBM v.23 (IBM SPSS Statistics for Windows, Armonk, NY). The paired sample t-test determined the significance between the MBF determined from $^{13}NH_3$ and the DB curve fitting technique based on coronary regions. Pearson's bivariate correlation coefficient was used to test the association between MBF of $^{13}NH_3$ and DCE-MRI using DB curves, as well as the association of ^{18}FDG[14] and MBF of the two methods. Changes of MBF between $^{13}NH_3$ and DB curves of DCE-MRI compared to baseline per coronary regions and changes of mean RPP were tested using non-parametric Kruskal-Wallis and Mann-Whitney test.

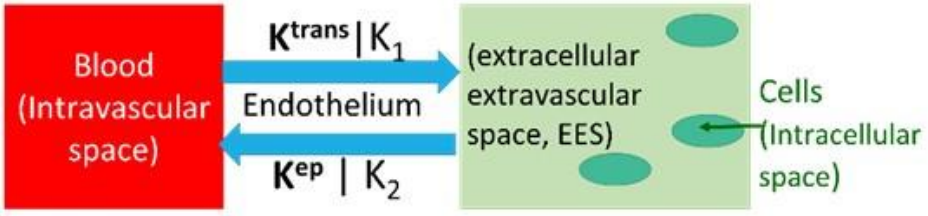

Figure 2.2 Regional uptake and clearance parameters K_1 and k_2 indicated in a one-tissue compartment model implemented in Flowquant software for $^{13}NH^3$ and Toft's Model with transfer constant K^{trans} and K_{ep} used by DB DCE-MRI deconvolution analysis

Figure 2.3 Myocardium contoured using 16-segment canine cardiac model on ITKsnap.

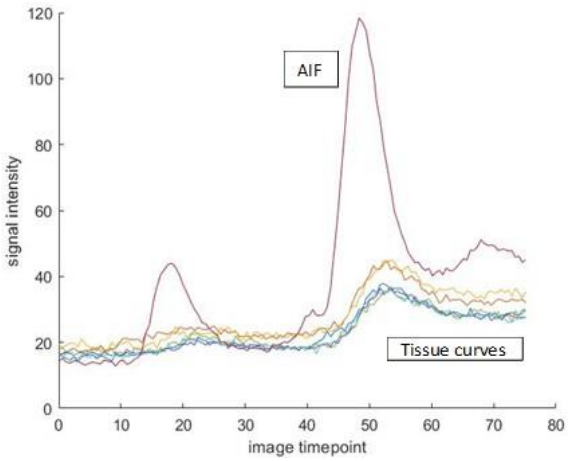

Figure 2.4 Ideal signal intensity curves for AIF and myocardial tissue within a dual bolus DCE-MR injection to prevent signal saturation. Note that the low dose bolus is injected first before the high dose bolus injection.

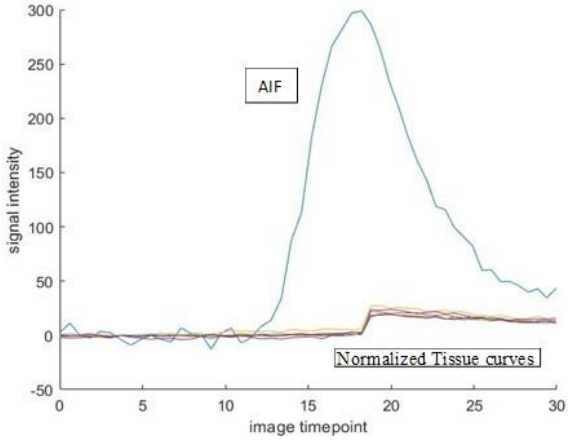

Figure 2.5 Ideal dual bolus curve fitting scenario with amplification of low contrast concentration bolus AIF signal intensity curve and truncation of low concentration tissue curves, followed by normalization of both curves.

2.3 Results

Figure 2.6 shows the results for both MBF methods rendered onto the 16-segments canine cardiac model (figure 2.3). Figures 2.7-8 show the results over time for MBF measured with $^{13}NH_3$ and DB DCE-MRI respectively for the entire myocardium which can be broken down to regions supplied by the LAD, LCX and that supplied potentially by both arteries as shown in figure 2.3.

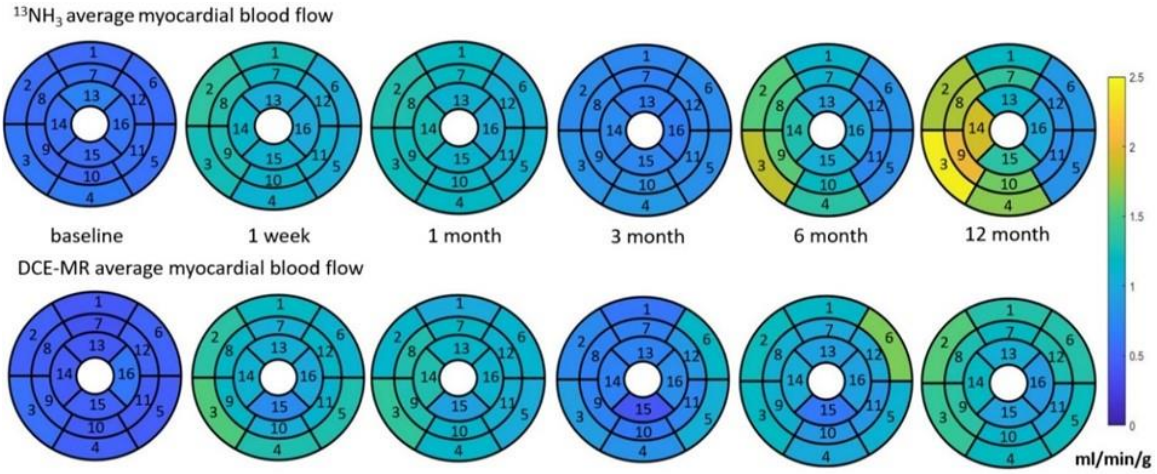

Figure 2.6 The absolute myocardial blood flow for each of the 16 segments averaged over all 5 animals. The $^{13}NH_3$ results are shown at the top and the DB DCE-MRI results at the bottom.

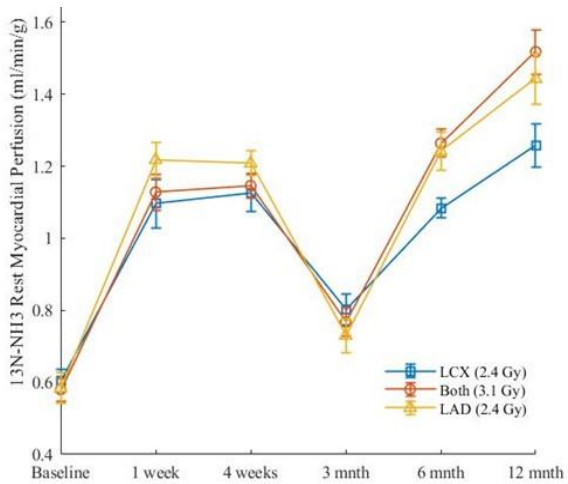

Figure 2.8 Changes and standard errors of means (SEM) in $^{13}NH_3$ rest MBF based on coronary regions.

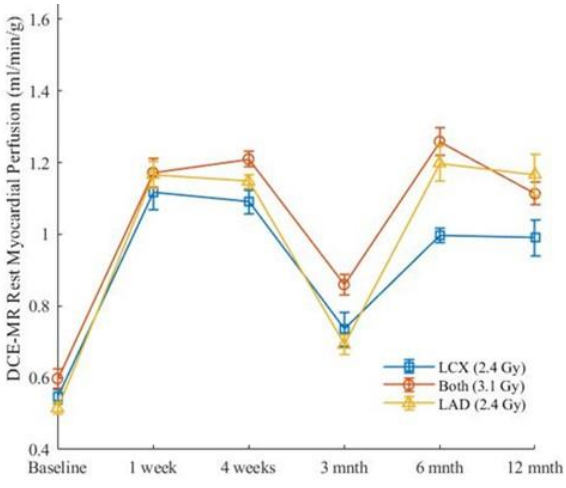

Figure 2.7 Changes and SEM in DB DCE-MRI rest MBF from DB curve fitting method based on coronary regions.

No difference was seen when $^{13}NH_3$ MBF in different coronary regions were compared to each other ($p = 0.06$). Significant changes indicated in $^{13}NH_3$ MBF in all myocardial regions for all timepoints ($p < 0.05$) using Kruskal-Wallis test. (See table 2.1 column 2). Comparing MBF follow-up timepoints to baseline MBF, only the 3-months follow-up timepoint showed insignificant changes ($p > 0.05$) in all myocardial regions. (See table 2.1 column 5) A positive correlation between ^{18}FDG and $^{13}NH_3$ MBF was observed for the LAD, LCX and that part of myocardium served by both coronary arteries. (See table 2.2) Note DB DCE-MRI MBF were statistically similar to $^{13}NH_3$ MBF for all coronary regions according to the pair t-test p values ($p > 0.05$). (See table 2.3-4) Six out of thirty data points from the DB DCE-MRI were removed from data analysis due to technical difficulties as shown in figure 2.9-10. Note that both MBF methods give, within statistical error, the same overall results: MBF post radiotherapy was increased at all timepoints measured except for the 3-months timepoint. This correlation of data from two different modalities for perfusion assessment was expected given that both were analyzed using a one-compartment tissue model (figure 2.2). The $^{13}NH_3$ results are highlighted given they corresponded to complete left ventricle tissue coverage, were not dependent on an assumption of extraction fraction estimate, did not fail in any of the measurements and provided overall greater statistical certainty in relationship to the ^{18}FDG values. No significant changes of mean RPP over all timepoints ($p = 0.97$) were observed using the Kruskal-Wallis test. (Figure 2.11) No specific focal enhancement was identified in all LGE-MR images at 6-months and 12-months follow-up.

Table 2.1 P-values of changes in time of myocardial MBF obtained from $^{13}NH_3$ MBF from non parametric Kruskal-Wallis test and p-values of MBF comparing follow-up versus baseline MBF from Mann-Whitney test based on coronary regions. $P < 0.05$ determines significant differences.

MBF	P-value of changes in all timepoints	P-values of comparing follow-up versus baseline MBF				
		1wk	1mon	3mon	6mon	1year
$^{13}NH_3$ LAD	.004	.009	.009	.142	.016	.016
$^{13}NH_3$ LCX	.014	.016	.016	.142	.009	.032
$^{13}NH_3$ BOTH	.004	.016	.009	.142	.016	.016

Table 2.2 Pearson bivariate correlation coefficient and p-values of ^{18}FDG standard uptake value and $^{13}NH_3$ MBF based on coronary regions for all timepoints.

	r-value	p-value
$^{13}NH_3$ LAD MBF V.S. ^{18}FDG LAD	.494	.008
$^{13}NH_3$ LCX MBF V.S. ^{18}FDG LCX	.465	.013
$^{13}NH_3$ BOTH MBF V.S. ^{18}FDG BOTH	.511	.005

Table 2.3 Paired T-Test P-values and Pearson bivariate correlation coefficient of MBF obtained from DB DCE-MRI compared to $^{13}NH_3$ and to ^{18}FDG standard uptake values for all time points and coronary regions. $R > 0.75$ and $R > 0.5$ indicates strong and moderate positive correlation, respectively. Insignificant difference was shown when DB DCE-MRI MBF in different coronary regions were compared ($p = 0.06$).

	Paired t-test p-value	Pearson bivariate correlation r-value
$^{13}NH_3$ LAD MBF V.S. DB LAD MBF	.057	.933
$^{13}NH_3$ LCX MBF V.S. DB LCX MBF	.251	.801
$^{13}NH_3$ BOTH MBF V.S. DB BOTH MBF	.867	.851
DB LAD MBF V.S. ^{18}FDG LAD	.006	.541
DB LCX MBF V.S. ^{18}FDG LCX	.175	.286
DB BOTH MBF V.S. ^{18}FDG BOTH	.033	.437
DB LAD V.S. DB LCX	.063	

Table 2.4 P-values of changes in time of myocardial MBF obtained from DB-DCE MBF from non-parametric Kruskal-Wallis test and p-values of MBF comparing follow-up versus baseline MBF from Mann-Whitney test based on coronary regions. $P < 0.05$ determines significant differences.

MBF	P-value of changes in all timepoints	P-values of comparing follow-up versus baseline MBF				
		1wk	1mon	3mon	6mon	1year
DB LAD	.007	.021	.021	.083	.014	.034
DB LCX	.043	.021	.021	.248	.014	.034
DB BOTH	.019	.021	.021	.083	.014	.034

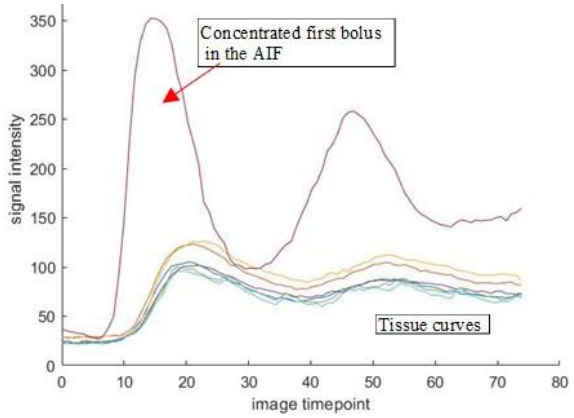

Figure 2.10 Residual contrast shown in LV pre-contrast injection of the high dose bolus injection.

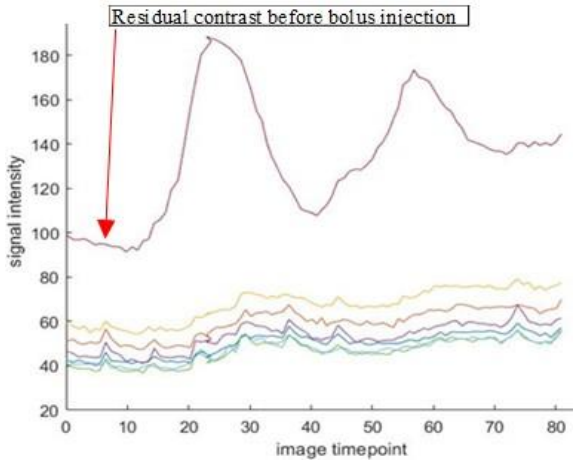

Figure 2.9 Higher blood contrast concentration following the first bolus with larger signal intensity compared to the second bolus indicating that a high dose bolus injection was injected first in error.

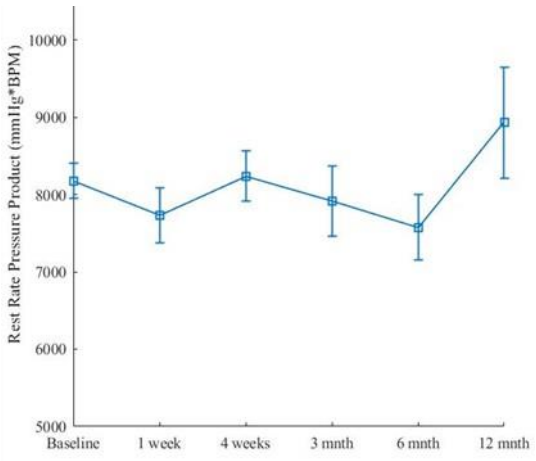

Figure 2.11 Rest rate pressure product and SEM of each imaging timepoint. Insignificant changes of mean RPP over all timepoints (p = 0.97) was determined using the Kruskal-Wallis test. Note one of the dogs did not perform blood pressure measurements at 3-month timepoint.

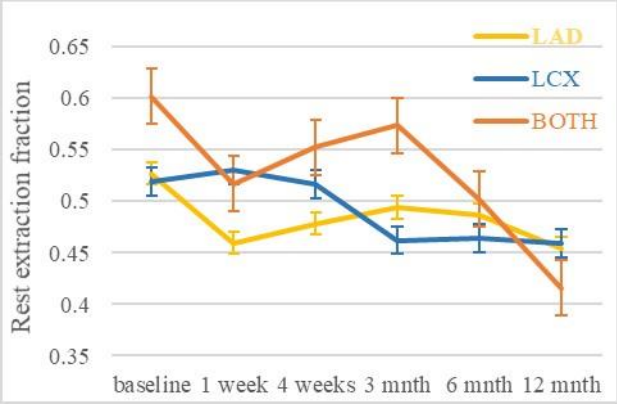

Figure 2.12 Rest extraction fraction average and SEM per coronary region determined from DB curve fitting method of DCE-MRI with K^{trans} divided by MBF from $^{13}NH_3$.The extraction fraction average per coronary region for all timepoints was 0.48 ± 0.03 (mean ± standard deviation) for LAD, 0.49 ±0.03 for LCX and 0.53 ± 0.07 for both coronary regions.

2.4 Discussion

In this study, an increase of myocardial blood flow developed as early as one-week post irradiation, with a dip at 3-months follow-up during rest perfusion. The 3-months follow-up was not different compared to baseline. All other timepoints showed a significant and progressive increase over the baseline value. Note that the consistency of the MBF measures between $^{13}NH_3$ vs. dual bolus DCE-MRI provided a level of confidence that the finding of the increase in MBF post radiotherapy is valid. As the RPP did not change at any time point compared to baseline, the increases seen in MBF cannot be explained by changes in the conventional myocardial oxygen demand factor.

It is of interest that at 12-months $^{13}NH_3$ MBF results progressed to their highest value whereas the DB DCE-MRI estimates of MBF at 12-months are similar to the other follow-up timepoints except 3-months. Due to technical issues (see figure 2.9-10), only data from 3 dogs DB DCE-MRI at 12-months were analyzed. At this 12-month timepoint, using Mann Whitney statistical analysis, only the LAD region's MBF was significantly different between the $^{13}NH_3$ and DB DCE-MRI ($p=0.03$). Furthermore, comparing all follow-up timepoints, $^{13}NH_3$ and DB-DCE MRI MBF were each insignificantly different except at 3-month when regional flows were compared ($p \geq 0.22$). The marginally significant disparity of $^{13}NH_3$ vs DB DCE-MRI MBF at 12 months only may be due to the intrasubject biological variations between the two modality measurements, in which DCE-MRI depends on functional capillary density, while $^{13}NH_3$ depends on glutamine synthetase reaction in the myocardial tissue. Another possibility is that the extraction fraction (EF) of Gd-DTPA may have been reduced perhaps due to loss of capillary density. As the EF of $^{13}NH_3$ is not reduced until much higher flows are reached, this could be an alternative explanation. It will be of interest to determine in future work if there are corresponding changes in histology (e.g. apoptosis, fibrosis) or in T1-values (caused by increases in the extracellular volumes, but which would require T1 values to be assessed before and after contrast enhanced MRI).

In contrast to our results reported here in the canine model, clinical assessments of MBF after left-sided breast radiotherapy have consistently shown reductions in rest MBF

determined primarily using SPECT imaging. However those assessments have all been at 6 or more months after radiotherapy.[7-11] The disparity between our findings and those previously reported may due to (1) the difference in human and canine's vasculature in which the dominant coronary artery in canines is the left circumflex and not the left anterior descending; (2) the greater radiation dose deposited in the heart (up to single fraction equivalent mean dose of 2.82 Gy in literature versus 1.7 Gy in our study) and the greater radiation dose deposited in the left ventricle (up to single fraction equivalent mean dose of 10.16 Gy in literature versus 2.7 Gy in our study). This greater radiation dose in the clinical SPECT studies resulted from selection criteria which followed-up primarily patients who received a high radiation dose in a portion of their left ventricle or heart during radiotherapy. In $^{13}NH_3$ PET studies in the literature, Rasmussen et al.[12] reported no differences in MBF between irradiated and non-irradiated myocardium when imaging breast cancer patients at an average of 7 years post-irradiation. Note however that this study did not have baseline measures for comparison. Without our baseline measurements, our post irradiation MBF values may not be considered increased. In contrast, although Yan et al.[13] did not perform baseline measurements, they used a control group of 18 dogs for the 18 exposed animals and did $^{13}NH_3$ measurements at 3, 6 and 12 months after a 20 Gy irradiation of the left anterior myocardium. No effects were seen at 3 months but a reduction in MBF was seen at 6 months with a further reduction in blood flow seen at 12 months.[13] In the same study, gradually decreasing focal areas of increased ^{18}FDG uptake were observed comparing irradiated and nonirradiated canine groups at 3, 6 and 12-months due to cardiac remodeling, without differences in the proinflammation phenotype macrophage marker CD68 and inflammatory cytokines.[13] In our canine study, we were aiming to simulate typical breast cancer radiotherapy dosage which is approximately ten times lower compared to Yan et al. For our canine study we observed a significant increase of global ^{18}FDG uptake which increased progressively from 3-months to 6-months and then again at 12-months. Currently, there are no serial follow-up studies post-irradiation using $^{13}NH_3$ or DB DCE-MRI along with concurrent cardiac inflammation data reported except for the Yan et al. [13] study; however, as noted above, the results of that study may not be relevant to the current practice of RT in left

sided breast cancer, because of the much higher administered dose in the previously reported study.

The correlation of myocardial blood flow to inflammation measured by ^{18}FDG did show a significant linkage with $^{13}NH_3$ myocardial blood. However, the Pearson correlation values were on average 0.5, indicating that only 25% of the change in ^{18}FDG uptake was associated with changes in blood flow based upon semi-quantitative measurement. Consider specifically the 3-month time point when resting blood flow returned to baseline value, while in the ^{18}FDG data, the increase at 1-month remained at 3-months. This suggests that at least part of the inflammatory signal is not mediated by changes in blood flow and is due to other additional and as yet undefined mechanisms. Also, it is not clear which is the primary driver of the pathophysiology-i.e. is the augmentation of flow an important driver of the inflammatory response, or alternatively, is the increase in flow a response to inflammatory injury. In our study, cardiac apoptotic tissue was not identified in our LGE-MR and ^{18}FDG results contrary to Yan et al.[13] The increase in rest $^{13}NH_3$ MBF at all time points, save at 3-months, suggests that this could be the result of an acute global inflammation in the myocardium despite the focal radiation targeted towards primarily the LAD region.[14] The global nature of the inflammation is also consistent with the finding that no specific focal enhancement was identified from the LGE-MR images at 6-months and 12-months follow-up, consistent with the evidence of increasing global ^{18}FDG uptake and increased global MBF values with a constant RPP. This global inflammatory and MBF response, seen as early as 1-week post irradiation, may project to late fibrosis within either myocardium or epicardial vessels. Note that any global change of scar/fibrosis would not be detected in this study using delayed contrast enhancement, as this would require pre and post contrast T1 maps with calculation of the extracellular volumes.

A limitation of our study is the small number of canines and the lack of an independent gold standard of perfusion such as the use of microspheres.[25] However, when calculating the absolute extraction fraction with K^{trans} obtained from the DB method divided by MBF determined using $^{13}NH_3$, the absolute extraction fraction average values per coronary regions obtained in this study across all timepoints (See figure 2.12) were between 0.48-0.57, consistent with the value reported by Tong et al.[23] using a gold standard

methodology. MBF determined from DB DCE-MRI was not statistically different from that determined from $^{13}NH_3$ for all coronary regions, with a strong correlation between the two, with r values between 0.80 and 0.93. (See table 2.3) An important indicator sensitive to coronary artery health[26] is myocardial perfusion reserve (MPR) which corresponds to the ratio of myocardial blood flow at stress divided by that at rest.[27] Although not assessed in our study, this would be a valuable measure to have in future canine and human studies. Moreover, the PET (voxel size of 2.08×2.08×2.03mm) and contrast enhanced MRI (voxel size of 1.875×1.875×1mm) in our canine study did not have the needed resolution in order to identify the transmural distribution of changes in flow (i.e. subendocardial vs. subepicardial).

2.5 Conclusion

In the canine, rest myocardial blood flow within the first year following heart irradiation generally progressively increases over time. This has been confirmed by two non-invasive independent methods. A possible interpretation is that the increase in resting MBF is a response to myocardial inflammation. Based on this data, future patient studies early after radiotherapy, should consider measurements of both myocardial blood flow and myocardial inflammation.

2.6 References

[1] Brenner DR, Weir HK, Demers AA, Ellison LF, Louzado C, Shaw A, et al. Projected estimates of cancer in Canada in 2020. Can Med Assoc J. 2020;192(9):199–205.

[2] Abe O, Abe R, Enomoto K, Kikuchi K, Koyama H, Masuda H, et al. Effects of radiotherapy and of differences in the extent of surgery for early breast cancer on local recurrence and 15- year survival: An overview of the randomised trials. Lancet. 2005; 366(9503):2087-106

[3] Noël G, Mazeron JJ. Favourable and unfavourable effects on long-term survival of radiotherapy for early breast cancer: an overview of the randomised trials. Cancer Radiother. 2001;5(1):92- 4

[4] Darby SC, McGale P, Taylor CW, Peto R. Long-term mortality from heart disease and lung cancer after radiotherapy for early breast cancer: Prospective cohort study of about 300 000 women in US SEER cancer registries. Lancet Oncol. 2005;6(8):557-65

[5] Drost L, Yee C, Lam H, Zhang L, Wronski M, McCann C, et al. A Systematic Review of Heart Dose in Breast Radiotherapy. Clinical Breast Cancer. 2018;18(5):e819-e824

[6] Darby SC, Ewertz M, McGale P, Bennet AM, Blom-Goldman U, Brnønum D, et al. Risk of ischemic heart disease in women after radiotherapy for breast cancer. N Engl J Med. 2013;368(11):987-98

[7] Lind PA, Pagnanelli R, Marks LB, Borges-Neto S, Hu C, Zhou SM, et al. Myocardial perfusion changes in patients irradiated for left-sided breast cancer and correlation with coronary artery distribution. Int J Radiat Oncol Biol Phys. 2003;55(4):914-20

[8] Zellars R, Bravo PE, Tryggestad E et al. SPECT Analysis of Cardiac Perfusion Changes After Whole-Breast/Chest Wall Radiation Therapy With or Without Active Breathing Coordinator: Results of a Randomized Phase 3 Trial. Int J Radiat Oncol Biol Phys. 2014;88(4):778–85

[9] Evans ES, Prosnitz RG, Yu X, Zhou SM, Hollis DR, Wong TZ, et al. Impact of patient-specific factors, irradiated left ventricular volume, and treatment set-up errors on the development of myocardial perfusion defects after radiation therapy for left-sided breast cancer. Int J Radiat Oncol Biol Phys. 2006;66(4):1125-34

[10] Hardenbergh PH, Munley MT, Bentel GC, Kedem R, Borges-Neto S, Hollis D, et al. Cardiac perfusion changes in patients treated for breast cancer with radiation therapy and doxorubicin: Preliminary results. Int J Radiat Oncol Biol Phys. 2001;49(4):1023-8

[11] Kaidar-Person O, Zagar TM, Oldan JD, Matney J, Jones EL, Das S, et al. Early cardiac perfusion defects after left-sided radiation therapy for breast cancer: is there a volume response? Breast Cancer Res Treat. 2017;164(2):253–62

[12] Rasmussen T, Kjær A, Lassen ML, Pedersen AN, Specht L, Aznar MC, et al. No changes in myocardial perfusion following radiation therapy of left-sided breast cancer: A positron emission tomography study. J Nucl Cardiol. 2019

[13] Yan R, Li X, Song J, Guo M, Cai H, Wu Z, et al. Metabolic Changes Precede Radiation-Induced Cardiac Remodeling in Beagles: Using Noninvasive 18F-FDG and

13N-Ammonia Positron Emission Tomography/Computed Tomography Scans. J Am Heart Assoc. 2020; 9(18): e016875

[14] El-Sherif O, Xhaferllari I, Sykes J, Butler J, Dekemp RA, Renaud J, et al. [18F]FDG cardiac PET imaging in a canine model of radiation-induced cardiovascular disease associated with breast cancer radiotherapy. Am J Physiol - Hear Circ Physiol. 2019; 316(3):H586-H595

[15] Gillette SM, Gillette EL, Shida T, Boon J, Miller CW, Powers BE. Late radiation response of canine mediastinal tissues. Radiother Oncol. 1992; 23(1):41-52

[16] Ishida M, Schuster A, Morton G, Chiribiri A, Hussain S, Paul M, et al. Development of a universal dual-bolus injection scheme for the quantitative assessment of myocardial perfusion cardiovascular magnetic resonance. J Cardiovasc Magn Reson. 2011;13(1):28

[17] Prato FS, Butler J, Sykes J, Keenliside L, Blackwood KJ, Thompson RT, et al. Can the inflammatory response be evaluated using 18F-FDG within zones of microvascular obstruction after myocardial infarction? J Nucl Med. 2015;56(2):299-304

[18] Schelbert HR, Phelps MD, Huang SC, MacDonalid NS, Hansen H, Selin C, et al. N-13 ammonia as an indicator of myocardial blood flow. Circulation. 1981;63(6):1250-1272

[19] Lortie M, Beanlands RSB, Yoshinaga K, Klein R, Dasilva JN, deKemp RA. Quantification of myocardial blood flow with 82Rb dynamic PET imaging. Eur J Nucl Med Mol Imaging. 2007; 34(11):1765-74

[20] Yushkevich PA, Piven J, Hazlett HC, Smith RG, Ho S, Gee JC, et al. User-guided 3D active contour segmentation of anatomical structures: Significantly improved efficiency and reliability. Neuroimage. 2006; 31(3):1116-28

[21] Tofts PS, Brix G, Buckley DL, Evelhoch JL, Henderson E, Knopp MV., et al. Estimating kinetic parameters from dynamic contrast-enhanced T1-weighted MRI of a diffusable tracer: Standardized quantities and symbols. J Magn Reson Imaging. 1999;10(3):223-32

[22] Borrazzo C, Galea N, Pacilio M, Altabella L, Preziosi E, Carni M, et al. Myocardial blood flow estimates from dynamic contrast-enhanced magnetic resonance imaging: Three quantitative methods. Phys Med Biol. 2018;63(3):035008

[23] Tong CY, Prato FS, Wisenberg G, Lee TY, Carroll E, Sandler D, et al. Measurement of the extraction efficiency and distribution volume for Gd-DTPA in normal and diseased canine myocardium. Magn Reson Med. 1993;30(3):337-46

[24] Stirrat J, Joncas SX, Salerno M, Drangova M, White J. Influence of phase correction of late gadolinium enhancement images on scar signal quantification in patients with ischemic and non-ischemic cardiomyopathy. J Cardio vasc Magn Reason. 2015;7(17):66

[25] Chatterjee N, Benefield BC, Harris KR, Fluckiger JU, Carroll T, Lee DC. An empirical method for reducing variability and complexity of myocardial perfusion quantification by dual bolus cardiac MRI. Magn Reson Med. 2017;77(6):2347-2355

[26] Rosen BD, Lima JAC, Nasir K, Edvardsen T, Folsom AR, Lai S, et al. Lower myocardial perfusion reserve is associated with decreased regional left ventricular function in asymptomatic participants of the Multi-Ethnic Study of Atherosclerosis. Circulation. 2006;114(4):289-97

[27] Nagel E, Klein C, Paetsch I, Hettwer S, Schnackenburg B, Wegscheider K, et al. Magnetic resonance perfusion measurements for the noninvasive detection of coronary artery disease. Circulation. 2003;108:432–43

Chapter 3

3 Dosimetric Planning Comparison for Left-sided Breast Cancer RT: The Clinical Feasibility of 4D-CT Based Treatment Planning Optimization

This chapter aims to provide an extensive dosimetric heart sparing comparison of free-breathing and 4D-CT based treatment planning, including robust optimization, and deep-inspiration breath-hold based treatment planning with combinations of forward and inverse-IMRT and VMAT. The goal is to demonstrate that for patients who are non-compliant for a breath-hold treatment, there are clinically feasible options for free-breathing treatment. However, the most effective way of cardiac and substructure dose-sparing is still IMRT with DIBH.

3.1 Introduction

Breast cancer is the most common cancer in women worldwide. Adjuvant radiation therapy (RT) is commonly used after breast conserving surgery to increase overall survival by decreasing the rate of cancer recurrence.[1] Traditionally, 3D conformal RT with tangential field directions is used in breast RT.[2] More modern techniques, including intensity-modulated radiation therapy (IMRT) and volumetric modulated arc therapy (VMAT) have been shown to provide higher target coverage and more effective sparing of critical organs.[3-5] However, a proportion of breast cancer survivors develop radiation-induced cardiac disease later in their cure life.[6] Darby et al. concluded a linear relationship between major coronary events such as myocardial infarction and death from ischemic heart disease and radiation dose without a threshold (7.4% per Gy mean heart dose).[7]

Traditionally, mean heart dose is commonly used as a reference measure for treatment planning constraints and in cardiotoxicity studies. However, there is increased evidence that cardiac substructure dose is associated with radiation-induced heart disease. Nilsson et al. previously reported an increase of stenosis in the left anterior descending artery (LAD) in irradiated left-sided breast cancer patients and an association between high-risk

RT and stenosis in hotspot areas for radiation, which indicated a linkage between radiation and location of coronary stenosis.[8] Veerle et al. performed a group dose-distribution analysis showing that the left ventricle (LV) received the highest dose among all cardiac structures due to the LV position relative to the left breast.[2] Arslan et al. retrospectively evaluated LV and LAD dose sparing in patients treated with free-breathing left-sided breast IMRT delivered with additional boost, presented significant reductions in the mean and max dose of the cardiac substructures in the re-optimized plan.[9] Currently, cardiac and its substructure dosimetric consensus constraints have not been fully evaluated nor established. Beaton et al. performed a retrospective case-control matched study and found that the risk of radiation induced cardiac death at 10-years appears to be very low if mean heart dose is <3.3 Gy and maximum LAD dose ($EQD2_3$ Gy) is <45.4 Gy.[10] Furthermore, cardiac dose parameters are limited and vary in endpoints. Based on the Quantitative Analyses of Normal Tissue Effects in the Clinic (QUANTEC) guidelines stated, the V_{25Gy}Heart should be <10% to decrease the cardiac mortality to <1%.[11] Hence, it is important to evaluate not just the radiation dose to the heart, but also the radiation to which the substructures are subjected.

Deep-inspiration breath-hold (DIBH) has been implemented in the breast cancer RT routine to further reduce cardiac exposure to irradiation in many centres.[12] The heart moves posteriorly and inferiorly during deep inspiration due to lung expansion and diaphragmatic movements. This maximizes the distance between breast and the heart and reduces cardiac dose deposition. Dose planning and clinical studies have concluded that moderate DIBH is efficient and can effectively decrease mean heart dose in breast cancer patients.[13-15] While DIBH techniques can potentially lower the radiation dose to heart, it requires patient compliance and longer treatment duration.

The RayStation treatment planning system v7 (RaySearch Laboratories, Sweden) optimization technique run in a Graphic Processor Unit (GPU) system can account for heart intrafractional motion at each breathing phase, if a 4D-CT scan is acquired. This method is called 4D Robust optimization. It has been used in RT to account for position uncertainties including patient setup and tumor motion relative to the target volume during treatment delivery.[16-17] 4D Robust optimization utilizes min-max optimization to

ensure dose planning stability by maximizing the plan quality in the worst-case scenario.[18] In contrast to conventional untagged average 4D-CT treatment planning, which the internal target volume is expanded with a fixed margin to create the planning target volume (PTV) that encompass the end-inhale and end-exhale target volume, Robust optimization discretizes each phase of 4D-CT target volumes into multiple scenarios. The min-max optimization method allows the prescription to hold true even in the worst-case scenario, and performs the dose calculation with the optimized treatment plan on the end-inhale 4D-CT dataset instead of the average 4D-CT dataset. The additional respiration motion information obtained from 4D-CT is useful. El-Sherif et al. showed dose estimates for the LAD were substantially susceptible to intrafraction respiratory motion, adjunct to small ranges of dose to the heart and LV.[19] The Robust optimization technique has been explored by Mahmoudzadeh et al. in the context of cardiac sparing for breast IMRT in a limited sample size under normal free-breathing conditions (six patients) and controlled breath-hold conditions using the active breathing control (two patients).[20] However, like Darby et al.[7], this study focused on whole heart dosimetric parameters only and did not take into account the dose to cardiac substructures, such as the LAD and the LV. Direct comparison among techniques of 4D Robust optimization, DIBH and standard 4D in combination with forward and inverse IMRT or VMAT has not been done in the literature.

In this study we performed an extensive dosimetric comparison among various treatment planning techniques. Fixed-beam tangents, IMRT, and VMAT along with motion management strategies, including traditional motion encompassment with 4D-CT, 4D-CT Robust optimization, and DIBH. This work aims to: (1) identify the clinical feasibility of aforementioned techniques in sparing of the heart and its substructures; (2) address whether 4D Robust optimization can outperform DIBH and conventional 4D-CT techniques; and (3) to determine the clinical feasibility of IMRT versus VMAT.

3.2 Methods

3.2.1 Patient selection

Fifteen consecutive early stage (T0-T2A) left-sided breast cancer patients who were treated from 2018-2019 with standard breast RT plans were selected. Mean age of patients was 60 ± 12 years (range 35-76).

3.2.2 CT simulation and delineation

Both DIBH and free-breathing four-dimensional computed tomography (4D-CT) simulation were performed on each patient using the Philips Brilliance Big Bore CT scanner (Philips Medical Systems, Cleveland, USA). Simulation imaging was performed with the patient in supine position, with scans taken from the upper border of hyoid bone to the diaphragm. 4D-CT scans were reconstructed into 10 phases using the Respiratory Gating for Scanners (RGSC) system (Varian Medical Systems, Palo Alto, USA). An untagged average 4D-CT dataset (UNTAG AVERAGE) that uses all the projection data acquired during the low-pitch helical CT scan was also generated and served as the primary dataset for the free-breathing scenario.

The breast volume was contoured, according to the delineation guidelines for adjuvant radiotherapy of early breast cancer by the Radiation Therapy Oncology Group (RTOG), and was approved by breast oncologists.[21] The anterior component of the target volume contours of the left breast were defined by a 5 mm contraction of the external contour. The pericardium was defined as the border of the LAD and the whole heart, while the left ventricle was contoured from the top left ventricle border to the apex cordis. The LAD, LV, both lungs, spinal cord, and the whole heart were delineated on all ten phases of the 4D-CT dataset, the untag average dataset, and the DIBH dataset (with supervision of a radiation oncologist) using RayStation 7 software (RaySearch Laboratories, Sweden).

3.2.3 Treatment planning

Eight treatment plans were generated for each patient. Forward IMRT, inverse IMRT, and VMAT were optimized on both the DIBH and UNTAG AVERAGE dataset. Additionally, 4D Robust IMRT and VMAT optimization, that uses the entire 4D-CT dataset, were also performed, giving a total of 120 treatment plans. A dose of 4250 cGy

in 16 fractions, the current clinical standard in our clinic, was prescribed for each patient, with a minimum of 90% coverage of the left breast target volume. Dose was calculated using collapsed cone convolution.

VMAT planning was composed of 2-4 partial arc beams ranging from 300° to 180° in the clockwise and counter-clockwise directions. Dose optimization for fixed tangential beams was performed using both forward and inverse step-and-shoot treatment planning techniques. The beam energy was chosen based on the distance between the radiopaque markers on the anterior-posterior set-point: 6 MV for separations less than 20 cm, 10 MV for separations between 20 and 23 cm and 15 MV (with or without additional 6 MV beams) for separations larger than 23 cm.

Objectives and constraints goals were prioritized as follows: (1) heart; (2) left lung; (3) left breast; (4) right breast; (5) right lung; and (6) remaining normal tissue, according to QUANTEC and dosimetric guidelines in our clinic (See Table 3.1 for details).[9] For the LV and LAD, no constraint was set up due to lack of literature consensus guidelines available. However, the dose of these two substructures were aimed to be reduced as low as possible.

Table 3.1 Objectives and constraints goals for inverse-IMRT and VMAT treatment plans with and without robust optimization

Objectives	Min dose: Left breast target volume with 4250 cGy
	Max DVH: 1% of Left breast target volume with 4460 cGy 10% of Heart with 250 cGy 8% of Heart with 1000 cGy 30% of Left lung with 250 cGy 10% of Left lung with 1200 cGy
	Dose Fall-Off: Left breast target volume: 4200 cGy to 4000 cGy in 2 mm
	Max EUD: Spinal cord: 17 cGy Right breast: 240 cGy Right lung: 37 cGy
	Uniform dose: Left breast target volume: 4250 cGy
Constraints	Min DVH: 97% of Left breast target volume with 4250 cGy
	Max Dose: Left breast target volume: 4460 cGy

3.2.4 Dosimetric assessment

Dose-volume histograms (DVHs) were used to compare following parameters: V_{5Gy}Heart (the volume of heart receiving at least 5Gy), $V_{50\%}$Lung (total lung volume receiving at least 2125 cGy) and the mean heart, mean LAD, mean LV dose and max LAD dose. Statistical analyses were performed in SPSS IBM v.23 (IBM SPSS Statistics for Windows, Armonk, NY) using Shapiro-Wilk test for normality, Kruskal-Wallis nonparametric one-way analysis of variance (ANOVA) to test for significance, and Wilcoxon-Mann-Whitney test to find between-subject significance.

3.3 Results

All treatment plans generated from the eight RT planning techniques were clinically feasible and reviewed by a certified dosimetrist, with a selection of sample patients contours approved by the radiation oncologists. All achieved minimum of 90% coverage of 4250 cGy prescription dose in 16 fractions. Dose distributions for each of the eight planning techniques for a representative patient are displayed in Figure 3.1.

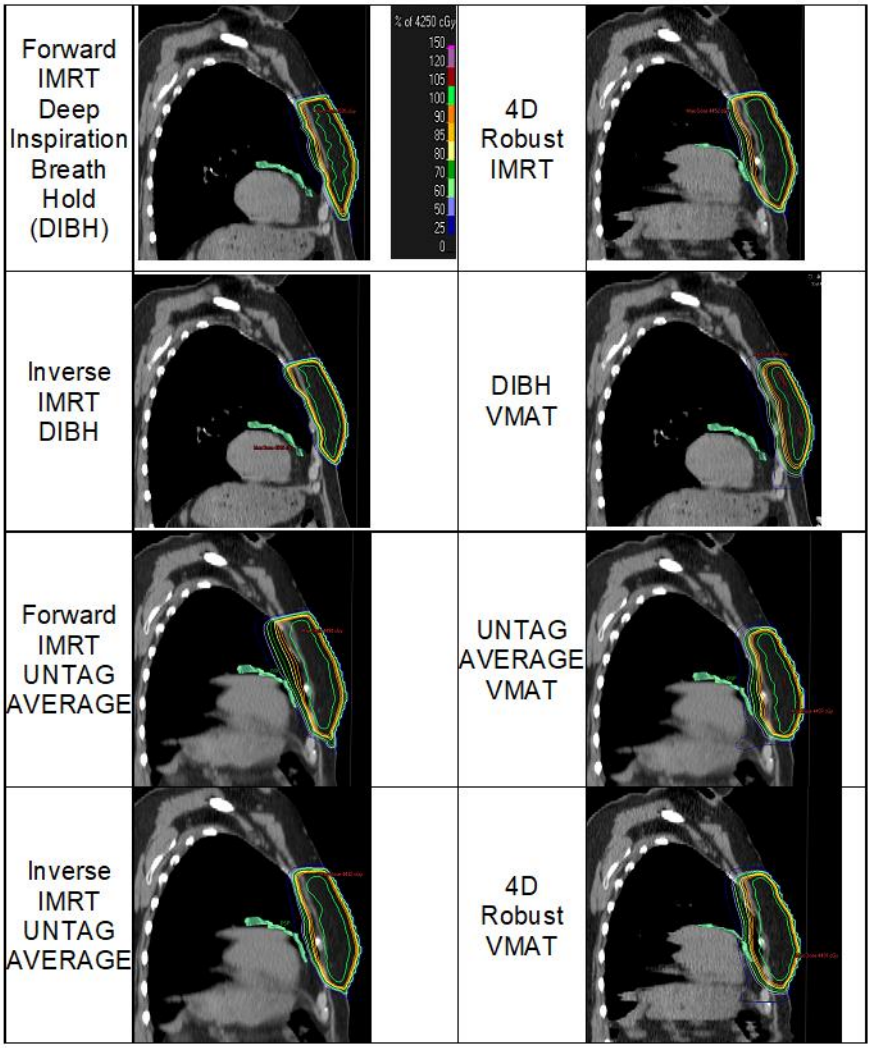

Figure 3.1 Whole-breast radiation treatment methods, with corresponding dose distribution of a representative left-sided breast cancer patient. The left anterior descending artery was three-dimensionally segmented in green on each CT image. Note that the 4D Robust and UNTAG AVERAGE radiation treatments were planned on the same 4D-CT dataset, but for simplicity, the dose distributions of 4D Robust technique were overlaid on the end-inspiration CT image of the 4D-CT dataset.

All cardiac and substructure dose metrics obtained from the eight planning techniques fulfilled the literature recommended constraints.[11] This included a mean heart dose below 330 cGy which was reported by Saiki et al. in breast cancer patients with outcomes of congestive heart failure;[22] and below 280 cGy which was corresponded to a significant elevated risk in coronary heart disease from a peptic ulcer disease study.[23] Furthermore,

all methods achieved a V_{5Gy}Heart <12%, mean LV dose <670 cGy, mean LAD dose <2380 cGy and a max LAD dose <4780 cGy, which were reported by Skyttä et al in patients who received breast radiotherapy with an outcome of >30% increase in cardiac damage biomarker, serum troponin T (hscTNT).[24] The mean LAD dose was below 1000 cGy, which was the suggested constraint from the Expert Panel of the German Society of Radiation Oncology (DEGRO).[25] And the max LAD dose was below 4540 cGy, which corresponded to a lower risk of radiation induced cardiac death presented by Beaton et al.[10]

All dose parameters, apart from the mean heart dose, were not normally distributed ($p < 0.05$) in each of the eight treatment methods, especially for inverse IMRT DIBH. Table 3.2 displayed the mean values for each parameter from the eight treatment planning techniques and the corresponding p-values from Kruskal-Wallis one-way analysis of variance test. Only $V_{50\%}$Lung ($p = 0.29$) was statistically equal among planning techniques.

Table 3.2 Mean values +/- standard deviation of all parameters compared. A p-value <0.05 determines significance from Kruskal-Wallis one-way analysis of variance.

	Mean Heart Dose (cGy)	V_{5Gy}Heart (%)	Mean LV Dose (cGy)	Mean LAD Dose (cGy)	Max LAD Dose (cGy)	$V_{50\%}$Lung (%)
Forward IMRT DIBH	74 ± 27	1.12 ± 1.43	89 ± 29	231 ± 141	976 ± 744	3.04 ± 1.54
Inverse IMRT DIBH	70 ± 30	1.37 ± 1.55	82 ± 34	242 ± 175	1112 ± 842	2.61± 1.29
Forward IMRT Untag Average	148 ± 58	4.06 ± 2.25	192 ± 68	453 ± 229	2351 ± 1057	3.44 ± 1.59
Inverse IMRT Untag Average	121 ± 38	3.43 ± 1.84	172 ± 6	379 ± 265	1987 ± 1268	2.4 ±1.2
4D Robust IMRT	120 ± 52	2.69 ± 1.82	170 ± 74	258 ± 120	1444 ± 959	2.28 ± 1.62
DIBH VMAT	147 ± 13	1.75 ± 1.7	176 ± 25	296 ± 123	1059 ± 743	3.22 ± 0.6
Untag Average VMAT	188 ± 36	5.39 ± 2.04	246 ± 56	370 ± 173	1530 ± 753	2.97 ± 1.25
4D Robust VMAT	173 ± 45	4.42 ± 2.56	245 ± 82	299 ± 101	1220 ± 716	3.13 ± 1.16
p-value	**<0.0001**	**<0.0001**	**<0.0001**	**0.008**	**.002**	**.287**

Results from Wilcoxon-Mann-Whitney test showed that only forward and inverse IMRT DIBH technique were considered as equal for all dose parameters ($p > 0.05$). (See table 3.3)

Table 3.3 P-values of each parameter obtained from Wilcoxon-Mann-Whitney test comparing each planning method to Forward IMRT DIBH technique. A significance value < 0.05 determines significance difference compared to Forward IMRT DIBH technique.

	Planning Method	Inverse IMRT DIBH	Forward IMRT Untag Average	Inverse IMRT Untag Average	4D Robust IMRT	DIBH VMAT	Untag Average VMAT	4D Robust VMAT
P-value	Mean Heart Dose (cGy)	.62	.00	.00	.00	.00	.00	.00
	V_{5Gy}Heart (%)	.68	.00	.00	.01	.19	.00	.00
	Mean LV Dose (cGy)	.33	.00	.00	.00	.00	.00	.00
	Mean LAD Dose (cGy)	.84	.00	.07	.41	.06	.01	.02
	Max LAD Dose (cGy)	.57	.00	.02	.16	.84	.02	.27
	$V_{50\%}$Lung (%)	.41	.51	.25	.22	.62	.97	.78

In figure 3.2a-f, significant difference between parameters from each planning methods compared to forward IMRT DIBH was indicated with *. Table 3.4 shows the p-value results from Wilcoxon-Mann-Whitney test comparing each parameter between IMRT and VMAT and between 4D Robust optimization, DIBH and standard 4D UNTAG AVERAGE treatment plans.

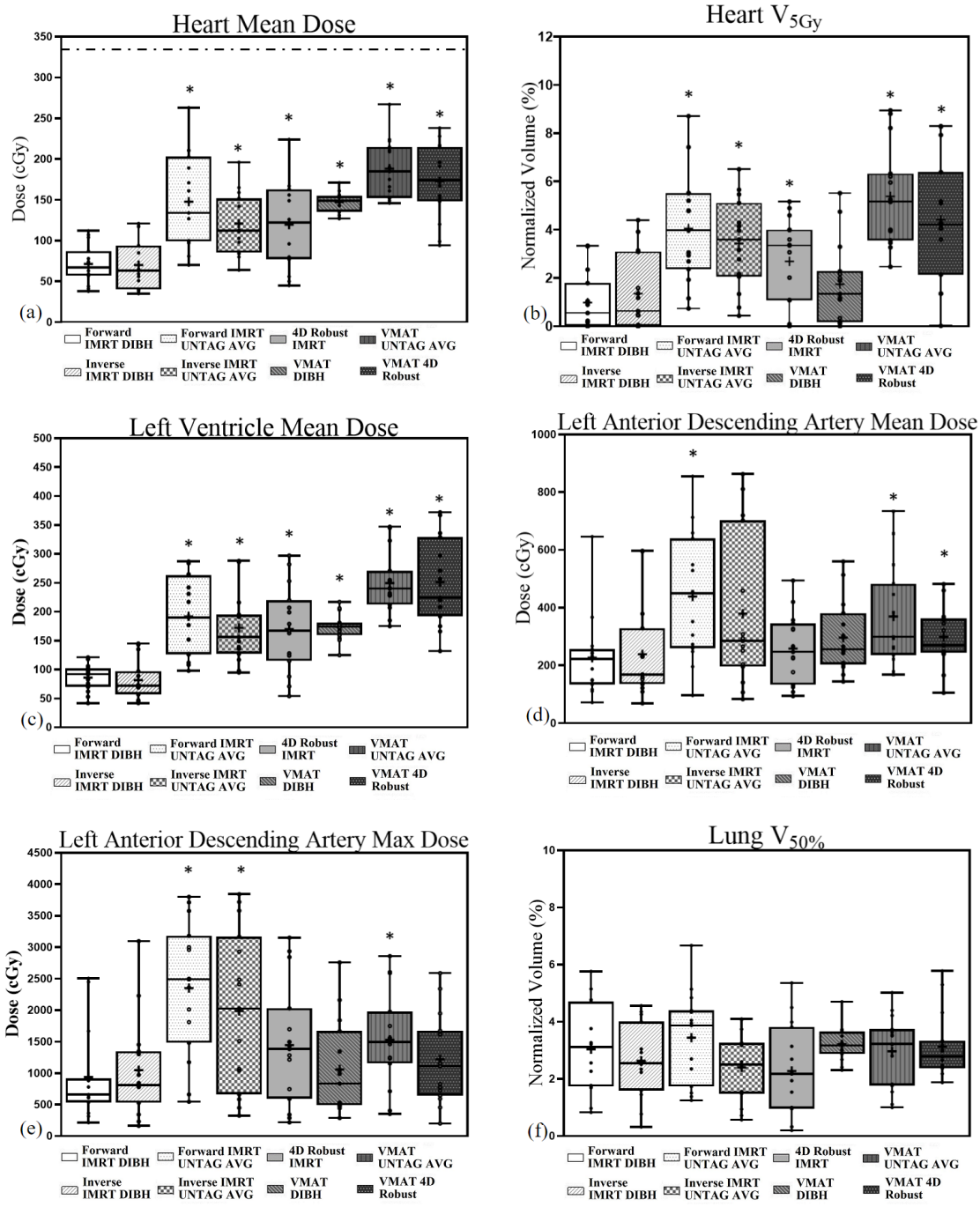

Figure 3.2 Boxplot displaying (a) mean heart dose, under literature threshold of 330 cGy. (b) V_{5Gy}Heart (c) mean left ventricle dose (d) mean left anterior descending artery dose (e) max left anterior descending artery dose (f) $V_{50\%}$ Lung. The plots whiskers displayed the minimum and the maximum value, the mean value was indicated with '+'. Wilcoxon-Mann-Whitney test results of significance difference between planning methods compared to forward IMRT DIBH technique was indicated with *.

Table 3.4 The p-value results from Wilcoxon-Mann-Whitney test comparing each parameter between free-breathing IMRT and VMAT and between 4D Robust, DIBH and standard 4D UNTAG AVERAGE treatment plans.

	Planning Method	Forward vs Inverse IMRT Untag Average	Inverse IMRT Untag Average vs 4D Robust IMRT	Inverse IMRT Untag Average vs Untag Average VMAT	4D Robust IMRT vs 4D Robust VMAT	Untag Average VMAT vs 4D Robust VMAT	DIBH VMAT vs 4D Robust VMAT
P-value	Mean Heart Dose (cGy)	0.237	0.934	**<0.001**	**0.011**	0.561	0.051
	V_{5Gy}Heart (%)	0.548	0.281	**0.026**	**0.034**	0.395	**0.004**
	Mean LV Dose (cGy)	0.547	0.95	**0.002**	**0.007**	0.852	**0.001**
	Mean LAD Dose (cGy)	0.431	0.407	0.724	0.272	0.351	0.724
	Max LAD Dose (cGy)	0.419	0.254	0.443	0.604	0.272	0.419

In correspondence to objective (2) to address whether 4D Robust optimization can outperform DIBH and standard 4D, figure 3.2a-2f showed that 4D Robust IMRT had statistically significantly greater V_{5Gy}Heart, mean heart and LV dose compared to DIBH IMRT ($p \leq 0.01$), except for mean and max LAD dose ($p > 0.1$). In comparison, DIBH with forward IMRT achieved a significant reduction in mean heart dose, V_{5Gy}Heart, mean LV and max LAD dose compared to free-breathing UNTAG AVERAGE IMRT ($p \leq 0.02$) except for mean LAD dose ($p = 0.07$). In table 3.5, among free-breathing methods, no difference in all cardiac and substructure dose including LAD and LV parameters were found ($p > 0.2$) in comparing between forward and inverse IMRT UNTAG AVERAGE, between inverse IMRT UNTAG AVERAGE and 4D Robust IMRT, and between UNTAG AVERAGE VMAT and 4D Robust VMAT. Among VMAT techniques, V_{5Gy}Heart and mean LV dose were significantly reduced in DIBH ($p < 0.005$) compared to 4D Robust VMAT, mean heart and LAD dose, max LAD dose were not different.

In correspondence to objective (3) to address the clinical feasibility, to determine whether we can reduce the complexity by using IMRT instead of VMAT. From figure 3.2a-f, DIBH IMRT had significantly less mean heart and LV dose ($p < 0.01$) than DIBH VMAT, whereas V_{5Gy}Heart, mean LAD and max LAD dose were not different ($p \geq 0.05$). And from table 3.4, inverse IMRT UNTAG AVERAGE had significantly less mean heart and LV dose, V_{5Gy}Heart compared to UNTAG AVERAGE VMAT ($p < 0.02$), mean and max LAD dose were not different ($p > 0.4$). Furthermore, 4D Robust IMRT had significantly less mean heart and LV dose and V_{5Gy}Heart, compared to 4D Robust VMAT ($p < 0.04$), mean and max LAD dose were not different ($p > 0.2$).

3.4 Discussion

In breast cancer patients, it is recommended to minimize the irradiated cardiac volume without compromising the target coverage to reduce the risk of radiation induced cardiac toxicity (RICT) without additional risk of recurrence in their later life post radiotherapy. Radiation-induced cardiac effects in early stage can lead to microvascular injuries caused by irradiating the myocardial endothelial cells, that can lead to acute inflammatory response, vascular damage and fibrosis.[26] Macrovascular damage can be seen as a latent effect, where the atherosclerotic process accelerates in the coronary arteries. Therefore, it is important to minimize the radiation toxicity with the use of sparing techniques, which reduce the heart and its substructures from radiation.

This comprehensive treatment planning study investigated cardiac sparing techniques including respiratory motion management techniques such as 4D-CT encompassment and DIBH, as well as advanced radiation therapy techniques such as forward/inverse IMRT and VMAT. The scope of treatment planning techniques evaluated in this study has not been comprehensively performed in the literature. The heart and its substructure doses including the mean dose to the LAD and left ventricle and max dose to LAD were evaluated in each plan. We were able to achieve clinically acceptable plans for all 8 techniques including 4D Robust optimization according to current guidelines from QUANTEC and the literature[10-11, 22-25]. Thus, we have shown the capability and clinical

feasibility of free-breathing 4D-CT based RT for patients who are not compliant with breath-hold RT and for centres where DIBH is limited.

In this study, 4D Robust IMRT had significantly greater cardiac and LV dose compared to DIBH IMRT ($p \leq 0.01$), but mean and max LAD dose were not different ($p > 0.1$). Furthermore, no significant difference between free-breathing IMRT methods (UNTAG AVERAGE IMRT and 4D Robust IMRT) was found. The mean LAD dose was not different comparing inverse UNTAG AVERAGE IMRT and DIBH IMRT ($p \geq 0.07$). This proved the use of 4D Robust Optimization was clinically feasible for patients who are not compliant with breath-hold and provided a further limitation of radiation dose to the LAD, but not to the heart and LV during free-breathing IMRT treatment (compared to standard 4D-CT based RT). In the literature, tangential treatment planning reported a mean heart dose and/or mean LV dose reduction using DIBH tangential RT in comparison to free-breathing tangential RT.[13, 27-29] Note however, these studies did not consider 4D-CT data sets and 4D Robust Optimization. In contrast, our results showed that DIBH IMRT can significantly reduce the heart and LV dose but not LAD dose compared to free-breathing techniques. These results agreed with Mahmoudzadeh et al., who showed that 4D Robust Optimization can potentially reduce, but not fully replace, the need for breath-hold in the tangential IMRT and can be applied to any case treated under free-breathing.[20]

Insignificant differences in all dose parameters ($p > 0.05$) between UNTAG AVERAGE VMAT and 4D Robust VMAT, along with significant reduction in mean LV dose and V_{5Gy}Heart ($p < 0.01$) in DIBH VMAT compared to UNTAG AVERAGE VMAT were found in our study. However, mean heart and LAD dose and max LAD dose were not different compared to DIBH VMAT and 4D Robust VMAT. This is contrary to the findings reported by Sakka et al.[28] in which mean heart and LAD dose in DIBH VMAT were significantly reduced compared to free-breathing VMAT. Therefore, the use of 4D Robust Optimization provided further radiation dose reduction to the LAD, but not the heart nor the LV compared to DIBH and standard 4D-CT based VMAT.

Significant reduction in mean heart and mean LV dose were observed in DIBH tangential IMRT compared to DIBH VMAT in our study ($p < 0.01$). This result was aligned with literature findings.[4, 29] Significant reduction in mean heart and LV dose and V_{5Gy}Heart were observed in 4D-CT based-IMRT compared to 4D-CT based VMAT ($p < 0.04$). This was supported by Sakka et al. findings of mean heart dose reduction in free-breathing IMRT compared to free-breathing VMAT.[28] This proved that the use of IMRT for its simplicity over VMAT was sufficient to provide the same dosimetic advantage for both 4D-CT based free-breathing and DIBH RT.

$V_{50\%}$Lung dose among all eight planning methods were statistically insignificant. Based on literature, Aznar et al. concluded that the lung exposure in breast cancer RT varied substantially between different countries and regimens, so the radiation related toxicity risk of lung cancer, pneumonitis and lung fibrosis can also vary.[30] Using breathing adaptation, prone or lateral decubitus patient positioning technique can further minimize the irradiated lung region and extent.[30]

Limitations of this study included the following: (1) twelve of the fifteen patients were qualitatively chosen for DIBH treatment based on the heart location and the expected irradiated volume under standard breast RT. Therefore, the results of this study were likely biased towards DIBH being the ideal treatment technique. However, VMAT and IMRT under 4D CT-based free-breathing conditions were still clinically feasible, which aligned with the published guidelines and are potential options for patients who are not compliant with breath-hold treatment, for situations where the distance between the heart and the chest wall is large, or in situations where centres are not able to offer DIBH; (2) The time duration per respiratory phase was not considered in 4D Robust optimization dose calculation; (3) Visualizing the LAD on both 4D-CT and DIBH CT datasets is difficult without the use of intravenous iodine contrast; (4) the time taken for contouring the LAD and LV and DIBH in IMRT/VMAT was not considered in this study, in future studies, cardiac atlas and automations can be utilized to improve the treatment planning efficiency in sparing of the cardiac substructures.

This study tested for the statistical significance for various heart sparing radiotherapy techniques including 4D Robust Optimization and DIBH, which aimed to provide breast cancer patients with the optimal treatment approach taking into account cardiac sparing, target coverage, and treatment complexity. In the future, clinical significance must be evaluated, including functional cardiac imaging and clinical outcomes, in order to establish a dose response relationship that can be used to drive future dose optimization objectives (ie. Cardiac substructures). Currently, there is minimal study (Beaton et al.[10]) that investigate the correlation of cardiac substructure radiation dose towards a clinical end point in the breast cancer population. This information may help aid in the design of new patient-specific treatment strategies that aim to minimize inadvertent heart damage and provide better dose constraint consensus guidelines for better quality radiation treatment standards.

3.5 Conclusions

This study demonstrated the clinical feasibility of free breathing 4D-CT based optimization in limiting radiation dose to the heart and its substructures with both IMRT/VMAT for an early-stage left-sided breast cancer patient cohort. 4D Robust Optimization cannot fully replace DIBH nor outperform standard 4D-CT based IMRT/VMAT except in terms of minimizing the LAD dose. In comparison, both forward and inverse IMRT DIBH technique was dosimetrically advantageous in heart sparing. This was compared to standard 4D-CT and DIBH based VMAT, 4D-CT Robust optimization and other free-breathing IMRT treatment techniques, given that the simplicity of IMRT in cardiac and substructure sparing outperformed VMAT technique. Despite the dosimetric advantage of DIBH with fixed-beam IMRT, all techniques had clinically acceptable plans according to published guidelines. Therefore, free breathing 4D-CT based techniques may be considered for patients who are not compliant for DIBH, where the heart and chest wall are far apart, or for centres where DIBH treatments are not available.

3.6 References

[1] Early Breast Cancer Trialists' Collaborative Group (EBCTCG), Darby S, McGale P, et al.: Effect of radiotherapy after breast-conserving surgery on 10-year recurrence and 15-year breast cancer death: meta-analysis of individual patient data for 10,801 women in 17 randomised trials. Lancet. 2011, 378:1707-1716.

[2] Van den Bogaard VAB, Ta BDP, van der Schaaf A, et al.: Validation and modification of a prediction model for acute cardiac events in patients with breast cancer treated with radiotherapy based on three-dimensional dose distributions to cardiac substructures. J Clin Oncol. 2017, 35:1171-1178.

[3] Byrne M, Archibald-Heeren B, Hu Y, et al.: Comparison of semiautomated tangential VMAT with 3DCRT for breast or chest wall and regional nodes. J Appl Clin Med Phys. 2018, 19:684-693.

[4] Karpf D, Sakka M, Metzger M, and Grabenbauer G G: Left breast irradiation with tangential intensity modulated radiotherapy (t-IMRT) versus tangential volumetric modulated arc therapy (t-VMAT): Trade-offs between secondary cancer induction risk and optimal target coverage. Radiat Oncol. 2019, 14:156.

[5] Beckham WA, Popescu CC, Patenaude VV, et al.: Is multibeam IMRT better than standard treatment for patients with left-sided breast cancer? Int J Radiat Oncol Biol Phys. 2007, 69:918-924.

[6] Henson K, McGale P, Darby S, Parkin M, Wang Y and Taylor C.: Cardiac mortality after radiotherapy, chemotherapy and endocrine therapy for breast cancer: Cohort study of 2 million women from 57 cancer registries in 22 countries. Int J Cancer. 2020, 147:1437-1449. 10.1002/ijc.32908

[7] Darby SC, Ewertz M, McGale P, et al.: Risk of ischemic heart disease in women after radiotherapy for breast cancer. N Engl J Med. 2013, 368:987-998.

[8] Nilsson G, Holmberg L, Garmo H, et al.: Distribution of coronary artery stenosis after radiation for breast cancer. J Clin Oncol. 2012, 30:380-386. 10.1200/JCO.2011.34.5900

[9] Arslan A, Aktas E, Sengul B, Tekin B: Dosimetric evaluation of left ventricle and left anterior descending artery in left breast radiotherapy. Radiol Med. 2021, 126:14-21.

[10] Beaton L, Bergman A, Nichol A, et al.: Cardiac death after breast radiotherapy and the QUANTEC cardiac guidelines. Clin Transl Radiat Oncol. 2019, 19:39-45.

[11] Gagliardi G, Constine L, Moiseenko V, et al.: Radiation dose-volume effects in the heart. Int J Radiat Oncol Biol Phys. 2019, 104:219-220.

[12] Mast ME, van Kempen-Harteveld L, Heijenbrok MW, et al.: Left-sided breast cancer radiotherapy with and without breath-hold: Does IMRT reduce the cardiac dose even further?. Radiother Oncol. 2013, 108:248-253.

[13] Mohamad O, Shiao J, Zhao Bo, et al.: Deep inspiration breathhold for left-sided breast cancer patients with unfavorable cardiac anatomy requiring internal mammary nodal irradiation. Pract Radiat Oncol. 2017, 7:e361-367.

[14] Vikström J, Hjelstuen MHB, Mjaaland I, and K. I Dybvik: Cardiac and pulmonary dose reduction for tangentially irradiated breast cancer, utilizing deep inspiration breath-hold with audio-visual guidance, without compromising target coverage. Acta Oncol. 2011, 50:42-50.

[15] Nissen HD and Appelt AL: Improved heart, lung and target dose with deep inspiration breath hold in a large clinical series of breast cancer patients. Radiother Oncol. 2013, 106:28-32.

[16] Byrne M, Hu Y and Archibald-Heeren B: Evaluation of RayStation robust optimisation for superficial target coverage with setup variation in breast IMRT. Australas Phys Eng Sci Med. 2016, 39:705-716.

[17] Jensen CA, Roa AMC, Johansen M, et al.: Robustness of VMAT and 3DCRT plans toward setup errors in radiation therapy of locally advanced left-sided breast cancer with DIBH. Phys Medica. 2018, 45:12-18.

[18] Fredriksson A, Forsgren A and Hårdemark B: Minimax optimization for handling range and setup uncertainties in proton therapy. Med Phys. 2011, 38:1672-1684.

[19] El-Sherif O, Yu E, Xhaferllari I, and Gaede S: Assessment of intrafraction breathing motion on left anterior descending artery dose during left-sided breast radiation Therapy. Int J Radiat Oncol Biol Phys. 2016, 95:1074-1082. 10.1016/j.ijrobp.2016.02.026

[20] Mahmoudzadeh H, Lee J, Chan TCY, and Purdie TG: Robust optimization methods for cardiac sparing in tangential breast IMRT. Med Phys. 2015, 42:2212-2222.

[21] Radiation Therapy Oncology Group. (Breast cancer atlas for radiation therapy planning: consensus definitions. (2009). Accessed March 20). https://www.rtog.org/LinkClick.aspx?fileticket=vzJFhPaBipE%253D&tabid=236.

[22] Saiki H, Petersen I, Scott CG, et al.: Risk of heart failure with preserved ejection fraction in older women after contemporary radiotherapy for breast cancer. Circulation. 2017, 135:1388-1396.

[23] Carr ZA, Land CEL, Kleinerman RA, et al.: Coronary heart disease after radiotherapy for peptic ulcer disease. Int J Radiat Oncol Biol Phys. 2005, 61:842-850.

[24] Skyttä T, Tuohinen S, Boman E, et al.: Troponin T-release associates with cardiac radiation doses during adjuvant left-sided breast cancer radiotherapy. Radiat Oncol. 2015, 10:141.

[25] Piroth MD, Baumann R, Budach W, et al.: Heart toxicity from breast cancer radiotherapy: Current findings, assessment, and prevention. Strahlenther Onkol. 2019, 195:1-12.

[26] Sardaro A, Petruzzelli MF, D'Errico MP, et al.: Radiation-induced cardiac damage in early left breast cancer patients: Risk factors, biological mechanisms, radiobiology, and dosimetric constraints. Radiother Oncol. 2012, 103:133-142.

[27] Bolukbasi Y, Saglam Y, Selek U, et al.: Reproducible deep-inspiration breath-hold irradiation with forward intensity-modulated radiotherapy for left-sided breast cancer significantly reduces cardiac radiation exposure compared to inverse intensity-modulated radiotherapy. Tumori. 2014, 100(2):168-178.

[28] Sakka M, Kunzelmann L, Metzger M and Grabenbauer G, et al.: Cardiac dose-sparing effects of deep-inspiration breath-hold in left breast irradiation. Strahlenther Onkol. 2017, 193:800-811.

[29] Pham TT, Ward R, Latty D, et al.: Left-sided breast cancer loco-regional radiation therapy with deep inspiration breath-hold: Does volumetric-modulated arc radiotherapy reduce heart dose further compared with tangential intensity-modulated radiotherapy? J Med Imaging Radiat Oncol. 2016, 60:545-553.

[30] Aznar MC, Duane FK, Darby SC, et al.: Exposure of the lungs in breast cancer radiotherapy: A systematic review of lung doses published 2010-2015. Radiother Oncol. 2018, 126:148-154.

Chapter 4

4 Assessing Acute Cardiac Inflammation One Month after Left-sided Breast Cancer RT with Hybrid PET/MRI

In this chapter, a pilot study of left-sided breast cancer patients (n = 15) is featured to investigate and demonstrate the feasibility of assessing early inflammation response and cardiac functionality changes at 1-month after radiotherapy using hybrid PET/MRI.

4.1 Introduction

Breast cancer is the most commonly diagnosed cancer and leading cause of cancer death in females worldwide.[1] Adjuvant radiation therapy (RT) of the breast plays a critical role in curative breast cancer management with local and regional control benefits and lower mortality rates.[2] However, patients with left-sided breast cancer are at an increased risk of radiation-related cardiac disease,[3,4] with an increase in the risk for undergoing percutaneous coronary intervention[5] and cardiac mortality,[6] due to the proximity of the heart to the irradiated breast.

A worldwide systematic review on whole breast RT studies after 2014 reported that the heart received a mean of 3.6 Gy heart dose based on 84 left-sided breast cancer studies.[7] The left anterior descending artery (LAD), however, had a substantially higher dose compared to the whole heart, with a mean dose of 12.4 Gy.[7] A linear relationship between major coronary events and mean heart dose of 7.4% per Gy from 2D-breast RT without a threshold, was also reported in a population-based case-control study.[8] However, the early effects of radiation are not well understood and the clinical symptoms do not typically manifest until 10–15 years after RT. It is therefore important to limit the exposure of the heart to ionizing radiation during RT to limit the development of cardiac sequelae.

A previous pre-clinical study of five canines imaged with hybrid ^{18}FDG/PET showed a progressive global inflammatory response during the initial year following RT.[9] ^{18}FDG/PET can identify an inflammatory reaction, as the activated proinflammatory

macrophages preferentially sequester glucose. The increased inflammatory signal uptake was detected as early as one-week post single fraction irradiation of a biologically equivalent LAD dose compared to a standard left breast RT under breath-hold condition.[9] The dose delivered to the whole heart and other coronary arteries were likewise the typical values observed in left breast RT.[7] Immunohistochemistry (CD45) at 12-months confirmed the presence of inflammatory cells.[9]

If inflammation occurs early, preceding but predictive of subsequent cardiac manifestations, then there may be a role for early treatment with anti-inflammatory and/or cardio-protective medication. With the use of multimodality imaging including hybrid positron emission tomography (PET) and magnetic resonance imaging (MRI), simultaneous acquisition over the same anatomical site allows assessment of acute cardiac inflammation and early cardiac irradiation functional changes non-invasively and longitudinally after RT. For optimal ^{18}FDG/PET assessment of the cardiac inflammatory response, suppressing the normal myocardial uptake of ^{18}FDG is required.[10]

Functional MR imaging including cine imaging assesses left ventricular function throughout the cardiac cycle with a short breath-hold of about 15 seconds. It is considered the gold standard for quantifying left ventricular ejection fraction (LVEF), end-diastolic volume (LVEDV) and end-systolic volumes (LVESV).[11] In addition, T1-mapping has the ability to detect pre-clinical myocardial fibrosis. The combination of pre-and post-contrast T1 maps can give a measure of the extracellular volume (ECV), where an increase relates to myocardial fibrosis and correlates to an increasing likelihood of cardiac events.[12] The optimal means of quantifying ECV is during a slow constant infusion of a gadolinium tracer, where a constant concentration of a tracer is supplied to the myocardium during the capture of 3D T1 maps.[13] Lastly, T2 relaxation rate increases correlate with an increase in extracellular water, i.e., edema.

Serial blood work such as high-sensitivity Troponin T (hs-TnT), high-sensitivity C-reactive protein (hs-CRP) and erythrocyte sedimentation rate (ESR) are the common surrogate markers of myocardial injury and inflammation. Hs-TnT level has great diagnostic accuracy in detecting acute myocardial infarction.[14] Meanwhile, hs-CRP with

a level greater than 3 mg/L is associated with higher cardiovascular risk.[15] ESR can identify acute inflammation by measuring the plasma viscosity.[16] These biomarkers can provide subclinical evidence of cardiotoxicity during RT.

4.1.1 Aim

In this study, we investigate the utility of hybrid PET/MRI and serial blood work to detect an early inflammatory response/cardiac functionality changes after radiation therapy in patients with left-sided breast RT.

4.2 Methods

4.2.1 Radiation Treatment and delivery

The clinical pilot study (NCT03748030) was approved by the Western University Human Research Ethics Board (HSREB ID 112991). Of 17 recruited left-sided breast cancer patients, stage T0-T3, one patient was ineligible, and one did not consent. All patients did not have a prior cardiac disease history and one patient was diagnosed with diabetes mellitus. None of the patients received any prior RT to the thorax or breast.

Patients in the study received their RT during 2020-2021. The majority of patients (73%) received standard deep inspiration breath-hold (DIBH) forward planned intensity-modulated radiotherapy (IMRT), 42.5 Gy in 16 fractions and did not receive adjuvant chemotherapy (67%). 7 of the 11 DIBH RT patients received additional boost doses of 10 Gy in 5 fractions. One patient only completed the first five fractions of her radiation treatment and discontinued due to breast swelling, pain and erythema.

Fifteen left-sided breast cancer patients treatment plans were retrospectively reviewed. Treatment planning optimization was performed using the Pinnacle^3 treatment planning system (Philips Radiation Oncology Systems, Fitchburg, USA). Contours of the heart, left ventricle (LV), and left anterior descending artery (LAD) were manually delineated on the treatment planning CT performed on the Philips Brilliance Big Bore CT scanner (Philips Medical Systems) using Mim maestro (Mim Software Inc., Cleveland, USA). The mean values for each dose metrics are shown in table 4.1. Note that this cohort of patients received a low dose in the reported cardiac regions compared to literature.

4.2.2 Imaging

PET/MR imaging was performed on a 3T-hybrid PET/MRI scanner (Biograph mMR Siemens Medical Systems, Malvern, USA) at baseline, within 1-month and within 1-year following the completion of RT. Patients were imaged in the supine position, with serial blood work drawn before imaging. In this paper, we are reporting the results at 1-month follow-up.

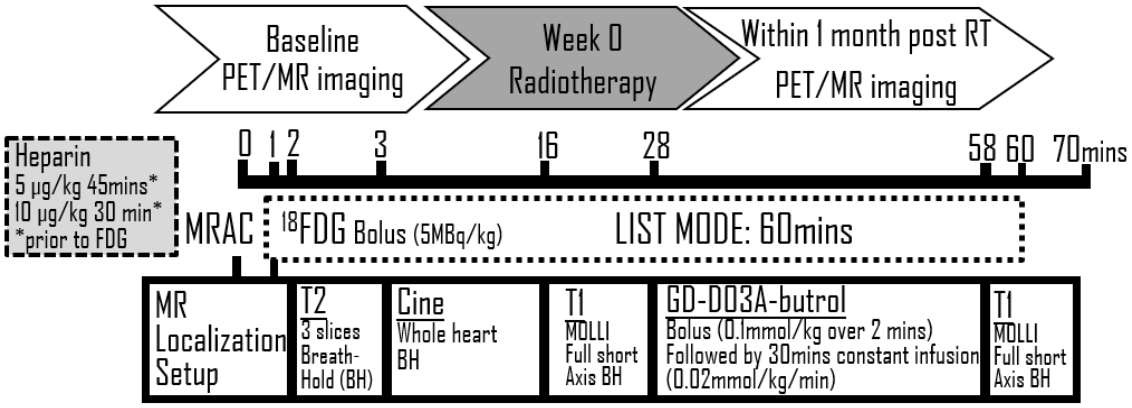

Figure 4.1 Overview of the timeline and hybrid PET/MR imaging protocol

4.2.2.1 PET imaging (Myocardial inflammation)

The suppression of glycolysis was achieved through fasting (12 hours prior imaging) and a 24-hour diet which was high in fat, low in carbohydrate and low in protein prior to the PET scan. Furthermore, the injection of heparin at 45 minutes (5 µg/kg) and 30 minutes (10 µg/kg) was performed prior to the injection of ^{18}FDG. A 60-minute list-mode scan of ^{18}FDG with a bolus injection at 5 MBq/kg was conducted. All PET data were reconstructed using an iterative three-dimensional ordered subset expectation maximization algorithm (OSEM)[17] with 3 iterations, 21 subsets, 10-minutes intervals, 172 x 172 x 127 matrix size and a 4 mm-Gaussian smoothing filter, yielding a voxel size of 2.08 x 2.08 x 2.03 mm. Attenuation was corrected for all PET scans using a two-point Dixon MR imaging pulse sequence (MRAC), which automatically segments and substitutes discrete attenuation coefficients of the lung, adipose tissue and soft tissue.[18] Myocardial contours were manually delineated on the PET images fused with the MRAC images using Mim maestro, according to the American Heart Association 16-segment model.[19]

Myocardial inflammation was assessed using the change from the baseline pre-radiation treatment study in the mean ^{18}FDG/PET standard uptake based on body weight (meanSUV_{bw}) in the myocardial tissue between 40-60 minutes post tracer injection. SUV at 1-month follow-up compared to baseline was calculated where the change was segmented based on each coronary vascular territory: left anterior descending (LAD), left-circumflex (LCX) or right coronary (RC) artery.

4.2.2.2 MR Imaging

T2-weighted images of the heart using 3 slice locations (apex, mid and base) were acquired concurrently with PET imaging using TrueFISP 2D sequence with 224.03 ms repetition time, 1.31 ms echo time, flip angle: 60, FOV matrix of 288 x 360 and slice thickness of 6 mm.

The T2-weighted images were followed by a 2D stack of standard non-contrast steady state free precession cine images and T1-weighted images of the whole heart before and during a gadolinium contrast (Gadovist; Bayer Inc, Mississauga, ON) infusion. The cine images of the whole heart were acquired using TrueFISP sequence, ECG-gated end-diastolic phase, flip angle: 50 degrees, 43.5 ms repetition time, 1.58 ms echo time, FOV matrix = 253 x 300, and a slice thickness of 6 mm.

The gadolinium contrast was injected as a bolus over 2 minutes (0.1 mmol/kg) and then followed by a constant infusion over 30 minutes 0.002 mmol/kg/min). The T1-weighted post gadolinium constant infusion images were acquired 10 minutes into the constant infusion. Both sets of T1-weighted images were acquired using the MOLLI sequence with 293.92 ms repetition time, 1.22 ms echo time, flip angle: 35 degrees, FOV matrix = 255 x 300 and slice thickness 6 mm.

Circle CVI42 v5.11 (Circle Cardiovascular Inc., Calgary, Canada) was used to assess cardiac function, including LV functional parameters (LVEDV, SV and LVEF) and a radiologist (AI) provided clinical assessment of the T2-weighted and T1-weighted post-contrast images. The extracellular volumes (ECV) were calculated using equation (1) with the extraction of T1 values of the blood pool and the myocardium between pre- and during- constant infusion, grouped based into three slices locations (apex, mid and basal). The hematocrit ratio was determined from the blood sample.

$$(1) ECV = (1 - hematocrit\ ratio)\left(\frac{\frac{1}{Post\ contrast\ T1\ myocardium} - \frac{1}{native\ T1\ myocardium}}{\frac{1}{Post\ contrast\ T1\ LV\ blood\ pool} - \frac{1}{native\ T1\ LVblood\ pool}}\right)$$

4.2.3 Bloodwork

Blood for the parameters noted earlier were drawn prior to the baseline pre-radiation scan and measured at 1-month follow-up.

4.2.4 Statistical Analysis

Statistical analyses were performed using SPSS IBM v.23 (IBM SPSS Statistics for Windows, Armonk, NY). Shapiro-Wilk normality test was utilized to check for normality among the values of standard uptake of ^{18}FDG per supplied coronary region, left ventricular functional parameters, blood work and ECV measurements before and 1-month after RT. Based on the Shapiro-Wilk test, all the blood work measurements (hs-TnT, hs-CRP and ESR) were not normally distributed ($p < 0.03$). Consequently, tests of significance for these parameters were performed using the Wilcoxon signed rank test. A paired t-test was performed for all other parameters. A bivariate correlation test was performed to compare these changes to relevant dosimetric parameters of the heart and substructures presented in table 4.1.

Dosimetric parameters of the heart and its substructures were tested for significance between the DIBH and free-breathing-RT group using Mann-Whitney U test. If any of the changes of the ^{18}FDG regional uptake, LV functional parameters, blood work and ECV measurements were significant at follow-up, Mann-Whitney U test was further performed to check for significance between the DIBH and Free-breathing-RT group.

4.3 Results

Table 4.1 Patient demographics of fifteen left-sided breast cancer patients along with the radiation dose metrics of the heart, left ventricle and the left anterior descending artery. The mean value is indicated with *

Age of patients n=15	*60y/o (38 - 79)
Staging	
T_{CIS}	3
T1	8 (1 recurrence BC)
T2	3
T3	1
Radiation Treatment (RT)	
Free-breathing RT	4 (27%)
Tomotherapy	2
IMRT	1
VMAT	1
DIBH IMRT	11 (73%)
Prescription dose	
42.5 Gy in 16 fractions	14
With 10 Gy in 5 fractions boost	7
48 Gy in 16 fractions	1
Mean Heart Dose	*1.79 Gy
Mean LV Dose	*2.07 Gy
Mean LAD dose	*2.78 Gy
$V5_{Gy}$ Heart	*9.46%
Max Heart Dose	*19.31 Gy
Max LAD dose	*8.41 Gy
Adjuvant chemotherapy	
Yes	5 (33%)
Herceptin	4
No	10 (67%)

Patient demographics of the observational study are shown in table 4.1. Results of regional uptake of ^{18}FDG/PET, LV functional parameters, ECV and blood work measurements are presented in figures 4.2 – 4.5. A significant increase in the ^{18}FDG/PET mean standard uptake (meanSUVbw) in the LAD territory ($p = 0.04$, 10%) was seen on average across patients (9 of the 10 patients) at 1-month follow-up. A non-significant correlation was observed between the increase of ^{18}FDG/PET uptake in the LAD territory and the LAD dose metrics (mean and max) with a r-value range of - 0.23 to - 0.24, $p > 0.5$. A non-significant correlation was observed with the heart dose metrics (mean heart dose and $V5_{Gy}$Heart) with a r-value of 0.12 - 0.17, $p > 0.6$ (see table 4.2). The SV was

significantly reduced ($p < 0.02$, 7%, 9 of 12 patients) at 1-month follow-up while LVEDV and LVEF were not significantly changed ($p > 0.08$) The majority of the LV functional parameters were within the normal range, except one patient who had borderline LV dilation.[20] The reduction in stroke volume (SV) was insignificantly correlated to all the heart and substructure dose metrics (r-value of 0.14 - 0.27, $p > 0.27$). In addition, a significant increase for ECV in apex and basal slices were identified (Apex: $p \leq 0.02$ by 6%, 10 of 12 patients and basal: 5%, 11 of 12 patients), while no significant change of ECV was observed for mid slices of the heart ($p > 0.5$). The ECV in apex and basal slice locations were weak to moderately correlated to all the heart, LV and LAD dose metrics (r-value of 0.19 - 0.57).

No significant changes ($p > 0.3$) of all blood work (hs-TnT, hs-CRP, ESR) measurements were reported. No gross abnormal enhancement, fibrosis or edema measured with T1- and T2-weighted images at both baseline and 1-month follow-up were detected. One patient had borderline LV dilation at 1-month follow-up.

For dose metrics, only the mean heart dose ($p = 0.04$) was significantly higher in free-breathing RT compared to DIBH RT patients. Maximum heart and LAD dose, $V5_{Gy}$Heart, mean LV and LAD dose were insignificant ($p \geq 0.06$). Changes of ^{18}FDG/PET uptake at the LAD territory, SV, ECV in apex and basal slices were not different ($p \geq 0.2$) between RT groups.

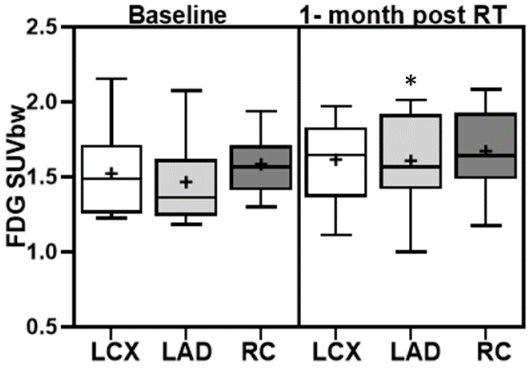

Figure 4.2 ^{18}FDG/PET mean standard uptake values of the myocardium based on body weight (SUVbw) of fifteen patients at baseline and 1-month follow-up. The uptake values for the entire myocardium were broken down to regions supplied by the LAD, LCX and RC. Note the mean standard uptake value is indicated with ‘ + ’ and the median value is indicated as the median bar in the boxplot, any significant differences at 1-month follow-up were marked with *

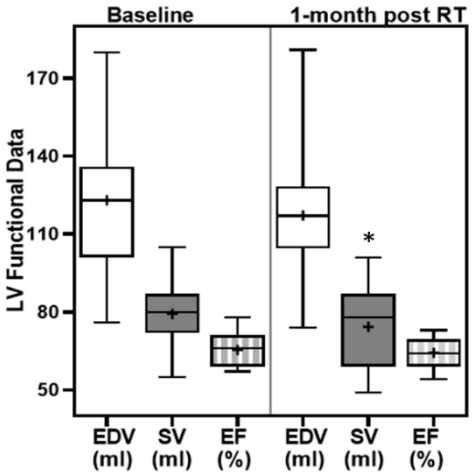

Figure 4.3 Mean cardiac functional parameters including the left ventricular end-diastolic volume (EDV), stroke volume (SV) and the left ventricular ejection fraction (EF) for the fifteen patients before and 1-month after radiotherapy. Significant reduction at 1-month post-RT was shown in SV.

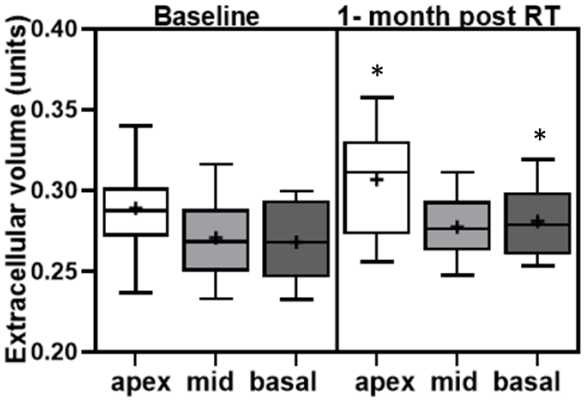

Figure 4.4 Mean Extracellular volume before and 1-month after radiotherapy. Significant increases of ECV in apex and basal slices were observed at 1-month follow-up.

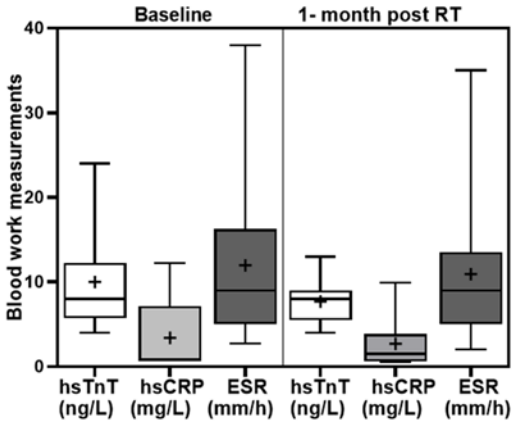

Figure 4.5 Mean blood work measurements of high-sensitivity Troponin T (hs-TnT) high-sensitivity C-reactive protein (hs-CRP) and erythrocyte sedimentation rate (ESR) before and 1-month after radiotherapy.

Table 4.2 Mean values of ^{18}FDG/PET standard uptake of the myocardium based on body weight (SUVbw) sorted according to the respective supplying coronary arteries using the AHA heart model, LV functional parameters (EDV, SV and EF), extracellular volume matrix values (at apex, mid and basal slice locations of the heart) and blood work measurements of high-sensitivity Troponin-T, high-sensitivity C-reactive protein and erythrocyte sedimentation rate at baseline and 1-month follow-up. The percentage comparing baseline and 1-month follow-up change of each respective measurement were reported.

N = 15		**LCX**	**LAD**	**RC**
^{18}FDG/PET meanSUVbw	baseline	1.52	1.47	1.61
	1-month follow-up	1.62	1.61	1.67
	% change	6%	10%	4%
		EDV (ml)	**SV (ml)**	**EF (%)**
Mean values of LV functional parameters	baseline	123	79.27	65.4
	1-month follow-up	115.92	74	64.25
	% change	-6%	-7%	-2%
		Apex	**Mid**	**Base**
Mean extracellular volume (ECV)	baseline	0.289	0.271	0.268
	1-month follow-up	0.307	0.275	0.279
	% change	6%	3%	5%
		hs-TnT (ng/L)	**hs-CRP (mg/L)**	**ESR (mm/h)**

Mean value of Blood Work measurements	baseline	10	3.39	12.64
	1-month follow-up	7.92	2.53	11.42
	% change	-21%	-25%	-10%

Table 4.3 Pearson bivariate correlation coefficient r-values and p-values between the changes of ^{18}FDG/PET standard uptake value in LAD supplied myocardial segments, stroke volume and extracellular volume matrices at apex and basal slices compared to the heart and substructure dose metrics.

Change of parameter		mean Heart dose	mean LV dose	mean LAD dose	$V5_{Gy}$ Heart	max Heart dose	max LAD dose
^{18}FDG LAD	r-value	0.12	0.04	-0.23	0.17	0.07	-0.24
	p-value	0.74	0.91	0.53	0.63	0.85	0.51
SV	r-value	0.25	0.32	0.22	0.21	0.14	0.37
	p-value	0.46	0.34	0.52	0.53	0.69	0.27
ECV apex	r-value	0.34	0.38	0.19	0.30	0.36	0.33
	p-value	0.28	0.22	0.55	0.35	0.26	0.30
ECV base	r-value	0.44	0.44	0.57	0.41	0.41	0.55
	p-value	0.17	0.18	0.07	0.21	0.21	0.08

4.4 Discussion

Currently, dose-sparing guidelines for cardiac substructures are not well established in breast RT. In terms of the whole heart, consensus guidelines recommend that the volume of the heart irradiated should be minimized as much as possible without compromising the breast target coverage. Quantitative Analyses of Normal Tissue Effects in Clinic (QUANTEC) recommended limiting the volume of heart receiving at least 25 Gy ($V25_{Gy}$) to less than 10% to maintain the risk of cardiac mortality under 1%.[21] In our study, the cardiac dose values among patients were lower than the QUANTEC guideline with a mean whole heart $V5_{Gy}$ of 9.46%. However, it is important to note that the LAD and LV can still receive a substantially higher dose than the remainder of the heart structures.[7] The mean LAD dose in our study was 2.78 Gy, which was recognized as a high regional dose region compared to the overall heart (mean heart dose of 1.79 Gy, see table 4.1).

While cardiac risk reduction strategies including the role of active breathing modalities,[22] patient positioning,[23-24] or accelerated partial breast irradiation[25] are discussed, few efforts in randomized controlled trials have validated the cardiac-sparing techniques or looked into the cardiac substructure early response to radiation in breast RT. In exploring differences that three patients received a higher mean heart dose in free-breathing RT, but no differences in other dosimetric parameters of the heart and its substructures compared to DIBH RT patients, this may have implications that DIBH RT can achieve better sparing in terms of the whole heart. With the use of hybrid PET/MRI, the significantly elevated uptake of ^{18}FDG/PET in LAD segments along with the increase of ECV in apical and basal slices with a reduction of SV suggested acute regional inflammation/functional changes in the myocardium as early as 1-month after the end of RT. It is important to note that the changes were observed in patients even with low dose myocardial irradiation compared to the recommended guidelines regardless of breath-hold techniques.

Jo et al.[26] conducted a retrospective study evaluating the irradiated myocardium segmented based on dose threshold in both the staging and post-RT PET/CT images of breast cancer patients who underwent 3D-CRT. The ^{18}FDG/PET uptake of the myocardium irradiated with more than 30 Gy significantly increased after RT even at the one-year follow-up. The degree of ^{18}FDG/PET uptake increase significantly correlated with the radiation dose to the myocardium. However, glucose suppression was not performed. In our study, where glucose was suppressed and the radiated dose to the myocardium was low, the ^{18}FDG/PET uptake increase in the LAD segments was weakly correlated to the whole heart dose metrics. Also of note, the myocardium was segmented according to the AHA heart model, which can provide better location of the radiosensitive substructure of the heart, i.e. the LAD myocardial segments.

In terms of MR functional parameters, our study demonstrated a significant reduction of SV at 1-month follow-up, no significant changes were shown in LVEDV and LVEF. This corresponds to the results of a systematic review conducted by Kaidar-Person et al., [27] which reported five out of six studies without LVEF reduction using SPECT imaging at 6-months follow-up and four studies with perfusion defects. Bergom et al.[28] evaluated

ECV and LV functional parameters in a pilot study of breast cancer patients who received 3D-CRT and adjuvant anthracycline-based chemotherapy using cardiac MR and did not report any clinically abnormal findings at a median follow-up of 8.3 years post RT. No evidence of increased ECV with increasing heart or ventricular radiation doses was reported,[28] contrary to our study which identified a weak to moderate correlation between the increase of ECV (at apex and basal slice locations) and the heart and substructure metrics. However, this study only performed a median long-term follow-up scan; hence, the changes in the LV functional parameters and ECV were not determined. Without measurements performed prior to 6 months, any early postulated effects of radiation on myocardial metabolism are purely conjecture.

Limitations of our study reported here include two patients had insufficient glucose suppression in their baseline ^{18}FDG/PET scan and two patients did not complete the one-month post-RT imaging. However, in the literature, it is reported that five percent of the time the suppression fails even under the best diet and fasting protocols.[29] The sample size of patients between breath-hold and free-breathing RT techniques was small; hence, in future a larger sample size is needed to increase the power of comparison of early cardiac response between RT techniques.

It is unlikely that the 70-minute hybrid PET/MRI protocol used in our study would be routinely used for patient management. Furthermore, it is noted that within 1-month post-RT, none of the patients have had clinically significant cardiac events, and therefore, we do not recommend that these findings influence present clinical practice. However, scar could manifest at a later stage, such that additional care to minimize the volume of cardiac substructure (LAD/LV) in the RT field and longitudinal follow-up are recommended. With patients returning for their 1-year post-RT imaging, longitudinal 1-year follow-up would increase the power to detect subsequent inflammation changes into cardiac sequelae such as progressive fibrosis or scar formation. Such evidence-based information can help establish guidelines to determine the need of cardiovascular risk assessment of patients prior to initiation of RT and long-term cardiovascular monitoring

of breast cancer survivors, in addition to the modification of the cardiovascular risk-based RT regimen.

4.5 Conclusion

In summary, we were successfully able to detect a significant increase of ^{18}FDG/PET uptake in the myocardial territory of the LAD along with a significant increase of extracellular volume matrices at the apex and basal locations of the heart at 1-month following the end of left-sided breast cancer radiotherapy. This may be related to a significant decrease in the left ventricular stroke volume noted at follow-up. No significant changes in blood work measurements including Troponin T, high-sensitivity C-reactive protein and erythrocyte sedimentation rate were seen. Among the fifteen left-sided breast cancer patients, our pilot study demonstrated the feasibility of using hybrid PET/MR imaging to assess cardiac responses to radiotherapy as early as one month follow-up. Validation of these metrics in the prediction of radiation-induced cardiac disease in a larger cohort could prompt a change in management of left-sided breast cancer patients with early cardiac changes detected with non-invasive imaging.

4.6 References

[1] Sung H, Ferlay J, Siegel R, Laversanne M, Isabelle S, et al. (2021) Global Cancer Statistics 2020: GLOBOCAN Estimates of Incidence and Mortality Worldwide for 36 Cancers in 185 Countries. CA Cancer J Clin 71(3):209-249.

[2] Early Breast Cancer Trialists Collaboration Group, McGale P, Taylor C, Correa C, Cutter D et al. (2014) Effect of radiotherapy after mastectomy and axillary surgery on 10-year recurrence and 20-year breast cancer mortality: meta-analysis of individual patient data for 8135 women in 22 randomised trials. Lancet 9935(1):2127-2135.

[3] Correa C, Litt H, Hwang W-T, Ferrari V, Solin L et al. (2007) Coronary artery findings after left-sided compared with right-sided radiation treatment for early-stage breast cancer. J Clin Oncol 25(21):3031-3037.

[4] McGale P, Darby S, Hall P, Adolfsson J, Bengtsson N-O et al. (2011) Incidence of heart disease in 35000 women treated with radiotherapy for breast cancer in Denmark

and Sweden. Radiother Oncol 100(2):167-175.

[5] Boero I, Paravati A, Triplett D, Hwang L, Matsuno R et al. (2015) Modern Radiation Therapy and Cardiac Outcomes in Breast Cancer. Int J Radiat Oncol Biol Phys 94(4):700-708.

[6] Henson K, McGale P, Darby S, Parkin M, Wang Y and C. Taylor. (2020) Cardiac mortality after radiotherapy, chemotherapy and endocrine therapy for breast cancer: Cohort study of 2 million womenn from 57 cancer registries in 22 countries. Int J Cancer 147(5):1437-1449.

[7] Drost L, Yee C, Lam H, Zhang L, Wronski M et al. (2018) A systemic review of heart dose in breast radiotherapy. Clin Breast Cancer 18(5):e819-824.

[8] Darby S, Ewertz M, McGale P, Bennet A, Blom-Goldman U et al. (2013) Risk of ischemic heart disease in women after radiotherapy for breast cancer. N Engl J Med 368(11):987-998.

[9] El-Sherif O, Xhaferllari I, Butler J, deKemp R, Renaud J et al. (2019) [18F]FDG cardiac PET imaging in a canine model of radiation-induced cardiovascular disease associated with breast cancer radiotherapy. Am J Physiol Heart Circ Physiol 316(3).

[10] Scholtens A, Verberne H, Budde and Lam M. (2016) Additional Heparin Preadministration Improves Cardiac Glucose Metabolism Suppression over Low-Carbohydrate Diet Alone in ^{18}F-FDG PET Imaging. J Nucl Med 57(4):568-573.

[11] Bellenger N, Davies L, Francis J, Coats A and Pennell D. (2000) Reduction in Sample Size for Studies of Remodeling in Heart Failure by the Use of Cardiovascular Magnetic Resonance. J Cardiovasc Magn Reson 2(4):271-278.

[12] Sado D, Flett A, Banypersad S, White S, Maestrini V et al. (2012) Cardiovascular magnetic resonance measurement of myocardial extracellular volume in health and disease. Heart 98(19):1436-1441.

[13] Smailovic H, Wilk B, Wisenberg G, Sykes, Butler J et al. (2021) Simultaneous measurements of myocardial glucose metabolism and extracellular volumes with hybrid PET/MRI using concurrent injections of Gd-DTPA and [18F]FDG. J Nucl Cardiol.

[14] Reichlin T, Hochholzer W, Bassetti S, Steuer S, Stelzig C et al. (2009) Early

diagnosis of myocardial infarction with sensitive cardiac troponin assays. N Engl J Med 361(9):858-867.

[15] Bassuk S, Rifai N and Ridker P. (2004) High-Sensitivity C-Reactive Protein: Clinical Importance. Curr Probl Cardiol 29(8):439-493.

[16] Harrison M. (2015) Erythrocyte sedimentation rate and C-reactive protein. Aust Prescr 38(3): 93-94.

[17] Hudson H and Larkin R. (1994) Accelerated image reconstruction using ordered subsets of projection data. IEEE Trans Med Imaging 13(4):601-609.

[18] Vontobel J, Liga R, Possner M, Clerc O, Mikulicic F et al. (2015) MR-based attenuation correction for cardiac FDG PET on a hybrid PET/MRI scanner: comparison with standard CT attenuation correction. Eur J Nucl Med Mol Imaging. 42(10):1574-1580.

[19] Cerqueria M, Weissman N, Dilsizian V, Jacobs A, Kaul S et al. (2002) Standardized myocardial segmentation and nomenclature for tomographic imaging of the heart. A statement for healthcare professionals from the Cardiac Imaging Committee of the Council on Clinical Cardiology of the American Heart Association. Circulation,

[20] Maceira A, Prasad S, Khan M and Pennell D. (2009) Normalized Left Ventricular Systolic and Diastolic Function by Steady State Free Precession Cardiovascular Magnetic Resonance. J Cardiovasc Magn Reson 8(3):417-426.

[21] Gagliardi G, Constine L, Moiseenko V, Correa C, Pierce L et al. (2010) Radiation dose-volume effects in the heart. Int J Radiat Oncol Biol Phys 76(3):S77-85.

[22] Eldredge-Hindy H, Lockamy V, Crawford A, Nettleton V, Werner-Wasik M et al. (2015) Active Breathing Coordinator reduces radiation dose to the heart and preserves local control in patients with left breast cancer: Report of a prospective trial. Pract Radiat Oncol 5(1):4-10.

[23] Jenny L-Y, Jason C-H, Sung-Hsin K, Hsing-Min C, Yu-Sen H et al. (2013) Prone breast forward intensity-modulated radiotherapy for Asian women with early left breast cancer: factors for cardiac sparing and clinical outcomes. J Radiat Res 54(5):899-908.

[24] Gortman A, Aherne N, Amalaseelan J, Last A, Westhuyzen J et al. (2020) Long-

term outcomes of patients with conserved breast cancer treated with adjuvant hypofractionated prone breast intensity-modulated radiation therapy. J Med Imaging Radiat Oncol 64(6):845-851.

[25] Ciérvide R, Montero Á, Potdevin G, García J, Aranda M et al. (2021) 5-year results of accerlerated partial breast irradiation (APBI) with SBRT (stereotactic body radiation therapy) and exactrac adaptive gating (Novalis) for very early breast cancer patients: was it all worth it? Clin Transl Oncol 23(11):2358-2367.

[26] Jo I-Y, Lee J-W, Kim W-C, Min C-K, Kim E-S et al. (2020) Relationship between changes in myocardial F-18 fluorodeoxyglucose uptake and radiation dose after adjuvant three-dimensional conformal radiotherapy in patients with breast cancer. J Clin Med 9(3):666.

[27] Kaidar-Person O, Zagar T, Oldan J, Matney J, Jones E et al. (2017) Early cardiac perfusion defects after left-sided radiation therapy for breast cancer: is there a volume repsonse? Breast Cancer Res Treat 164(2):253-262.

[28] Bergom C, Rubenstein J, Wilson J, Welsh A, Ibrahim E-S et al. (2020) A Pilot Study of Cardiac MRI in Breast Cancer Survivors After Cardiotoxic Chemotherapy and Three-Dimensional Conforomal Radiotherapy. Front Oncol 10:1-10.

[29] Larson S, Pieper J, Hulten E, Ficaro E, Corbett J et al. (2020) Characterization of a highly effective preparation for suppresion of myocardial glucose utilization. J Nucl Cardiol 27(3):849-861.

Chapter 5

5 Multimodality Imaging Assessment of the Heart Before and After Stage III Non-small Cell Lung Cancer Radiation Therapy

In this chapter, through collecting comprehensive functional imaging data with imaging sessions before and 6-weeks after NSCLC RT in 2 patients, here we are able to demonstrate the capability of these methods to assess early functional response in the heart after RT.

5.1 Introduction

Radiation may induce unintentional injury of myocardial tissue during and after treatment of non-small cell lung cancer (NSCLC) due to the close proximity of the heart to the target. The Radiation Therapy Oncology Group 0617 clinical trial showed a reduction in median overall survival (OS) for higher radiation doses compared with standard doses in the treatment of NSCLC, with V_{5Gy}Heart being an OS predictor in the first year and median long-term follow-up at the fifth year.[1] Radiation therapy (RT)-related cardiac damage may occur through acute inflammation in both the myocardium and microvasculature and may not be diagnosed until a late stage of the disease. Previously, our laboratory demonstrated, in canines imaged with [^{18}F] fluorodeoxyglucose (^{18}FDG)/positron emission tomography (PET), a progressive global inflammatory response during the initial year after RT.[2] The response was detected as early as 1 week post single fraction irradiation and was confirmed with immunohistochemistry at 12 months.[2]

Early diagnosis of acute myocardial functional responses to RT has allowed timely and appropriate treatment with cardio-protective drugs such as angiotensin-converting enzyme–inhibitors and/or beta-blockers to reduce the mortality associated with radiation.[3,4] However, if inflammation occurs early, preceding but predictive of subsequent functional changes, then there may be a role for early treatment with anti-inflammatory and/or cardio-protective medication.

With the use of multimodality imaging, we aimed to assess the effects of RT on inflammatory response, left ventricular function, and myocardial perfusion noninvasively as early as 6 weeks post RT. ^{18}FDG/PET with glucose suppression of normal myocytes can identify an inflammatory reaction, as the activated proinflammatory macrophages preferentially sequester glucose, for example, cardiac sarcoidosis.[5] In addition, both functional computed tomography (CT) and magnetic resonance imaging (MRI) are often used to quantitatively measure cardiac function to assess cardiac injury after RT. CT perfusion has been shown to have good diagnostic accuracy to identify hemodynamically significant coronary lesions in comparison to the catheter-based fractional flow reserve technique.[6] Huang et al. previously reported mean CT myocardial perfusion reserve (MPR) values in nonischemic (2.53 ± 0.7) and ischemic segments (1.56 ± 0.41).[7] The capability of functional MRI to acquire cine images of wall motion throughout the cardiac cycle during short breath holds of 10 to 20 seconds has developed as the gold standard for the quantitation of left ventricular ejection fraction (LVEF), end-systolic, end-diastolic, and stroke volumes (SV).[8] Marceira et al. established reference ranges for healthy men (normal 95% confidence interval of LVEF: 58%-75%; left ventricle end-systolic volume (LVESV): 30-75 mL; left ventricle end-diastolic volume (LVEDV): 115-198 mL; and LVSV: 76-132 mL).[9] The reproducibility of cine MRI in identifying patients with heart failure was also verified.[10]

5.2 Case Presentations

In this report, 2 NSCLC patient cases are presented. The patients included in this study were recruited under the clinical trial (RICT-Lung: NCT03416972) in 2019 and under the Western University Health Sciences research ethics board approval (109084). Patient 2 of this study was also recruited under the Canadian PET-BOOST clinical trial (NCT02788461)[11], which was funded by the Canadian Pulmonary Radiotherapy Investigators Group and under the Ontario Cancer research ethics board approval (1215).

5.2.1 Patient Characteristics

Patient 1 (65 years of age) presented with a 4.7 × 3.2 × 4.2 cm moderately differentiated stage III squamous cell carcinoma, T3N2M0,[12] of the left upper lobe, PD-L1 negative (Fig 5.1). Apart from RT, patient 1 received concurrent chemotherapy with carboplatin and paclitaxel for 6 consecutive weeks followed by 1 year of durvalumab immunotherapy. Patient 1 had a history of coronary artery disease (CAD) with 3 prior myocardial infarctions treated with a total of 5 stents in the left circumflex (LCX) and right coronary (RC) arteries (Fig 5.2a). Extensive calcified plaque in the left anterior descending artery (LAD) was also identified in the baseline CT image (Fig 5.2b).

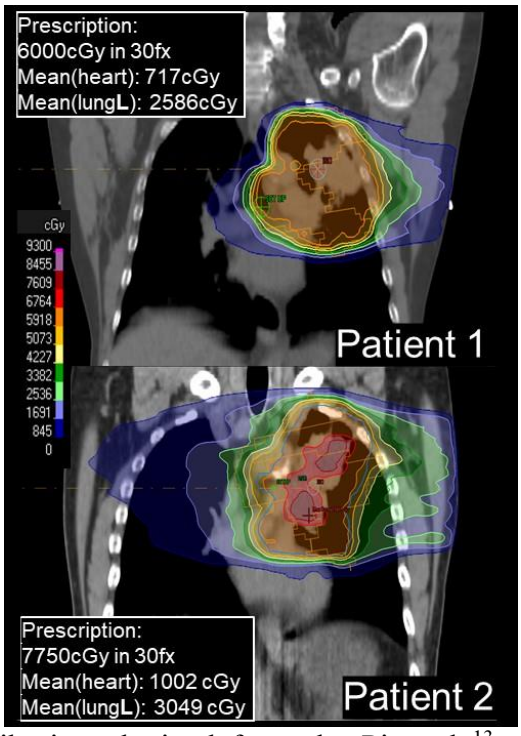

Figure 5.1 Dose distribution obtained from the Pinnacle[13] treatment planning system (Philips Radiation Oncology Systems, Fitchburg) and treatment prescription of each patient, along with their mean heart and left lung doses. Both patients were treated on the 6 MV TrueBeam linear accelerator (Varian Medical Systems, Palo Alto) using volumetric-modulated arc therapy (VMAT). Patient 1 (65 years of age) received standard 60 Gy in 30 fractions. Patient 2 (63 years of age) received 60 Gy in 30 fractions with a simultaneous integrated boost up to 77.5 Gy to the metabolic active tumor subvolume. Note patient 2 received a greater mean heart dose than patient 1.

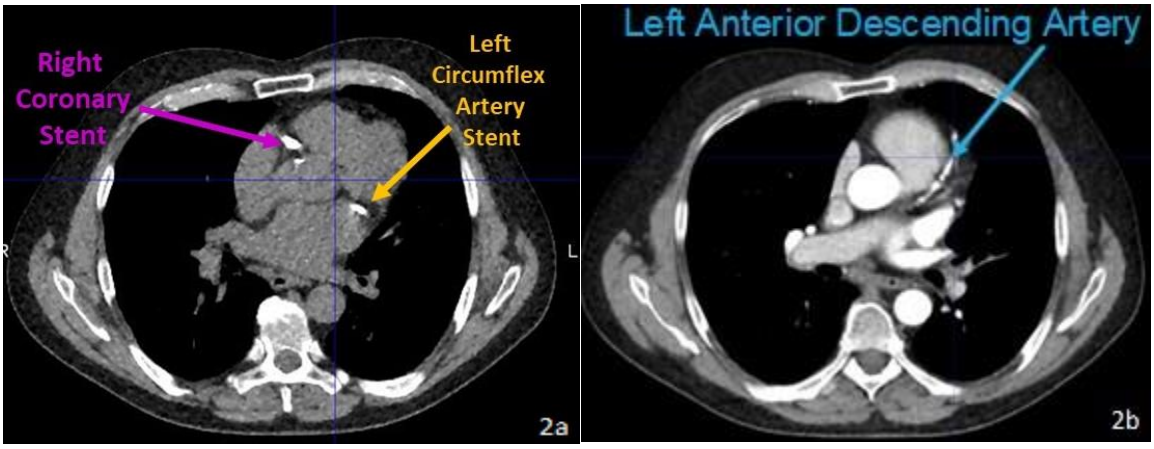

Figure 5.2 (a) Patient 1 presented with a history of coronary artery disease including 3 previous myocardial infarctions and intervention with 5 stents. (b) Patient 1 presented with extensive calcified plaque in the left anterior descending artery.

Patient 2 (63 years of age) presented with a $5.2 \times 5.2 \times 8$ cm poorly differentiated adenocarcinoma, T4N2M0, in the left upper lobe with mediastinal invasion. The tumor was EGFR-negative, ALK-negative, and PD-L1 strongly positive. Patient 2 was treated with concurrent chemotherapy of cisplatin and vinblastine every 21 days for 4 cycles, followed by 1 year of durvalumab immunotherapy.

5.3 Treatment planning and delivery

Both patients were treated with 6 MV beams from a medical linear accelerator (TrueBeam Varian Medical Systems, Palo Alto, CA) using volumetric modulated arc therapy. Treatment planning optimization was performed using the Pinnacle[13] treatment planning system (Philips Radiation Oncology Systems, Fitchburg, MA). Patient 1 was prescribed a standard 60 Gy in 30 fractions to the left upper tumor. For Patient 2, the planning target volume received a dose of 60 Gy in 30 fractions, while a simultaneous integrated radiation boost of 77.5 Gy was delivered to the metabolic active tumor subvolume. The regions of interest for both patients satisfied the dosimetric guidelines of a standard 60 Gy in 30 fractions NSCLC RT plan in our clinic.

Patient 1 received a mean dose of 7.2 Gy to the heart, 1.1 Gy to the left ventricle (LV), 29.8 Gy to the LAD, 2.0 Gy to the LCX, and 1.0 Gy to the RC artery. Patient 2 received a

mean dose of 10.0 Gy to the heart, 4.2 Gy to the LV, 39.8 Gy to the LAD, 2.2 Gy to the LCX, and 1.8 Gy to the RC artery.

In terms of dose distributed in the myocardial segments according to the coronary artery vascular territory, patient 1 received 1.3 Gy to the LCX territory, 0.8 Gy to the LAD territory, and 0.5 Gy to the RC territory, which was less than patient 2, who received 4.2 Gy to LCX territory, 2.8 Gy to the LAD territory, and 1.3 Gy to the RC artery territory.

5.4 Multimodality imaging

Multimodality functional imaging sessions were performed in a single institution at baseline and 6 weeks post RT (see Fig 5.3 for imaging protocol).

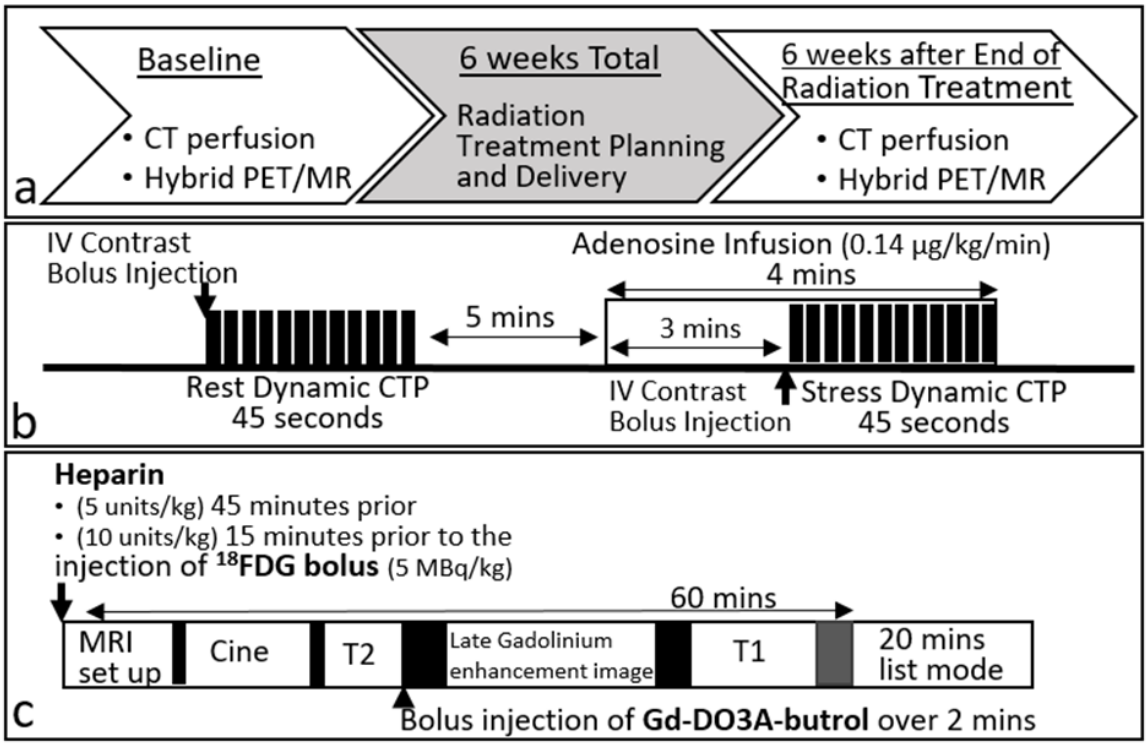

Figure 5.3 Overview of the (a) timeline, (b) CT perfusion, (c) hybrid PET/MRI imaging protocol

5.4.1 CT perfusion

Initially, an electrocardiogram-gated dynamic contrast-enhanced CT (Iopamidol 370; Bracco Diagnostics, Plainsboro, NJ) was performed on a 256 slice-GE Revolution CT

scanner (GE Health care, Waukesha, WI). The scan parameters were the following: 50 cm FOV, 100 kV, 100 mA, 15 passes, minimum 0.8 seconds between passes, 0.28 second rotation time, for a total exposure time of 47.7 seconds. Two free-breathing dynamic scans were obtained including a rest and an adenosine-induced (0.14 μg/kg/min) stress scan. Mid-diastolic phase CT images were selected, non-rigidly registered, and averaged into a slice thickness of 2.5 mm. Myocardial perfusion maps were generated with a model-based deconvolution method[14] using the CT Perfusion software (GE Healthcare), with segments delineated according to the approximately horizontal long-axis 6-segment heart model.[15] Absolute myocardial perfusion at rest and post-adenosine was determined as well as MPR.

5.4.2 Myocardial inflammation

The ^{18}FDG/PET imaging protocol was performed on a 3T-hybrid PET/MR scanner (Biograph mMR; Siemens Medical Systems, Malvern, PA). Both patients fasted for 12 hours before imaging. Intravenous heparin (5 units/kg) was injected initially 45 minutes and then (10 units/kg) 15 minutes before the injection of ^{18}FDG (5 MBq/kg). PET imaging acquisition was performed in list mode 1 hour after the second injection for 20 minutes, whereas a bellows device was used for respiratory triggering. All PET data were reconstructed using an iterative 3-dimensional (3D) ordered subset expectation maximization algorithm[16] with 3 iterations, 21 subsets, 172 × 172 × 127 matrix size, and a 4-mm Gaussian smoothing filter, yielding a voxel size of 2.08 × 2.08 × 2.03 mm. Attenuation was corrected for all PET scans using a 2-point Dixon MRI pulse sequence. Mean standardized uptake based on body weight of each myocardium segment was analyzed and compared using MIM v7.0.5 (MIM Software Inc, Cleveland, OH).

5.4.3 MRI

The MR 2D stack of standard non-contrast steady state free precession cine imaging of the whole heart was also performed in the same imaging session as PET. The cine images were collected using the TrueFISP sequence (6 mm slice thickness, 50.82 ms repetition time, 1.58 ms echo time, FOV matrix = 300 × 300). Late gadolinium enhancement (LGE) images were collected using the T1-weighted postcontrast agent (Gadovist; Bayer Inc,

Mississauga, ON) Flash3D sequence, 421.09 ms repetition time, 1.2 ms echo time, flip angle 20, and FOV matrix = 270 × 320. T2-weighted images were acquired using TrueFISP 2D sequence with 262.35 ms repetition time, 1.36 ms echo time, and FOV matrix = 300 × 300. Circle CVI42 v5.11 (Circle Cardiovascular Inc, Calgary, Canada) was used to obtain cardiac functional measurements including the LVEDV, LVESV, LVEF, and SV, and for a radiologist (A.I.) to provide clinical assessment of the LGE and T2-weighted images.

5.5 Results

Both patients manifested a global increase in the ^{18}FDG/PET myocardial uptake at 6 weeks post RT (Table 5.1 and Fig 5.4). For CT MPR measurements, different responses were seen between patient 1 who had CAD and patient 2 who did not. Patient 1 had MPR reduction in half of the segments, while patient 2 had a reduction of MPR in all segments (Tables 5.1 and 5.2).

Table 5.1 ^{18}FDG/PET mean SUVbw and CT MPR values of the 2 patients are presented. Segments with reduction of MPR at 6 weeks post RT were underlined. The uptake and MPR values were sorted according to the respective supplied coronary arteries using the approximately horizontal long-axis heart model.[15] ^{18}FDG/PET increase factor is the calculated ratio of mean ^{18}FDG uptake between follow-up and baseline. MPR value is the ratio between adenosine-induced stress perfusion and rest perfusion

			Left circumflex		Left anterior descending			Right coronary
			Basal lateral	Mid lateral	Apical lateral	Apical septal	Mid septal	Basal septal
^{18}FDG myocardial mean standard mean uptake based on body weight (SUV_{bw})	Patient 1	Baseline	1.92	1.56	1.02	1.33	1.46	1.63
		Follow-up	3.45	3.28	2.6	3.25	4.11	3.44
	Increase factor		1.8	2.1	2.55	2.44	2.82	2.11
	Patient 2	Baseline	1	0.56	0.21	0.73	1.03	1.21
		Follow-up	1.78	1.52	1.02	1.41	1.92	1.97
	Increase factor		1.78	2.71	4.86	1.93	1.86	1.63
CT myocardial perfusion reserve = stress perfusion/ rest perfusion	Patient 1	Baseline	2.42	1.55	1.34	1.58	1.74	2.07
		Follow-up	1.77	2.28	1.07	1.65	2.1	1.74
		Percentage change (%)	–26.9	47.1	–20.2	4.4	20.7	–15.9
	Patient 2	Baseline	2.61	2.27	2.39	2.43	2.78	2.81
		Follow-up	1.37	1.71	1.8	1.66	1.63	1.41
		Percentage change (%)	–47.5	–24.7	–24.7	–31.7	–41.4	–49.8

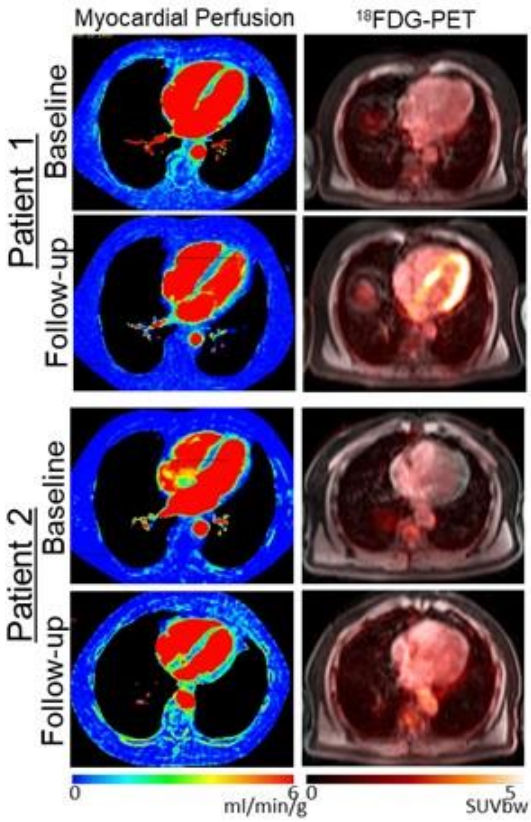

Figure 5.4 Baseline and 6-week follow-up of rest computed tomography (CT) myocardial perfusion images and [^{18}F]fluorodeoxyglucose (^{18}FDG)/positron emission tomography (PET) images of the heart. Note global increase of myocardial uptake can be seen in post radiation therapy (RT) PET imaging of both patients.

Table 5.2 CT myocardial perfusion values under rest and adenosine-induced stress scans of the 2 patients are presented. The perfusion values are sorted according to the respective supplying coronary arteries using the approximately horizontal long-axis heart model.[15]

		Left circumflex		Left anterior descending			Right coronary
	CT perfusion (mL/min/100g)	Basal lateral	Mid lateral	Apical lateral	Apical septal	Mid septal	Basal septal
Patient 1 baseline	Rest	344.72	351.17	605.13	576.93	423.24	471.08
	Stress	834.22	544.32	810.87	911.55	736.44	975.14
Patient 1 follow-up	Rest	142.50	125.72	182.63	178.18	142.69	166.88
	Stress	251.62	287.18	195.04	294.15	298.99	290.67
Patient 2 baseline	Rest	56.02	70.48	81.30	92.51	67.61	60.29
	Stress	146.14	159.67	194.25	224.83	187.89	169.55
Patient 2 follow-up	Rest	119.90	113.14	121.29	161.95	122.03	129.24
	Stress	164.81	193.17	218.86	268.40	198.36	182.18

For both patients, the LVEF was reduced and LVESV was increased at 6 weeks post RT (Table 5.3). For patient 1, an increase in LVEDV and SV was observed, while for patient 2, a reduction in LVEDV and SV was observed at 6 weeks post RT. At follow-up imaging of patient 2, there was a small mid myocardial focus of LGE in the basal inferolateral segment that was not observed at baseline. This corresponded to the region of lowest MPR value. The area of the scar (see Fig 5.5 for scar with LGE) demonstrated a borderline increase in quantitative T2 relaxation up to 53 ms.

Table 5.3 Presented are cardiac functional parameters including the LVESV, LVEDV, SV, and the LVEF for the 2 patients before and after radiation therapy

		LVESV (mL)	LVEDV (mL)	SV (mL)	LVEF (%)
Patient 1	Baseline	49	138	89	65
	Follow-up	55	151	96	64
	% change	11.5	9.2	8	–1.5
Patient 2	Baseline	64	166	102	61
	Follow-up	75	164	89	54
	% change	16.7	–1.4	–12.8	–11.4

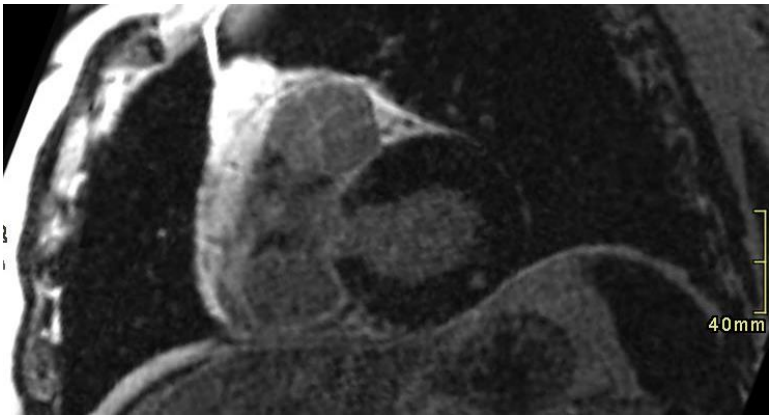

Figure 5.5 6-weeks follow-up Late Gadolinium Enhancement Image of Patient 2 demonstrating a small mid myocardial focus in the basal inferolateral segment

Within 1 year post RT, patient 1 developed increasing cough, shortness of breath after 5 minutes of walking, and hypotension. At 18 months post RT, a slight increase in the size of small pericardial and pleural effusions along with innumerable bilateral pulmonary nodules and new lesions were observed on a follow-up CT thorax image. Based on the evidence of disease progression in the lungs while on durvalumab, patient 1 did not qualify for immunotherapy and passed away at 19 months post RT. For patient 2, no respiratory symptoms, dyspnea on exertion, or chest pain was reported at 1 month follow-up and at every 3 months follow-up to 30 months post RT. No further cardiac functional imaging was performed beyond 6 months for either patient.

5.6 Discussion

Currently in the literature, there is no study comparing the cardiac effects before and after NSCLC RT using multimodality imaging. Most of the studies that assessed cardiac functional response of RT were performed in breast and Hodgkin lymphoma patients.[17,18] Demissei et al. reported a significant increase in cardiovascular biomarkers in patients after completion of lung cancer RT; however, the changes in biomarkers were not significantly associated with the changes in echocardiography-derived measures of cardiac functional parameters (LVEF, longitudinal circumferential strain).[19] Vinogradskiy et al. evaluated ^{18}FDG/PET imaging changes in terms of the whole heart, with the Kaplan-Meier curves showing an overall trend of improved OS, corresponding with increasing mean standard uptake cardiac values.[20] However, the study did not use a protocol for suppression of myocyte glucose uptake, and the time interval between baseline and follow-up imaging (range, 201-1131 days) was inconsistent. Our study is the first to report cardiac functional changes after NSCLC RT using multimodality imaging. Patient 1 CT MPR <2, particularly in the LAD-supplied apical segments at both timepoints, were consistent with the impaired hyperemic response documented in the literature, as indicative of a functionally significant luminal narrowing ≥50% on CT angiography.[21] Patient 2 baseline MPR values were consistent with no hemodynamically significant attenuation of hyperemia, as reported by Huang et al.[7] Different responses were observed in MPR in patient 1 compared with patient 2, who did not have CAD. A global reduction of MPR, with the range of 1.37 to 1.8 at follow-up as measured for patient 2, could now be considered to be indicative of an impaired hyperemic response.[7]

In terms of MR functional parameters, both patients had a reduction in LVEF and increase in LVESV; however, different responses were observed in LVESV and SV in patient 1 compared with patient 2, who did not have CAD. At both imaging timepoints, the MR functional measurements reported for patient 1 were within the normal range, whereas for patient 2 at follow-up, the LVEF was slightly under the normal range by 4%.[9] The LGE of myocardial focus in patient 2 at follow-up may be consistent with local edema suggestive of acute inflammation in the cardiac region, which received the highest

radiation dose. From the ^{18}FDG/PET results, the elevated global myocardial uptake suggested an acute inflammation response to RT for both patients.

It is unlikely that such a complex set of tests used here would be routinely used for patient management. Current routine tests typically include echocardiography and blood work. As a scar would be expected to develop only subsequent to inflammation, the ^{18}FDG/PET signal suggesting inflammation may be more sensitive to a pathologic response to RT than MR, which is looking for scar development. However, the additional step of suppression of myocardial uptake of ^{18}FDG is required for optimal ^{18}FDG/PET test results. The assessment of MPR with any modality (performed here with CT) requires the use of a pharmacologic stressor such as adenosine, which was used in this study.

Our pilot study with 2 patients with NSCLC representing 2 different baseline cardiac conditions demonstrated the feasibility of using multimodality imaging in detecting early functional changes of the heart. The presence of these changes might indicate a risk for late manifestations and may be a focus of future therapeutic interventions to improve radiation-mediated outcomes. Therefore, further long-term follow-up studies in a larger cohort need to confirm the functional responses (^{18}FDG/PET, MPR, and LV function) as accurate predictors of radiation-induced clinically important cardiac toxicity before the routine use of these expensive imaging modalities. If validated, we expect mitigation strategies could be applied and/or developed to protect the heart from radiation toxicity at an early timepoint.

5.7 Conclusions

In summary, these 2 cases demonstrate the feasibility of using multimodality imaging to assess cardiac responses to radiation therapy as early as 6 weeks after the end of radiation therapy. Quantitative assessment included CT perfusion, ^{18}FDG/PET measured inflammation uptake, and MR cardiac functional metrics before and after radiation therapy (6 weeks) that were obtained from 2 dynamic imaging sessions. Both patients with NSCLC experienced a global increase in ^{18}FDG/PET myocardium uptake, increase in LVESV, and decrease in LVEF, while CT MPR and MR functional measurements

suggested a different response in the patient with a history of CAD (regional ranges of CT MPR and increase of LVEDV and SV) compared with the patient with no history of CAD (global MPR, LVEDV, and SV reduction). Validation of these results in additional patients with and without CAD can advance decision making for NSCLC treatment.

This article was published in *Advances in Radiation Oncology*, 7(4), by Oi-Wai Chau, A Islam, E Yu, M Qu, J Butler, H Biernaski, A Sun, J-P Bissonnette, A MacDonald, C Graf, A So, G Wisenberg, T-Y Lee, F S Prato and S Gaede, titled "Multimodality Imaging Assessment of the Heart Before and After Stage III Non-small Cell Lung Cancer Radiation Therapy", 100927, Copyright Elsevier (2022)

5.8 References

[1] Bradley J, Hu C, Komaki R, Masters G, Blumenschein G et al. Long-Term Results of NRG Oncology RTOG 0617: Standard Versus High-Dose Chemoradiotherapy With or Without Cetuximab for Unresectable Stage III Non-Small-Cell Lung Cancer. J clin Oncol. 2020;38(7):706-714

[2] El-Sherif O, Xhaferllari I, Sykes J, Butler J, A. deKemp R et al. [18F]FDG cardiac PET imaging in a canine model of radiation-induced cardiovascular disease associated with breast cancer radiotherapy. Am J Physiol Heart Circ Physiol. 2019;316(3):586-595

[3] Ohtsuka T, Hamada M, Hiasa G, Sasaki O, Suzuki M et al. Effect of beta-blockers on circulating levels of inflammatory and anti-inflammatory cytokines in patients with dilated cardiomyopathy. J Am Coll Cardiol. 2001;37(2):412-417

[4] Kortekaas K, Meijer A, Hinnen JW, Falman R, Xu B et al. ACE inhibitors potently reduce vascular inflammation, results of an open proof-of-concept study in the abdominal aortic aneurysm. PLoS One. 2014;9(12): e111952

[5] Wisenberg G, Thiessen J, Pavlosky W, Butler J, Wilk B et al. Same day comparison of PET/CT and PET/MR in patients with cardiac sarcoidosis. J Nucl Cardiol. 2020; 27(6):2118-2129

[6] Bamberg F, Becker A, Schwarz F, Marcus RP. Greif M et al. Detection of Hemodynamically Significant Coronary Artery Stenosis: Incremental Diagnostic Value of Dynamic CT-based Myocardial Perfusion Imaging. Radiology. 2011; 260(3):689-698

[7] Huang L, Wu MT, Hu C, Mar GY, Lee TY et al. Quantitative low-dose rest and stress CT myocardial perfusion imaging with a whole-heart coverage scanner improves functional assessment of coronary artery disease. Int J Cardiol Heart Vasc. 2019; 24:100381

[8] Grothues F, Smith G, Moon J, Bellenger N, Collins P et al. Comparison of interstudy reproducibility of cardiovascular magnetic resonance with two-dimensional echocardiography in normal subjects and in patients with heart failure or left ventricular hypertrophy. Am J Cardio. 2002; 90(1): 29-34

[9] Maceira A, Prasad S and Pennell D. Normalized left ventricular systolic and diastolic function by steady state free precession cardiovascular magnetic resonance. J Cardiovasc Magn Reason. 2006;8(3): 417-426

[10] Bellenger N, Davies L, Francis J, Coats A and Pennell D. Reduction in Sample Size for Studies of Remodelling in Heart Failure by the Use of Cardiovascular Magnetic Resonance. J Cardiovasc Magn Reason. 2000; 2(4): 271-278

[11] Raman S, Bissonnette J-P, Warner A, Le L, Bratman S et al. Rationale and protocol for a Canadian multicenter Phase II randomized trial assessing selective metabolically adaptive radiation dose escalation in locally advanced non-small-cell lung cancer (NCT02788461). Clin Lung Cancer, 2018; 19(5):699-703

[12] Frank D. The eight edition TNM stage classification for lung cancer: What does it mean on main street? J Thoraic Cardiovasc Surg 2018;155: 356-9

[13] Cadman P, McNutt T and Bzdusek K. Validation of physics improvements for IMRT with a commercial treatment-planning system. J Appl Clin Med Phys. 2005;6(2):74-86

[14] So A, Hsieh J, Li JY, Hadway J, Kong HF and Lee TY. Quantitative myocardial perfusion measurement using CT perfusion: a validation study in a porcine model of reperfused acute myocardial infarction. Int J Cardiovasc Imaging. 2012;28: 1237–48.

[15] Cerqueira M, Weissman N, Dilsizian V, Jacobs A, Kaul S et al. Standardized myocardial segmentation and nomenclature for tomographic imaging of the heart. Circulation. 2002;105(4):539-542

[16] Hudson H, Larkin R. Accelerated image reconstruction using ordered subsets of projection data. Med. Imaging, IEEE Trans. 1994;13:601–609.

[17] Kaidar-Person O, Zagar T, Oldan J, Matney J, Jones E et al. Early cardiac perfusion defects after left-sided radiation therapy for breast cancer: is there a volume response? Breast Cancer Res Treat. 2017;164(2):253-262

[18] Heckmann M, Totakhel B, Finke D, Anker M, Müller-Tidow et al. Evidence for a cardiac metabolic switch in patients with Hodgkin's lymphoma. ESC Heart Failure 2019;6(4);824-829

[19] Demissei B, Freedman G, Feigenberg S, Plastaras J, Maity A et al. Early Changes in Cardiovascular Biomarkers with Contemporary Thoracic Radiation Therapy for Breast Cancer, Lung Cancer, and Lymphoma. Int J Radiat Oncol Biol Phys. 2019;103(4):851-860

[20] Vinogradskiy Y, Diot Q, Jones B, Castillo R, Kwak J et al. Evaluating Positron Emission Tomography-Based Functional Imaging Changes in the Heart After Chemo-Radiation for Patients With Lung Cancer. Int J Radiat Oncol Biol Phys. 2020;106(5):1063-1070

[21] Fiechter M, Ghadri J, Gebhard C, Fuchs T, Pazhenkottil A et al. Diagnostic value of 13N-ammonia myocardial perfusion PET: added value of myocardial flow reserve. J Nucl Med. 2012;53(8):1230-1234

Chapter 6

6 Conclusion and Future work

6.1 Future Work

6.1.1 Longitudinal studies

A larger sample size and longitudinal follow-up studies for both cancer type survivors should be considered to assess the clinical significance of the cardiac dose sparing techniques presented in this thesis (in chapter 3) using multi-modality imaging (presented in chapter 4 and 5) and serial biomarkers, such as troponin, high sensitivity C-reactive protein and natriuretic peptide. It is aimed to detect any clinical end-points (presented in the introduction chapter) which confirms the diagnosis of radiation-induced cardiac disease after treatment and further correlate on cardiac morbidity and cardiac dose sparing distribution.

In this proceeding section, the 1-year follow-up results of the pilot study - RICT-BREAST (NCT03748030, presented in chapter 4) for left-sided breast cancer patients are featured to investigate and demonstrate the clinical feasibility of assessing the medium long-term inflammation response and cardiac functionality changes at 1-year post radiotherapy using hybrid PET/MRI.

In summary, PET/MR imaging cardiac is performed on a 3T-hybrid PET/MRI scanner (Biograph mMR Siemens Medical Systems, Malvern, USA), with serial blood work drawn at baseline, within 1-month and within 1-year following the completion of RT of a total of 15 left-sided breast cancer patients. (see figure 6.1 for the imaging timeline and PET/MRI protocol) A list-mode ^{18}FDG/PET scan with glucose suppression is acquired. Myocardial inflammation is quantified by the change of mean ^{18}FDG standard uptake and analyzed based on the coronary vascular territory (left anterior descending (LAD), left circumflex or right coronary artery). MR assessments, including LV functional and extracellular volume matrices (ECV), are extracted from T1 (pre and during-constant infusion of gadolinium) and cine images, respectively, acquired simultaneously during PET acquisition. Cardiac injury and inflammation biomarker measurements of hs-TnT,

hs-CRP and erythrocyte sedimentation rate are compared at follow-up. At the current stage, five patients had returned for their 1-year follow-up scan. The results of blood work and imaging functional parameters were compared and presented in the following section.

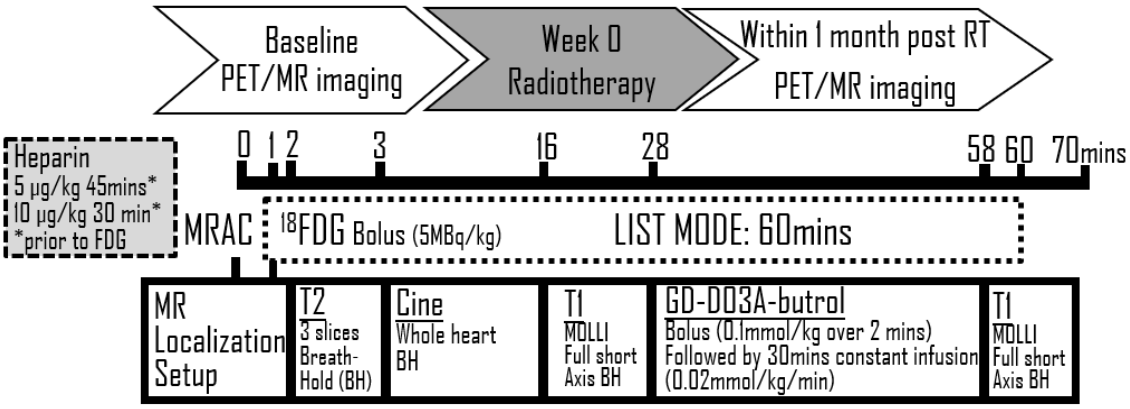

Figure 6.1 Overview of the timeline and hybrid PET/MR imaging protocol for RICT-Breast pilot study

6.1.2 Updated Results for RICT-BREAST (1-year follow-up)

Table 6.1 Patient demographics of the first five left-sided breast cancer patients along with the radiation dose metrics of the heart, left ventricle and the left anterior descending artery. The mean value is indicated with *.

Age of patients n=5	*62y/o (38 - 79)
Staging	
T1	2 (1 recurrence BC)
T2	2
T3	1
Radiation Treatment (RT)	
Free-breathing RT	3
Tomotherapy	1
IMRT	1
VMAT	1
DIBH IMRT	2
Prescription dose	
42.5 Gy in 16 fractions	2
With 10 Gy in 5 fractions boost	2
48 Gy in 16 fractions	1
Mean Heart Dose	* 2.75 Gy
Mean LV Dose	* 3.38 Gy

Mean LAD dose	* 1.29 Gy
$V5_{Gy}$ Heart	* 15.6%
Max Heart Dose	* 24.14 Gy
Max LAD dose	* 6.19 Gy
Adjuvant chemotherapy Yes Herceptin No	 3 3 2

The patient demographics of the first five patients who returned for their 1-year follow-up imaging session are shown in table 6.1. Note that these patients (stage 1 to stage 3) were treated with a variety of treatment techniques including IMRT, VMAT and Tomotherapy with a combination of DIBH or free-breathing RT. Results of regional uptake of ^{18}FDG/PET, LV functional parameters, extracellular volume matrix (ECV) and blood work measurements are presented in table 6.2, 6.3 and in figures 6.1 – 6.4.

At 1-year follow-up, one patient (38y/o) who was treated with Tomo Therapy (42.5 Gy in 16 fractions with 10 Gy in 5 fractions boost) was reported with LV borderline dilation but normal in shape and wall thickness. All patients were assessed by a Radiologist (A.I.). No segmental wall motion abnormality or no gross abnormal enhancement, scar, fibrosis or edema measured with T1- and T2-weighted images were detected at 1-year follow-up.

Table 6.2 Presented are the mean values of ^{18}FDG/PET standard uptake of the myocardium based on body weight (SUVbw) sorted according to the respective supplying coronary arteries using the AHA heart model, LV functional parameters (EDV, SV and EF), extracellular volume matrix values (at apex, mid and basal slice locations of the heart) and blood work measurements of high-sensitivity Troponin-T (hs-TnT), high-sensitivity C-reactive protein (hs-CRP) and erythrocyte sedimentation rate (ESR) at baseline, 1-month and 1-year follow-up. The percentage change comparing baseline, 1-month and 1-year follow-up of each respective measurement are reported.

N = 5		**LCX**	**LAD**	**RC**
^{18}FDG/PET meanSUVbw	baseline	1.42	1.34	1.55
	1-month follow-up	1.53	1.48	1.57
	1-year follow-up	1.38	1.33	1.48
	% change (1-year vs **baseline**)	-2.38	-0.98	-4.8
	% change (1-year vs **1-month**)	-9.89	-10.33	-6.14
		EDV (ml)	**SV (ml)**	**EF (%)**
Mean values of LV functional parameters	baseline	132	86.6	66.6
	1-month follow-up	124	79	64.6
	1-year follow-up	120	66.2	62.2
	% change (1-year vs **baseline**)	-9.09	-23.56	-6.61
	% change (1-year vs **1-month**)	-3.23	-16.2	-3.72
		Apex	**Mid**	**Base**
Mean extracellular volume (ECV)	baseline	0.295	0.267	0.272
	1-month follow-up	0.311	0.283	0.286
	1-year follow-up	0.315	0.288	0.288
	% change (1-year vs **baseline**)	6.94	7.87	5.66
	% change (1-year vs **1-month**)	1.5	1.77	0.48
		hs-TnT (ng/L)	**hs-CRP (mg/L)**	**ESR (mm/h)**
Mean value of Blood Work measurements	baseline	14.2	1.1	7.3
	1-month follow-up	8	1.2	9.5
	1-year follow-up	9.6	1.55	9.5
	% change (1-year vs **baseline**)	-32	48	30
	% change (1-year vs **1-month**)	20	32	0

Table 6.3 Summary table of individual patient results are presented, with worsening changes at follow-up compared to baseline highlighted in red.

	Stage		T2N0	T1N0	T2N0	T3N1	T1N0
	Treatment technique		DIBH IMRT	4D-CT IMRT	Tomotherapy	4D-CT VMAT	DIBH IMRT
	Dose Prescription		42.5Gy in 16fx	42.5Gy in 16fx	42.5Gy in 16fx, 10Gy in 5fx	48Gy in 16fx	42.5Gy in 16fx,10Gy in 5fx
	Adjuvant chemotherapy with Herceptin		Yes	No	Yes	Yes	No
Dose Parameters (Gy)	mean Heart		0.541	59.5	8.347	3.71	0.56
	Heart$V5_{Gy}$ (%)		0	0	66	12	0
	max Heart		8.692	24.309	38.64	40.609	8.456
	mean LV		0.782	79	8.275	6.527	0.53
	mean LAD		1.233	1.518	0.658	2.16	0.88
	max LAD		2.916	5.068	1.395	20.146	1.414
1-month vs baseline	FDG (mean SUVbw)	LCX	-0.13	0.28	0.39	-0.03	0.08
		LAD	-0.18	0.39	0.3	0.06	0.13
		RC	-0.15	0.25	0.18	-0.12	-0.05
1-year vs baseline		LCX	-0.06	-0.22	-0.07	-0.18	0.35
		LAD	-0.16	-0.20	-0.04	0.00	0.34
		RC	-0.17	-0.16	-0.10	-0.15	0.21
1-month vs baseline	EDV (ml)		-13	-7	1	-4	-25
	SV (ml)		-2	-8	-4	1	-25
	EF (%)		5	-2	-2	-2	-9
1-year vs baseline	EDV (ml)		-29	-2	-11	-6	-12
	SV (ml)		-22	-45	-11	-5	-19
	EF (%)		-4	-7	-2	0	-9
1-month vs baseline	ECV	apex	-0.001	0.035	0.031	0.028	-0.014
		mid	0.016	0.005	0.018	0.023	0.019
		basal	0.001	0.017	0.024	0.013	0.015
1-year vs baseline		apex	0.0016	N/A	-0.0035	0.0212	0.0549
		mid	0.0032	N/A	0.0053	0.0322	0.0589
		basal	0.0043	N/A	-0.0050	0.0147	0.0491
1-month vs baseline	hs-TnT		-12	0	-16	-3	0
	hs-CRP		-0.1	0.2	0	0.4	0.3
	ESR		-3	-3	20	2	-1
1-year vs baseline	hs-TnT		-14	-2	-19	10	2
	hs-CRP		0.9	0.2	0	0.9	N/A
	ESR		3	0	13	0	N/A

A global reduction of overall ^{18}FDG/PET mean standard uptake (meanSUVbw) was observed in the first five patients, comparing 1-year follow-up to baseline (-2.38% in the LCX territory, -0.98% in the LAD territory and -4.8% in the RC territory) and 1-month follow-up (-9.89% in the LCX territory, -10.33% in the LAD territory and -6.14% in the RC territory). (See figure 6.2)

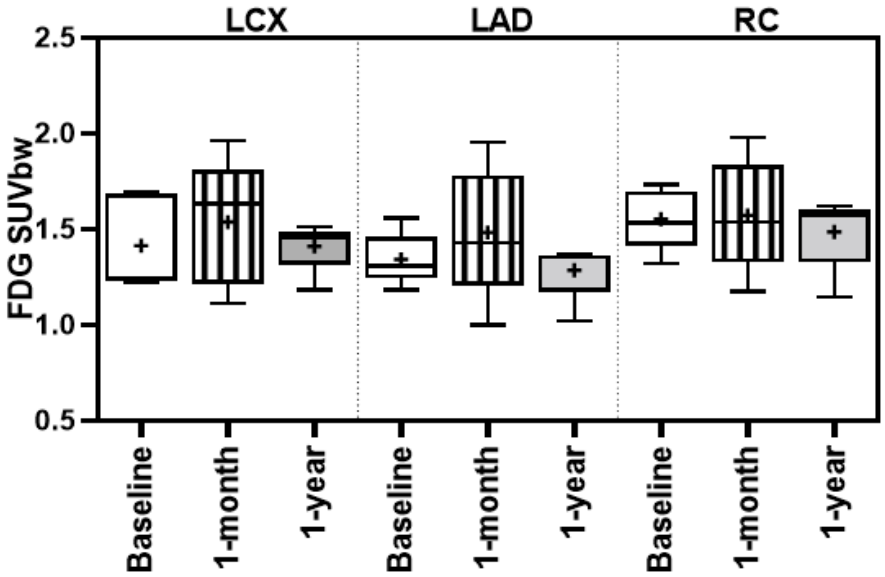

Figure 6.2 ^{18}FDG/PET mean standard uptake values of the myocardium based on body weight (SUVbw) (n = 5) at baseline, 1-month and 1-year follow-up. The uptake values for the entire myocardium were broken down to regions supplied by the LAD, LCX and RC. Note the mean SUV is indicated with ' + ' and the median value is indicated as the median bar in the boxplot.

Reduction of LV functional parameters were manifested in the first five patients, comparing 1-year follow-up to baseline (-9.09% in end-diastolic volume (EDV), -23.56% in stroke volume (SV) and -6.61% in ejection fraction (LVEF)) and 1-month follow-up (-3.23% in EDV, -16.2% in SV and -3.72% in LVEF). (See figure 6.3)

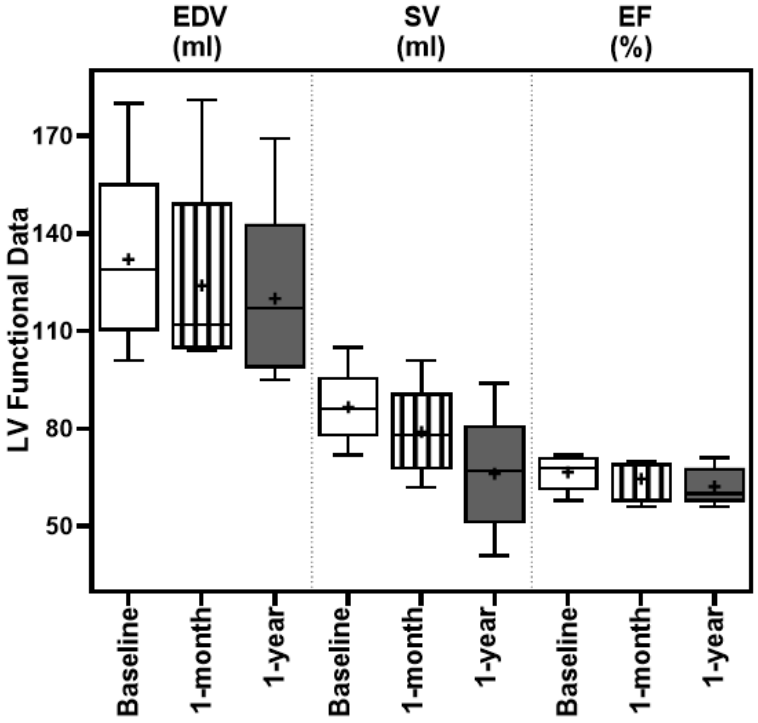

Figure 6.3 Mean cardiac functional parameters including the left ventricular end-diastolic volume (EDV), stroke volume (SV) and the left ventricular ejection fraction (EF) before, 1-month and 1-year after radiotherapy (n = 5).

Regarding extracellular volume matrix (ECV) values, at 1-year follow-up, only 4 out of the 5 patients results were analyzed due to technical difficulties in generating T1 maps for one patient. A global elevation ECV across all slices were shown comparing 1-year follow-up to baseline (6.94% in apex slices, 7.87% in middle slices and 5.66% in basal slices location) and comparing 1-year follow-up to 1-month follow-up (1.5% in apex slices, 1.77% in middle slices and 0.48% in basal slices location). (See figure 6.4)

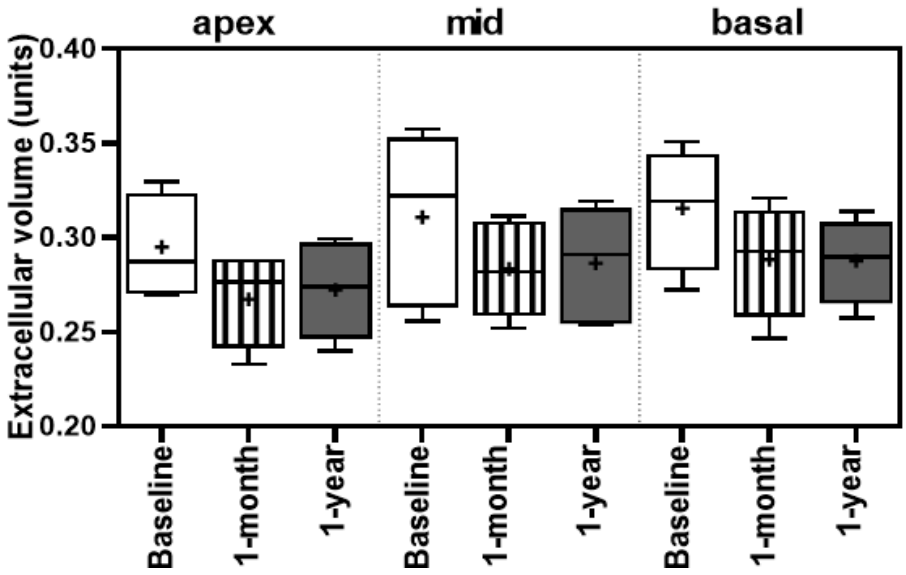

Figure 6.4 Mean Extracellular volume before, 1-month and 1-year after radiotherapy (n = 5).

Blood work results of high-sensitivity C reactive protein (hs-CRP) and erythrocyte sedimentation rate (ESR) of one patient at 1-year follow-up were excluded considering an expected total knee surgery inflammation response. At 1-year follow-up, high-sensitivity troponin T level was reduced (-32%) compared to baseline but elevated (20%) compared to 1-month follow-up. hs-CRP was reported up to 48% elevation compared to baseline and 32% compared to 1-month follow-up. Whereas, ESR was reported with 30% increase compared to baseline but no change compared to 1-month follow-up. (See figure 6.5)

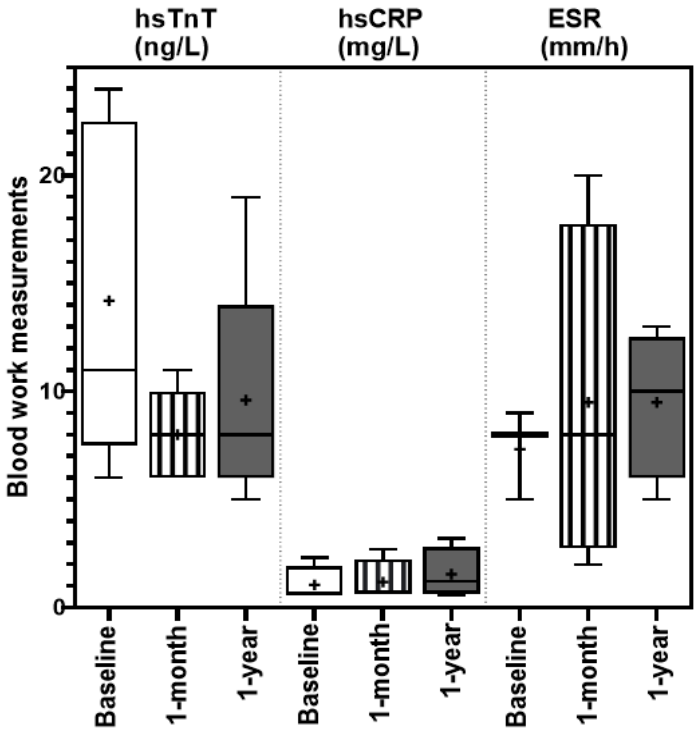

Figure 6.5 Presented are the mean blood work measurements of high-sensitivity Troponin T (hs-TnT) high-sensitivity C-reactive protein (hs-CRP) and erythrocyte sedimentation rate (ESR) before,1-month and 1-year after radiotherapy (n = 5).

Overall, our hybrid PET/MR imaging protocol is capable of detecting median-long term (1-year follow-up) functional changes in the first five patients, particularly in the reduction of LV functional parameters, the elevation of MR extracellular volume matrix, along with serial blood work changes of hs-CRP. However, myocardial inflammation response, which was determined from ^{18}FDG/PET, showed global reduction at 1-year follow-up. It is important to note that the changes may be attributed to advanced mitigation strategies of breast cancer radiation treatments or inflammation does not generally persist in this first five patients at one year follow-up. To validate the clinical significance of the advanced mitigation strategies, a larger sample size of the patient population should be considered, along with a cardiac-specific significant clinical end-point detection at a longer-term follow-up using hybrid PET/MRI.

6.1.3 Pre-treatment risk stratification

With the confirmation of clinical significance, multi-modality cardiac imaging can be utilized to perform pre-treatment risk stratification on both breast and NSCLC cancer patients as well as other cancer types including esophagus cancer, Hodgkin lymphoma and other thoracic cancer; in adjunct with serial blood work and standard screening such as echocardiography. With non-invasive cardiac imaging assessment at baseline including tests on myocardial blood flow, MR extracellular volume matrix (ECV) or cine imaging for left ventricle functional, this can further provide additional information on patients' cardiac condition, which is required to design and deliver a patient-specific treatment.

6.1.4 Automation

With a possible large sample dataset to be collected, an automated cardiac atlas for cardiac substructure can be generated. This can enhance the contouring efficiency during treatment planning. Note contrast-enhanced CT images are required for better visualization of the cardiac substructure and accurate contouring, hence a large sample CT dataset with contrast is also needed.

6.1.5 Anti-inflammation treatment

With the detection of early inflammation, early treatment with anti-inflammatory and/or cardioprotective medication can be issued. This includes standard cardioprotective drugs such as angiotensin receptor blockers, beta-blockers and ACE-inhibitors, which can prevent the deterioration of the heart toward heart failure. Furthermore, canakinumab, a therapeutic monoclonal antibody agent currently tested in clinical trials which targets a cytokine that is central to the inflammatory response, can be potentially issued and assessed for clinical efficacy using multi-modality imaging.[1]

6.2 Conclusion

In this thesis, we established a clinically feasible protocol to assess early cardiac functional changes and inflammation response to current radiation treatment techniques that are dedicated to minimizing cardiac dose and radiation-induced cardiac toxicity. This

included multi-modality cardiac imaging assessment using hybrid PET/MR and CT perfusion imaging with serial blood work performed and obtained from animal model to patient pilot studies for both left-sided breast cancer and non-small cell lung cancer. Additionally, an extensive dosimetric heart sparing comparison of free-breathing, 4D-CT based treatment planning, including robust optimization and deep-inspiration breath-hold based treatment planning with combinations of forward and inverse-IMRT and VMAT was completed to present clinical feasible free-breathing options for patients who are non-compliant with breath-hold treatment.

References or Bibliography

[1]Ridker P, EverettB, Thuren T, MacFadyen J, Chang W, Ballantyne C, et al. Antiinflammatory Therapy with Canakinumab for Atherosclerotic Disease. N Engl J Med.2017;377(12):1119-1131

Appendices

Ethics approval for published material in Chapter 2

Fwd: eSirius Notification - New Protocol Modification Has Been APPROVED2014-005::1

3/18/15

------- Forwarded Message -------
Subject:eSirius Notification - New Protocol Modification Has Been APPROVED2014-005::1
Date: Wed, 18 Mar 2015 15:39:22 -0400
From:
To:
CC:

Western

AUP Number: 2014-005
PI Name: Prato, Frank
AUP Title: The Use of Hybrid PET/MR imaging to assess radiation-induced toxicity: A Canine Pilot Study (Pilot)

Official Notification of AUS Approval: A MODIFICATION to Animal Use Protocol 2014-005 has been approved.

The holder of this Animal Use Protocol is responsible to ensure that all associated safety components (biosafety, radiation safety, general laboratory safety) comply with institutional safety standards and have received all necessary approvals. Please consult directly with your institutional safety officers.

Submitted by: Copeman, Laura
on behalf of the Animal Use Subcommittee

The University *of* Western Ontario
Animal Use Subcommittee / University Council on Animal Care
Health Sciences Centre, • London, Ontario • CANADA – N6A 5C1
PH: 519-661-2111 ext. 86768 • FL 519-661-2028
Email: auspc@uwo.ca • http://www.uwo.ca/animal/website/

Ethics approval for published material in Chapter 4 (RICT-BREAST)

Western Research

Date: 5 February 2019

To: Dr. Stewart Gaede

Project ID: 112991

Study Title: Assessing Acute Cardiac Inflammation after Left-Sided Breast Cancer Radiotherapy with Hybrid PET/MRI (RICT-BREAST)

Application Type: HSREB Initial Application

Review Type: Full Board

Meeting Date: December 4, 2018

Date Approval Issued: 05/Feb/2019

REB Approval Expiry Date: 05/Feb/2020

Dear Dr. Stewart Gaede

The Western University Health Science Research Ethics Board (HSREB) has reviewed and approved the above mentioned study as described in the WREM application form, as of the HSREB Initial Approval Date noted above. This research study is to be conducted by the investigator noted above. All other required institutional approvals must also be obtained prior to the conduct of the study.

Documents Approved:

Document Name	Document Type	Document Date
letterofinformation-071218	Written Consent/Assent	07/Dec/2018
RICT-BREAST PROTOCOL-071218	Protocol	07/Dec/2018

Documents Acknowledged:

Document Name	Document Type	Document Date
HRSSRC - GAEDE - RICT - F18 - LETTER OF NO OBJECTION	Radionuclide Safety and Scientific Review Approval	31/Jan/2019

No deviations from, or changes to, the protocol or WREM application should be initiated without prior written approval of an appropriate amendment from Western HSREB , except when necessary to eliminate immediate hazard(s) to study participants or when the change(s) involves only administrative or logistical aspects of the trial.

REB members involved in the research project do not participate in the review, discussion or decision.

The Western University HSREB operates in compliance with, and is constituted in accordance with, the requirements of the TriCouncil Policy Statement: Ethical Conduct for Research Involving Humans (TCPS 2); the International Conference on Harmonisation Good Clinical Practice Consolidated Guideline (ICH GCP); Part C, Division 5 of the Food and Drug Regulations; Part 4 of the Natural Health Products Regulations; Part 3 of the Medical Devices Regulations and the provisions of the Ontario Personal Health Information Protection Act (PHIPA 2004) and its applicable regulations. The HSREB is registered with the U.S. Department of Health & Human Services under the IRB registration number IRB 00000940.

Please do not hesitate to contact us if you have any questions.

Sincerely,

Karen Gopaul, Ethics Officer on behalf of Dr. Joseph Gilbert, HSREB Chair

Note: This correspondence includes an electronic signature (validation and approval via an online system that is compliant with all regulations).

Ethics approval and permission to reproduce previously published material in Chapter 5 (RICT-LUNG)

Western Research

Date: 13 May 2021

To: Stewart Gaede

Project ID: 109084

Study Title: Identification of acute radiation-induced cardiac toxicity after non-small cell lung cancer radiotherapy with advanced multi-modality imaging (RICT-LUNG)

Reference Number/ID: N/A

Application Type: HSREB Amendment Form

Review Type: Delegated

Full Board Reporting Date: 08/June/2021

Date Approval Issued: 13/May/2021 14:48

REB Approval Expiry Date: 07/Jun/2021

Dear Stewart Gaede ,

The Western University Health Sciences Research Ethics Board (HSREB) has reviewed and approved the WREM application form for the amendment, as of the date noted above.

Documents Approved:

Document Name	Document Type	Document Date	Document Version
12May2021 - RICT Lung Ethics Protocol - cc	Protocol (Western)	12/May/2021	
12May2021 - RICT Lung Protocol - cc	Protocol	12/May/2021	
12May2021 - LOI RICT-Lung - cc	Consent Form	12/May/2021	

Documents Acknowledged:

Document Name	Document Type	Document Date	Document Version
12May2021 - RICT Lung Ethics Protocol - trcked	Summary of Changes	12/May/2021	
12May2021 - RICT Lung Protocol - trcked	Summary of Changes	12/May/2021	

REB members involved in the research project do not participate in the review, discussion or decision.

The Western University HSREB operates in compliance with, and is constituted in accordance with, the requirements of the TriCouncil Policy Statement: Ethical Conduct for Research Involving Humans (TCPS 2); the International Conference on Harmonisation Good Clinical Practice Consolidated Guideline (ICH GCP); Part C, Division 5 of the Food and Drug Regulations; Part 4 of the Natural Health Products Regulations; Part 3 of the Medical Devices Regulations and the provisions of the Ontario Personal Health Information Protection Act (PHIPA 2004) and its applicable regulations. The HSREB is registered with the U.S. Department of Health & Human Services under the IRB registration number IRB 00000940.

Please do not hesitate to contact us if you have any questions.

Sincerely,

Ms. Nicola Geoghegan-Morphet , Ethics Officer on behalf of Dr. Philip Jones, HSREB Chair

Note: This correspondence includes an electronic signature (validation and approval via an online system that is compliant with all regulations).

Obtain permission request - Journal (1252358) [220428-019239]

RP Rights and Permissions (ELS) <Permissions@elsevier.com>
Fri 4/29/2022 9:07 AM
To: Oi Wai Chau

You don't often get email from permissions@elsevier.com. Learn why this is important

Dear ,

We hereby grant you permission to reprint the material below at no charge in your thesis subject to the following conditions:

1. If any part of the material to be used (for example, figures) has appeared in our publication with credit or acknowledgement to another source, permission must also be sought from that source. If such permission is not obtained then that material may not be included in your publication/copies.

2. Suitable acknowledgment to the source must be made, either as a footnote or in a reference list at the end of your publication, as follows:

"This article was published in Publication title, Vol number, Author(s), Title of article, Page Nos, Copyright Elsevier (or appropriate Society name) (Year)."

3. Your thesis may be submitted to your institution in either print or electronic form.

4. Reproduction of this material is confined to the purpose for which permission is hereby given.

5. This permission is granted for non-exclusive world English rights only. For other languages please reapply separately for each one required. Permission excludes use in an electronic form other than submission. Should you have a specific electronic project in mind please reapply for permission.

6. As long as the article is embedded in your thesis, you can post/share your thesis in the University repository.

7. Should your thesis be published commercially, please reapply for permission.

This includes permission for the Library and Archives of Canada to supply single copies, on demand, of the complete thesis. Should your thesis be published commercially, please reapply for permission.

This includes permission for UMI to supply single copies, on demand, of the complete thesis. Should your thesis be published commercially, please reapply for permission.

8. Posting of the full article/ chapter online is not permitted. You may post an abstract with a link to the Elsevier website [http://www.elsevier.com,]www.elsevier.com, or to the article on ScienceDirect if it is available on that platform.

Kind regards,
Subash Balakrishnan
Copyrights Coordinator
ELSEVIER | HCM - Health Content Management
Visit Elsevier Permissions

Curriculum Vitae

Name: Oi Wai Chau (April)

Post-secondary Education and Degrees:
The University of Western Ontario
London, Ontario, Canada
2013-2017 B.Sc. Medical Biophysics
The University of Western Ontario
London, Ontario, Canada
2017-2022 Ph.D. Medical Biophysics (CAMPEP)

Honours and Awards:
Translational Breast Cancer Research Scholarship
2017-2020
Western Graduate Research Scholarship
2017-2022

Related Work Experience
Teaching Assistant MPH9010/9011
The University of Western Ontario, 2022

Publications:

Oi-Wai Chau, A Islam, E Yu, M Qu, J Butler, H Biernaski, A Sun, J-P Bissonnette, A MacDonald, C Graf, A So, G Wisenberg, T-Y Lee, F S Prato, S Gaede. Multimodality Imaging Assessment of the Heart Before and After Stage III Non-small Cell Lung Cancer Radiation Therapy. Advances in Radiation Oncology. 2022;7(4):100927. DOI: 10.1016/j.adro.2022.100927

Oi-Wai Chau, H Fakir, M Lock, R Dinniwell, F Perera, A Erickson, S Gaede. Dosimetric Planning Comparison for Left-Sided Breast Cancer Radiotherapy: The Clinical Feasibility of Four-Dimensional-Computed Tomography-Based Treatment Planning Optimization. Cureus. 2022;14(5):e24777. DOI:10.7759/cureus.24777

H Young, C Park, O-W Chau, T-Y Lee, S Gaede. Technical Note: Volumetric Computed Tomography for Radiotherapy Simulation and Treatment planning. J Appl Clin Med Phys. 2021;22(8):295-302. DOI: 10.1002/acm2.13336

Oi-Wai Chau, A Islam, M Lock, E Yu, R Dinniwell, B Yaremko, M Brackstone, W Pavlosky, J Butler, H Biernaksi, M Kovacs, C Graf, G Wisenberg, F S Prato, S Gaede. Assessing Acute Cardiac Inflammation One Month after Left-sided Breast Cancer Radiotherapy with Hybrid PET/MRI. Under Review. 2022

Oi-Wai Chau, O El-Sherif, M Mouawad, J Sykes, J Butler, H Biernaski, R deKemp, J Renaud, G Wisenberg, F S Prato, S Gaede. Changes in Myocardial Blood Flow in a Canine Model of Left Sided Breast Cancer Radiotherapy. Under Review. 2022

J Chhina, H Sendzik, O-W Chau, J Navarro, S Gaede, S Frisbee. Cardiovascular Disease Associated with Radiation Therapy for Breast Cancer: A Comprehensive Review and Synthesis of the Literature. Submission in Preparation. 2022